Journal of Materials Chemistry A

ROYAL SOCIETY OF CHEMISTRY

REVIEW

View Article Online
View Journal | View Issue

Cite this: J. Mater. Chem. A, 2021, 9, 15140

Recent advancements in solid electrolytes integrated into all-solid-state 2D and 3D lithium-ion microbatteries

Albina Jetybayeva,[ab] Berik Uzakbaiuly,[abc] Aliya Mukanova, *[abc] Seung-Taek Myung [d] and Zhumabay Bakenov *[abc]

With the increasing role of microelectronics and autonomous wireless devices in everyday life, the miniaturization of power sources has attracted a lot of attention. Solid-state Li-ion microbatteries proved to be a good candidate for micro-energy storage devices due to their high energy density. As the electrolyte is one of the key components in a battery, much research has been conducted to develop high-quality materials for successful integration in the microbattery technology. Several types of solid electrolytes, including inorganic glass, crystalline and polymer materials, have been investigated in both two-dimensional (2D) and three-dimensional (3D) architecture, and these systems are reviewed in this work along with the general overview of microbatteries concepts. The latest advancements, performance and remaining issues of both 2D and 3D solid structures with different solid electrolytes are discussed. The paper also focuses on reviewing the electrochemical properties of solid electrolytes reported in various literature. So far, it was observed that LiPON electrolyte satisfying most of the electrolyte specifications appears to be one of the most studied and the most appropriate candidates for solid-state microbatteries, performing well in several 2D and innovative 3D structures. Along with that, polymer electrolytes with innovative 3D architectures deposited with effective techniques, such as electrodeposition, formed an excellent electrode–electrolyte interface and showed high power and energy densities. Therefore, these electrolytes hold great promise for further 3D microbatteries development. The important information on solid electrolytes and their application in microbatteries is systemized and provided, including the electrolyte composition, ionic conductivity, microbattery electrodes, preparation methods and conditions, architecture, electrochemical test conditions and their performance to elucidate the electrolyte candidates and their microbattery structures with high capacity and long cycle life.

Received 30th March 2021
Accepted 11th June 2021

DOI: 10.1039/d1ta02652f

rsc.li/materials-a

1. Introduction

The rapid development of micro- and nano-electromechanical systems (MEMS/NEMS) resulted in the advancements of small-scale devices such as microsensors, micro drug delivery systems, micromachines.[1–4] These devices require an autonomous power supply with a stable current or the ability to deliver high-peak currents within a confined volume (<10 mm^3).[1] Lithium-ion battery (LIB) technology is an excellent candidate, as it has become a mature energy storage solution with the highest energy per weight.[5–7] The early microbatteries were structured in thin film, two-dimensional (2D) architectures, where the straightforward layered fabrication and easy integration in devices were advantageous for industrial production.[8] However, 2D structures have power, energy, and size limitations; thus, it is challenging to satisfy the increasing demand for rapidly developing devices. As a result, a large interest in three-dimensional (3D) microbatteries arose, as 3D architectures allow power and energy density enhancement without the undesired volume increase.[3,4,9–11]

However, to significantly reduce the size of traditional Li-ion batteries and keep the energy efficiency, it is necessary to remove inactive materials, such as separators, as well as introduce alternative electrodes and electrolytes. The commercial electrolytes, although being highly ionically conductive, cause safety issues, like leakage risks.[12,13] Thus, solid-state electrolytes have been actively developed and integrated into the microbatteries. Meanwhile, a newer generation of promising

[a]Institute of Batteries, 53 Kabanbay Batyr Ave., Nur-Sultan 010000, Kazakhstan. E-mail: aliya.mukanova@nu.edu.kz
[b]Department of Chemical and Materials Engineering, Nazarbayev University, Nur-Sultan, Kazakhstan
[c]National Laboratory Astana, Nazarbayev University, 53 Kabanbay Batyr Ave., Nur-Sultan 010000, Kazakhstan
[d]Department of Nano Technology and Advanced Materials Engineering, Sejong University, Gunjadong, Gwangjin-gu, Seoul 05006, South Korea

electrode and electrolyte materials have been continuously investigated.

The solid electrolyte is an important component in the solid-state cell, as in most cases its unsatisfactory bulk and interfacial performance pose the main constraints in the various Li-ion microbattery (LIMBs) technologies' commercialization.[12,14,15]

In order to successfully implement the solid electrolyte in the microbattery, it should satisfy the following basic specifications:[16,17]

- High ionic conductivity 10^{-4} S m^{-1} at room temperature[18] (at least $>10^{-7}$ S m^{-1})[19]
- Compared to ionic conductivity, significantly lower electronic conductivity[20,21]
- High electrochemical, chemical and thermal stability against electrode materials[19,20]
- Mechanical integrity to prevent Li dendrites formation[17]
- Easy synthesis and manufacture on a large scale[22]
- Low cost and toxicity.

Solid electrolytes are typically divided into organic and inorganic types. Organic type is mainly presented by polymer-based electrolyte, which has recently been the subject of more studies due to the high achievable ionic conductivity (up to 10^{-4} S cm^{-1}), relatively easy fabrication methods, flexibility, and the ability to constrain the volume changes of electrodes, such as Si.[23,24]

Inorganic electrolytes are usually classified into crystalline and glass-based on the material structure. Crystalline electrolytes include materials such as Li superionic conductor (LISICON), Na superionic conductor (NASICON), perovskites and garnet-type electrolytes.[25,26] Glass electrolytes are mainly represented by lithium phosphate-containing compounds and amorphous phase of some crystalline electrolytes.[8,27,28]

The choice of electrolyte type for microbattery depends on the application requirements. Undoubtedly, the integration of solid electrolytes into microbatteries requires specific preparation techniques. Each technique has its advantages and drawbacks that usually also have a critical impact on the decision of which type should be preferred. Among the most common techniques to obtain thin films are radio-frequency (RF) magnetron sputtering (MS), Pulsed Laser Deposition (PLD), Atomic Layer Deposition (ALD), Chemical Vapor Deposition (CVD), Electrodeposition (ED), nitrogen Ion Beam Assisted Deposition (IBAD), thermal evaporation (TE), and others.[19,29–33]

In fact, when 'micro-sized' electrolytes are developed, the same problems as for 'bulk' electrolytes exist along with additional specific problems. The ionic conductivity is less of a concern in microbatteries due to the shorter path for lithium ions;[34] however, a lot of studies have been devoted to keeping it on a satisfying level or improving it. Equally critical is a morphology where weakness can easily result in short circuits. Another important aspect is reducing the interface resistance between the electrolyte and the interface. The structure of a 3D microbattery implies increasing the surface area allowing a decrease in the interfacial resistance.

Summarizing the above, the development of solid-state microbatteries, including attempts to create 3D types, are the focus interest of many researchers. Therefore, this work is to track the progress of the research results.

During the recent two decades, a growing number of research on Li solid electrolytes used in all-solid-state microbatteries and reviews on these studies has been done. Several review papers covered the general principles, overall information on the materials used for electrodes and electrolytes, and deposition techniques of all-solid-state thin film and 3D microbatteries.[1,7,35–39] Other articles discussed all-solid-state microbatteries modelling and simulations evaluating the effect of 2D or 3D structures and mechanical stresses on the microbattery performance.[23,40] The reviews with a particular focus on the microbatteries with Si anode[41] and $LiCoO_2$ (LCO) cathode[42] also provided useful information on several solid electrolytes integrated into these structures. Moreover, the recent overviews for the emerging deposition techniques applied for microbatteries, such as PLD and ALD discussed the development of solid-state electrolytes.[29,43,44] All these previous studies contain very important information, however, there are no specific reviews fully covering and revising the topic of solid-state electrolytes integrated into microbatteries. One review by Xia *et al.*[19] focused on solid-state electrolytes including glass-like and crystalline materials and their properties for potential application in thin-film microbatteries. However, it was published a decade ago and did not include solid polymer electrolytes. There are many new studies published recently on glass, crystalline, polymer electrolytes, which were not covered up until now. In addition, various types of 3D-shaped microbatteries were developed and can be discussed as well.

Therefore, this review article presents an overview of the polymer, crystalline and glass-based solid electrolytes integrated and tested in LIMBs. The recent advancements, performance, and remaining challenges of thin-film and 3D solid structures with various solid electrolytes are discussed. The initial part shortly reviews the microbatteries concepts, while the following parts focus on each type of solid electrolytes in different microbattery architectures.

This review was structured as follows, first an overall brief introduction to solid-state electrolytes currently used in microbatteries and the general overview of solid-state microbattery technology with its main materials and concepts will be provided. Then the types of solid-state electrolytes will be covered in detail separately for polymer, inorganic crystalline, and inorganic glass electrolytes. Firstly, organic electrolytes, as the common electrolyte materials for batteries applications, will be reviewed. Then the materials applied mainly in their crystal structure (inorganic crystalline electrolytes) will be discussed, as they are less integrated into microbatteries. Next materials more frequently used in their amorphous state (inorganic glass electrolytes) will be covered as the most developed type for microstructures. The inorganic electrolytes are differentiated into crystalline and glass category in this review since most of the specific materials are mainly used in microbatteries in either crystalline or glass state. For example, LiPON is predominantly applied as amorphous material, while NASICON as a crystal one. Finally, the table and summarizing plots are presented to show the current situation. The provided material

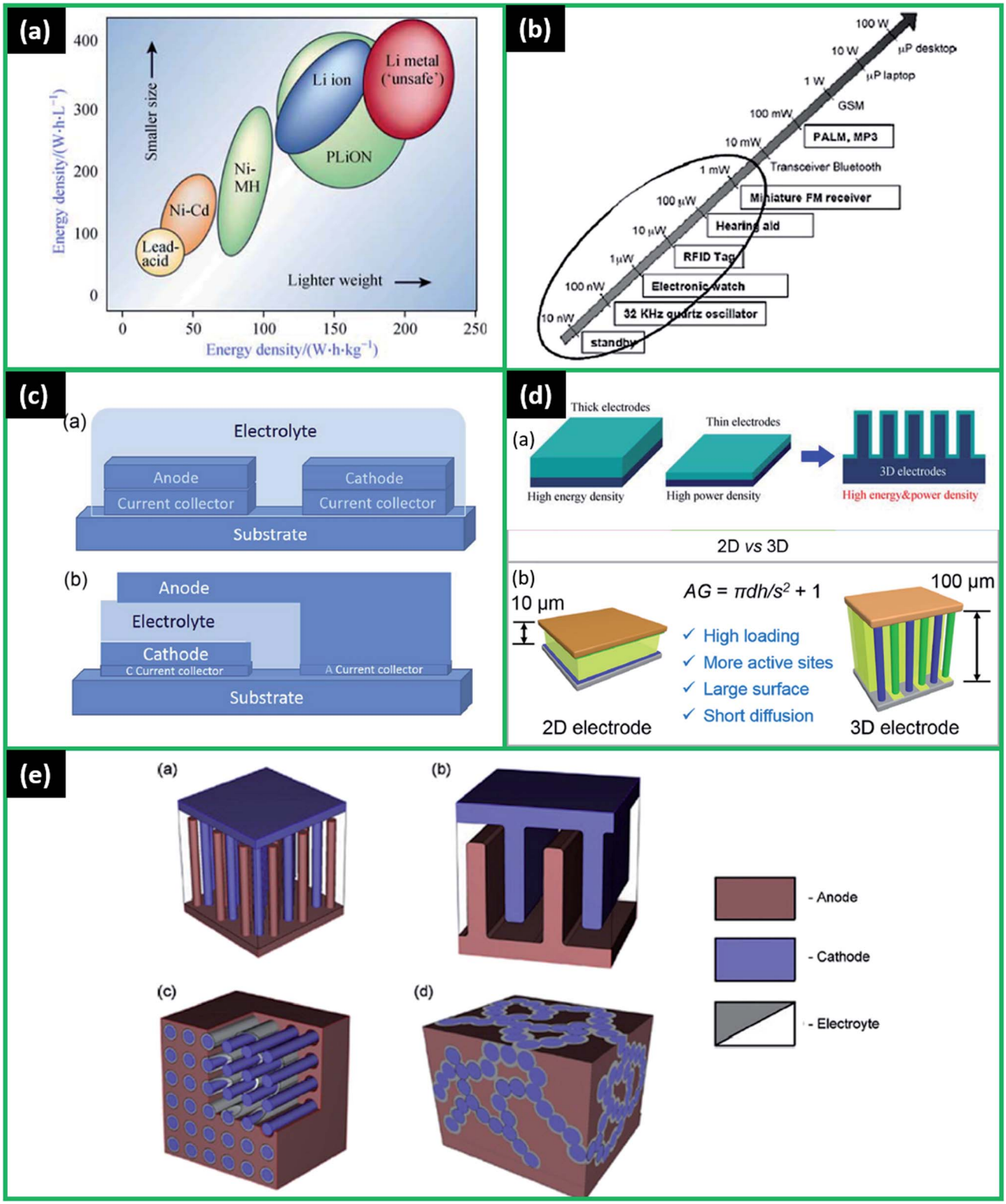

Fig. 1 (a) Comparison of the different battery technologies in terms of volumetric and gravimetric energy density. Reproduced with permission from ref. 41; (b) typical electrical consumption for different mobile devices. Reproduced with permission from ref. 50; (c) representative configuration of (a) planar (b) stacked microbatteries. Reproduced with permission from ref. 1; (d) (a) advantages of the 3D battery structure, (b) superiority of 3D *vs.* 2D electrodes is illustrated with schematics (where AG – area gain of 3D, *d* – nanorod diameter, *s* – nanorod spacing, and *h* – rod height). Reproduced with permission from ref. 41 and 49; (e) 3D micro LIB structures: (a) interdigitated rod electrodes, (b) interdigitated plates or 3D-trench, (c) concentric tube, (d) 3D aperiodic sponge. Reproduced with permission from ref. 66.

can serve as a good source for further research and development in solid-state microbattery technology.

2. All-solid-state microbatteries overview

With the increasing interest in advanced micro- and nano-devices, such as radio-frequency identification tags, stand-alone sensor systems, implantable medical devices, labs-on-chip, Complementary Metal Oxide Semiconductor (CMOS) memory chips, smart cards, and others the demand for micro-energy systems is rising drastically.[19,29,41,43] The energy systems can be classified based on the energy generation and storage systems, such as solar cells,[45] micro-fuel cells,[46] micro thermo-electric generators,[47] nuclear microbatteries, and rechargeable LIMBs.[48] LIMBs are considered a promising solution for powering a wide variety of small devices due to relatively higher energy density (Fig. 1a), a wider range of operating temperatures, good cycling stability, and mature manufacturing technology.[41]

The principle of work for rechargeable microbatteries is similar to standard LIBs where Li-ions transfer between anode and cathode, and charge carriers produce electrical energy. The electrodes are also separated by an electrolytic solution or solid-state electrolyte.[37] The greatest difference between traditional batteries and LIMBs is the volume, where a microbattery is typically smaller than 0.01 cm^3.[1] As a result, geometry along with suitable materials are critical for microbatteries' power densities.[1,37] The energy consumption for typical microelectronic devices is about 10 mW and may range between tens of nanowatts and tens of milliwatts (Fig. 1b).[1,49,50] Most of the microbatteries can generate these energy and power densities in the span of 30–300 $\mu W\ h\ cm^{-2}\ \mu m^{-1}$ and 0.0001–10 $mW\ cm^{-2}\ \mu m^{-1}$, respectively, which in many cases might be insufficient to fit inside of microdevices and fulfil their energy requirements.[1,49] Therefore, making the advancement in materials and cell geometry is a primary goal to increase the energy density of microbatteries.

Replacing liquid electrolytes with solid-state electrolytes in microbatteries is in more demand these days, as it is safer, it brings higher thermal and electrochemical stability, enables Li metal anode, and automatically excludes the necessity of additional electrical insulators.[19,37] Separators with liquid electrolyte have an average thickness of 20 μm or more, whereas solid electrolytes typically have thicknesses of 1 μm in microbatteries.[37] Furthermore, liquid electrolytes also lead to more complicated packaging to avoid safety issues.[7]

With the recent successful developments in solid-state ion-conducting materials, the rapid progress towards LIMBs solidification, miniaturization, and commercialization was observed. The first all-solid-state microbatteries had a 2D thin-film structure. The structure of 2D usually has several layers deposited either in a planar or a stacked way (Fig. 1c).[1]

The most commonly used materials for thin-film microbatteries include LCO for a cathode,[51–56] Li metal for an anode,[44,56–58] and liquid Li-ion compounds and solid materials, such as lithium phosphorus oxynitride (LiPON),[37,56,57,59] LISICON,[60] NASICON,[61] poly(ethylene oxide) (PEO)-based polymer[62–64] and others for electrolytes. The early studies showed that all-solid-state 2D microbattery, having a more homogeneous current distribution, proved to be more stable and more resistant to high temperatures during cycling.[56,65] Moreover, good compatibility of microbatteries with the manufacturing processes of solar panels and circuits resulted in the commercialization of some thin-film batteries' designs (Table 1).[7,19,29,57] Nevertheless, 2D microbatteries struggle to provide sufficient power and energy to the increasing demand of the fast-growing small power applications, especially MEMS devices.[1] The possible approach to increase the energy density of 2D all-solid-state microbatteries is to increase the thickness of electrodes.[43] However, this will compromise the power density, as the diffusion path of Li-ions will become longer and the expanded size will complicate integration into microdevices. Besides the major problem of large footprint area needed to deliver the required capacity, another issue is the dependency of the current density distribution on the relative distance between the electrodes.[1]

For microbatteries, the key issue is to fit within the small size of microdevices and at the same time to have high energy and power densities.[1] Since 3D designs result in high energy density while occupying a minimal footprint area, they have been extensively researched.[9] Compared to 2D designs with the limited surface area, 3D-structured cells demonstrated higher microbattery performance compared to 2D microbatteries in

Table 1 Some industrial thin film microbatteries (reproduced with permission[1,29,307])

Manufacturer	Electrochemical chain	Specifications
Cymbet Co.	EnerChip™ $LiCoO_2$/Li	60 $\mu A\ h\ cm^{-2}\ \mu m^{-1}$/5000 cycles/4–4.15 V
Infinite Power Solutions	$LiCoO_2$ or V_2O_5/LiPON/Li	"Thinergy" 40 $\mu A\ h\ cm^{-2}\ \mu m^{-1}$/4.1 V
Front Edge Technology	$LiCoO_2$/LiPON/Li	"Nanoenergy" 0.9 $\mu A\ h\ cm^{-2}\ \mu m^{-1}$
Ulvac Inc.	$LiCoO_2$/Li_3PO_4/Li	50 $\mu A\ h\ cm^{-2}\ \mu m^{-1}$
STMicroelectronics	$LiCoO_2$/LiPON/Li	700 μA h/discharge/5 mA/3.9 V
Excellatron	$LiCoO_2$–$LiMnO_2$–LiPON–Sn_3N_4	0.3 μm thick/0.1 mA h/2000 cycles/3.9–4.1 V
Enfucell	MnO_2-based cell	Voltage rating > 3 V
GS Caltex	n/a	300 μm thick/3.9 V/8000 cycles
Ilika Inc.	Stereax® M250 medical	174 $\mu A\ h\ cm^{-2}$, 3.5 V
Wyon	CP1254	160 μA h/3.7 V/2 mm thick
Varta		60 mA h/3.7/5.4 mm thick

several studies.[7,37] In the 3D arrangement, the larger specific surface area allows usage of more active material in the same footprint area, directly increasing aerial capacity, and thus, energy and power densities as well (eqn (1) and (2)). The quantification of advantages of 3D architectures was also provided by Long *et al.*[9] In addition, in 3D structure, the shorter Li-ion diffusion lengths result in higher power density (Fig. 1d).[41,49] Thus, both the energy and power density can be increased.

$$E = \frac{C \times V}{\theta \times \rho} \quad (1)$$

where: E – energy density [W h kg^{-1}]; C – aerial capacity [mA h cm^{-2}]; V – voltage [V]; θ – thickness [μm]; ρ – density [kg m^{-3}].

$$P = \frac{E}{\Delta t} \quad (2)$$

where: P – power density [W kg^{-1}]; Δt – discharge time [h].

There are many studies on the various 3D designs for microbatteries, and the most common ones are demonstrated in Fig. 1e.[1,66] Among them, interdigitated architectures are more easily manufactured and have a lower risk of short circuits between the electrodes. In other designs, pinholes in the extremely thin electrolyte/separator layer can be formed as a result of electrode materials' volume change and, thus, cause the battery to fail.[1] Therefore, it is critical to find the optimal distance between the electrodes that will allow the maximum possible energy density without significantly raising the short-circuit risk. Up to now, several review papers have specifically covered the 3D architectures of batteries, their structures, modelling, and common materials.[9,10,16,67–69]

Undoubtedly, the choice of materials for the battery has a fundamental role to achieve desirable performance. Thus, careful selection is crucial. As a cathode material in 3D all-solid-state LIMBs compounds such as LCO,[70–72] spinel structures, such as $LiNi_{0.5}Mn_{1.5}O_4$ (LNMO),[73–75] $LiFePO_4$ (LFP),[76,77] vanadium oxides,[31,78] and others have been utilized. Currently, extensively studied LCO with relatively high capacity, stability, and mature manufacturing procedure prevails as a cathode material, while other promising materials are under development.[7,37,71]

For the anode, Li metal is the commonly used material due to its high specific capacity, low electrochemical potential, and weight.[7,37,44,70,79] Moreover, for solid-state electrolytes, the problem with Li dendrite formation is of less concern.[7] Other anode materials include elements of the IVA group (Sn, C, Si, *etc.*).[31,80,81] For example, Li–Si alloy has demonstrated high specific capacity (3580 mA h g^{-1}), with the only concern of Si volume expansion that can be possibly mitigated by proper architecture or other methods.[37,71,72,82] Titanium-based structures (TiO_2, $Li_4Ti_5O_{12}$ (LTO)) are also among the anode candidates. LTO, for example, can show good cyclability with a small volume change and yet relatively low capacity (160 mA h g^{-1}).[7,73–75,83] As LTO suffers from a high charge–discharge potential of 1.5–1.6 V, it acts as a high-voltage anode or low-voltage cathode, and this narrows the cell potential.[37] So LTO can be used in applications where stability and low-temperature applications are prioritized over energy content.[37] Many studies have also suggested and tested TiO_2 structures as anodes due to good lithium intercalation behaviour, reasonable capacity retention, and lower risk of Li dendrites formation compared to carbonaceous materials.[68,84–86] The interest grew especially in using TiO_2 for 3D designs as self-supporting oxide satisfying the criteria of 3D electrodes with high capacity and cyclability.[68,84–87] In addition to the many experimental investigations, theoretical calculations of the highest achievable capacity have been done for the optimized architectures of TiO_2 micropillars.[88]

Over the last decade, many studies have been investigating the important component for microbatteries – solid-state electrolyte.

In this review paper, the focus is to cover the recent advances in LIMBs from the point of view of various solid electrolytes and to identify new potential variants for the next-generation all-solid-state microbatteries.

3. Polymer electrolytes

Polymer electrolytes (PE) are one of the promising solid electrolytes for Li microbatteries due to several advantages including good ionic conductivity (up to 10^{-4} S cm^{-1}), improved flexibility, ability to accommodate volume changes, easy processing, and the recently improved mechanical strength (10^6–10^8 Pa) which helps to prevent Li dendrites formation.[23,24,89–91] The essential benefits of using a polymer electrolyte in the 2D and 3D structured microcells can be its ability to reach the very narrow spaces between the electrodes and, consequently, to provide good contacts. PEs are fabricated by dissolving Li salts ($LiPF_6$, $LiClO_4$, LiFSI, LiTFSI, LiDFOB, *etc.*) in the polymer matrix (polyethylene oxide (PEO), poly(methyl methacrylate) (PMMA), polyacrylonitrile (PAN), polyvinylidene fluoride (PVDF), and its derivatives, *etc.*).[24,89] They can be categorized as solid polymer electrolytes, composite polymer electrolytes, and gel polymer electrolytes. Solid polymer electrolytes (SPEs) are dry polymers and are solvent-free systems in which organic liquid is not used.[92] The early SPE demonstrated low ionic conductivity of approximately 10^{-7} S cm^{-1}.[93] Later, it was found that it is the amorphous phases rather than crystalline that act as the transmission host for Li-ions that move through polymer chains.[94] Thus, several methods were suggested to increase the presence of the amorphous phase, including crosslinking, addition of large side-groups to the polymer chains, and addition of plasticizers.[37,94] Composite polymer electrolytes are SPEs where polymers could be blended, cross-linked, doped, reinforced by additives and inorganic fillers,[92] whereas, gel polymer electrolytes are also known as plasticized PEs.[92] Polymers are plasticized and get swollen by a liquid electrolyte. Generally, PEs can be produced by several techniques, including the evaporation method, drop-casting from a polymer solution, *in situ* plasma polymerization, and electrodeposition.[94–97] Despite being attractive alternatives to glass electrolytes, PEs have several disadvantages, such as low voltage window, unreliable electrochemical and thermal stability, and deficient mechanical integrity to suppress the Li dendrite growth.[23] The minimization

of these disadvantages is the aim of most studies, as well as the investigation of electrode/electrolyte compatibility and optimal cycling conditions. There are numerous in-depth reviews on SPEs based on various polymer matrices, active/inactive fillers, composite and hybrid components. The readers are asked to refer to those for further investigation.[92,98–100] In this section, we are going to review PEs that are used to fabricate all solid-state LIMBs.

3.1 Solid polymer/composite polymer electrolytes

Among SPEs, polyethylene-based electrolytes are one of the most commonly used polymer electrolytes due to a promising achievable ionic conductivity (10^{-7}–10^{-4} S cm^{-1}),[94] good compatibility with solid-state Li microbattery materials,[73] and thermal stability.[101] In addition, they possess faster dynamics at room temperature and excellent capability to solvate large concentrations of lithium salts.[102] Deposition of the electrolytes were mainly done by drop casting or dip coating and electrodeposition, as well as other deposition methods onto electrode materials, which were produced by traditional methods. Since dip/drop coating of PEs may not coat complex structures of electrodes uniformly for high capacity/power batteries, the research has also been focused on other electrolyte deposition methods. The electrodeposition technique was proposed to produce more conformal coating of the electrolyte. Other methods of deposition of SPEs include a range of techniques, such as infiltration of polymers into structured electrodes, spin coating, deposition onto electrodes, and patterning using photolithography or UV-polymerization, as well as CVD growth onto electrodes.

3.1.1 Drop casting/dip coating of electrolytes

3.1.1.1 Polyethylene polymers. Drop casting and dip coating are widely used deposition techniques of SPEs. Several investigations of 2D thin-film batteries with PEG-based electrolytes have been conducted, with the results being less successful compared to cells with LiPON electrolyte due to polymer electrolyte stability issues. For instance, the covalent silica–PEO–LiTFSI (SiO_2–PEG) hybrid solid electrolyte was prepared *via* sol–gel and organic polymerization methods and tested in thin film Li/SiO_2–PEG/$Li_4Ti_5O_{12}$ cell, where the electrolyte and the cathode were dip-coated thin films.[63] It was found that the produced electrolyte had good ionic conductivity of 2.6×10^{-5} S cm^{-1} with a Li-ion transference number of 0.37, while the microbattery demonstrated a decrease of capacity from 2.75 to 0.8 mA h g^{-1} after 500 cycles at the current density of 1.0 mA cm^{-2} and in the potential window of 1–2 V.[63] Further capacity fading was observed due to the deterioration of the electrolyte/electrode interface, proved by the increased resistance of the cell.[63]

In another study of thin-film battery, PEO based BAB block copolymer with the improved ionic conductivity of 2×10^{-4} S cm^{-1} was integrated into the cell with LMO cathode and $Li_{4/3}Ti_{5/3}O_4$ anode composite electrodes that were micro-injected onto Au current collectors.[64] The resulting microbattery showed an initial energy density of 8.48 μW h cm^{-2}, which was lower compared to the cell fabricated by the sputtering method. Nevertheless, the important advantage of this technique is it being a cheap and simple process.[64]

3D designs with SPE were more successful and received larger attention as the ability of SPE conformal deposition allowed the relatively reliable electrode–electrolyte interface formation and, as a result, improved performance. One of the first constructed 3D microbatteries with SPE contained the drop-casted polymer electrolyte polymethyl methacrylate–polyethylene glycol (PMMA–PEG) combined with titanium nanotubes (TiO_2nts) anode and an LNMO cathode (Fig. 2a).[73] Cells were assembled by squeezing together the TiO_2nts that were grown by anodization of Ti foil and LNMO casted on Al foil. The cell demonstrated the stable capacity of 80 mA h g^{-1} (30 μA h cm^{-2} μm^{-1}) in the potential window of 1–3.3 V and at the rate of C/10. The coulombic efficiency and capacity retention remained at 96.7% and 91.5%, respectively, for 35 cycles. Nevertheless, it was found that the performance of this microbattery can be significantly improved if the large surface area of TiO_2nts would have been fully utilized.[73]

3.1.1.2 Non-polyethylene polymers. Non-polyethylene polymers have also been studied in an attempt to introduce more appealing properties of PEs, such as higher cationic transference number. Sun *et al.*, for example, fabricated a novel polymer electrolyte of poly(ether amine) (PEA)-based monomer where one of the oligomer chains was substituted by the methacrylic group to add the polymerizable functionality.[103] It was then mixed with LiTFSI salt, and the resulting SPE demonstrated ionic conductivity of 8×10^{-6} S cm^{-1} at 60 °C. Using UV-polymerization, SPE with a thickness of 1 μm was integrated into thin-film LFP/SPE/Li battery (with standard LFP composite electrodes), which had 140 mA h g^{-1} capacity that faded after 12 cycles due to the formation of Li dendrites.[103]

Later, the same research group investigated another SPE based on poly(trimethylene carbonate) (PTMC) in two different 3D structures: carbon foams dip-coated with LFP and electrodeposited Cu nanopillars with Li counter electrode (Fig. 2b).[104] The new SPE was proposed due to the expected higher ionic conductivities (10^{-5} S cm^{-1}) compared to PEO (10^{-5}–10^{-8} S cm^{-1}). It was found that, although the functionalized P(TMC-OH) electrolyte resulted in the conformal coating of LFP unlike PTMC-based electrolyte without functionalization, both showed poor electrochemical performance and the latter even led to short circuits as a result of poor contact. That unsatisfactory behaviour was also attributed to the limited interfacial contact with Li electrode, insufficient ionic conductivity and lack of electronic wiring. The Cu 3D structure with P(TMC-OH) electrolyte, on the other hand, demonstrated more promising performance, with stable cycling at a capacity of 0.2 mA h cm^{-2} and a current rate of 8 μA cm^{-2}.[104]

Tan *et al.* tested a microbattery with electrodeposited nanotubes of Cu_2Sb and Li metal electrodes.[105] Poly(propylene glycol) diacrylate (PPDGA) and polyetheramine (glyceryl poly(-oxypropylene)) (PEA) blend with LiTFSI was chosen as an electrolyte, the conductivity properties of which were found to be in the order of 10^{-6} S cm^{-1}.[106] The battery showed moderate electrochemical performance with the capacity of 0.05 mA h cm^{-2} at C/50 rate and voltage range of 0–2 V after 50

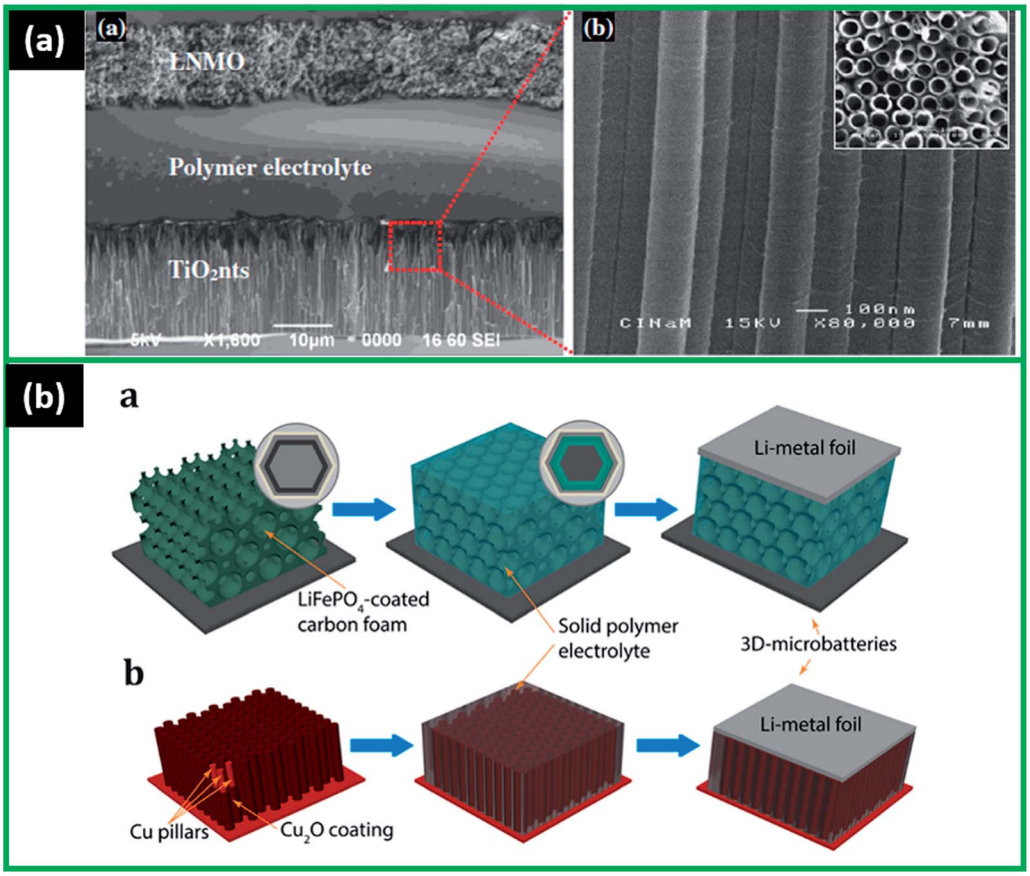

Fig. 2 (a) (a) SEM images of cross section of the all-solid-state battery composed of TiO_2nts/polymer electrolyte/LNMO: (b) enlarged view of the self-organized TiO_2nts. The inset shows the top view of the nanotubes. Reproduced with permission from ref. 73; (b) schematic illustrations showing the step-by-step fabrication of the all-solid-state Li-polymer 3D-microbatteries based on: (a) a $LiFePO_4$-coated carbon foam electrode and (b) a Cu_2O-coated Cu nanopillar electrode. Reproduced with permission from ref. 104. Copyright (2018) American Chemical Society.

cycles. That was approximately 10 times larger than that of 2D microbattery, which proved that the bigger footprint area resulted in higher energy produced. However, the capacity for 3D structure showed a diminishing trend which was expected due to the loss of contact between the electrodes and electrolytes during cycling as a result of the electrode's volume changes.[105]

3.1.2 Deposition by electrochemical methods. Since dip/drop coating of PEs may not coat complex structures of electrodes uniformly for high capacity/power batteries, research has also been focused on other deposition methods of electrolytes. Thus, the electrodeposition technique was proposed to produce a more conformal coating of the electrolyte.[101,107]

3.1.2.1 Polyethylene polymers. The microbattery of TiO_2nts/PMMA–PEG/LNMO (Fig. 3a) demonstrated a twofold increase of capacity (to 150 mA h g^{-1} (70 μA h cm^{-2} μm^{-1}) at C/10 after 10^{th} cycle) due to the complete filling of electrodes by the electrodeposited electrolyte.[74] Moreover, even after the 100^{th} cycle, the capacity of electrodeposited polymer microbattery was two times larger than the one for the drop casted electrolyte.[74] Similarly, as a good candidate for 3D Li-ion microbatteries, PEO–PMMA electrolyte electrodeposited on the anodized nanostructured titania electrode was tested in Li/PEO–PMMA(LiTFSI)/TiO_2nts coin cell.[108] In this cell, the capacity decreased from 83 to 65 μA h cm^{-2} μm^{-1} after 50 cycles at C/5. The enhanced interface between electrode and electrolyte by proper covering and filling of nts area by PEO–PMMA using the electrodeposition allowed improved capacity compared to LiPON. Moreover, the thickness of the electrolyte (<1 μm) proved the ability to withstand the volume variations of the electrodes.[108] The research team under the same main investigator attempted to improve the microbattery performance by electrodepositing PMMA–PEG on porous lithium nickel manganese oxide (LNMO) spread on Al disk.[75] After that, the electrodes were pressed together with a drop of electrolyte in between. The TiO_2nts/PMMA–PEG/LNMO microbattery demonstrated the capacity of 89 mA h g^{-1} (44 μA h cm^{-2} μm^{-1}) between 1–3.3 V and at C/10, corresponding to the 72% capacity retention.[75] It was found that, again, the electrodeposition of polymer electrolyte on LNMO significantly improved the performance of the microbattery.[75]

Recently Abdelhamid *et al.* electrochemically grafted and polymerized (PEO)-acrylate-based electrolyte and obtained pinhole-free and homogeneous film on 3D metal cylindrical micropillars.[109] The resulting electrolyte had relatively high ionic conductivity (10^{-4} S cm^{-1}).[109] Although the testing of

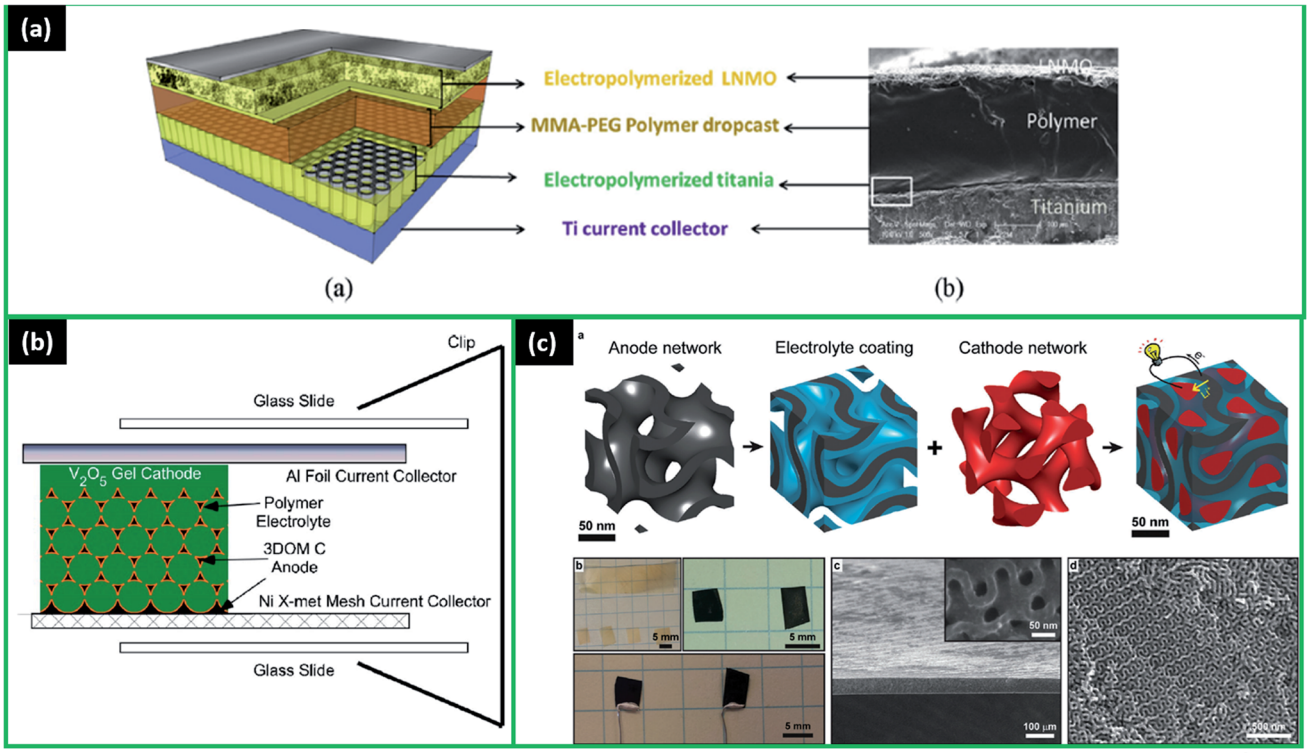

Fig. 3 (a) (a) Schematic representation and (b) cross-sectional SEM image of the all-solid-state battery composed of TiO_2nts$_{(EP)}$/polymer/LNMO$_{(EP)}$. Reproduced with permission from ref. 74; (b) schematic of a three-dimensional solid-state interpenetrating cell. Reproduced with permission from ref. 1; (c) assembly of a penta-continuous interpenetrating and nanostructured hybrid from double gyroidal mesoporous carbon (GDMC) monoliths: (a) schematic illustration of the synthesis pathway, (b) photographs of the as-made BCP-organic hybrids (top left), GDMC monoliths after carbonization (top right), and GDMC monoliths electrically contacted in the edge-on geometry (bottom), (c and d) SEM images of a GDMC monolith exhibiting uniform thickness (c), surfaces with open and accessible gyroidal mesoporosity (c, inset), and uniform gyroidal cross-section (d). Reproduced with permission from ref. 81.

microbattery has not been conducted, it is expected that homogeneous SPE film will positively impact the microbattery performance. Moreover, this approach was shown as a promising way to control electrolyte formation by varying the potential and duration of the polymerization process.

3.1.2.2 Non-polyethylene polymers. The other non-PEO based polymer electrolytes in thin film and 3D microbatteries have also been studied recently. The early investigation of the 3D structures was done on the interpenetrating cell consisting of infiltrated VO cathode ambigel assembled with a macroporous polymer electrolyte coated carbon anode.[80] The poly(phenylene oxide) (PPO) was used as an electrolyte and electrodeposited on the three-dimensionally ordered (3DOM) carbon, where the macropore scale of the structure was then filled with vanadia aerogel-like material cathode (Fig. 3b).[80] When cycling, the initial discharge capacity was observed to be around 9 mA h g^{-1}, which reduced to approximately 1 mA h g^{-1} after 10 cycles between 1.6–3.3 V. Although the capacity was improved due to the increased area, the issue with the cathode's electronic and ionic conductivities hindered the wide implementation of this 3D battery.[80]

The research by Werner *et al.* investigated the innovative gyroidal 3D structure with poly(phenylene oxide) (PPO) solid electrolyte. The polymer was electrodeposited on gyroidal mesoporous carbon (GDMC) monoliths (anode), and then lithium sulfide–polymer composite was infiltrated as a cathode (Fig. 3c).[81] The electrochemical testing of this structure demonstrated 0.225 mA h cm^{-2} capacity in the voltage window of 1.5–3 V and 0.125 mA cm^{-2} current rate with almost no fading after 10 cycles. These results, with the capacity being improved almost 45 times, were better than the previously developed solid-state 3D prototype with nanoscale dimensions.[80] The polymer electrolyte (10 nm) also showed sufficient stability with a conformal and layer impermeable to the cathode, which helped to avoid short circuits.[81] However, the small open-circuit voltage due to the current leakage and large polarization in electrolyte introduced some issues.[81] Moreover, the volume changes of sulfur caused the loss of connection with the current collector and formed electronically disconnected parts, leading to small specific capacity (20% of theoretical value).[81]

Another microbattery consisted of TiO_2nts and Li anode was tested with a new polymer electrolyte-*p*-sulfonated poly(allyl phenyl ether) (SPAPE).[96] The electrolyte was electrochemically deposited on TiO_2nts, which were also electrodeposited, forming a conformal layer. The cycling showed that the microbattery could deliver approximately 60 μA h cm^{-2} capacity after the 4th cycle (at a C/8 rate). In general, the performance of the cells had

an improved areal capacity, and its retention depended on the electrochemical synthesis parameters of the polymer electrolyte.[96] Later the same SPAPE electrolyte was investigated on carbon nanotubes (CNT). The CNT/SPAPE/Li microbattery delivered a capacity of 750 mA h g^{-1} (276 μA h cm^{-2}) even after 110 cycles at 1C, which is 67% more than pristine CNT.[110]

3.1.3 Other methods. Such techniques as infiltration of polymers into structured electrodes, spin coating, deposition onto electrodes, and patterning using photolithography or UV-polymerization as well as CVD growth onto electrodes can be also considered as other methods of SPEs deposition.

3.1.3.1 Polyethylene polymers. A few examples of particular application of the above-mentioned techniques on the microbattery will be discussed. Firstly, Hur *et al.* fabricated an interesting 3D microbattery Si/SU-8/$LiNi_{0.8}Co_{0.15}Al_{0.05}O_2$ (NCA), where SU-8 is a promising polymer electrolyte that has a structure similar to PEG (Fig. 4a).[82] The SU-8 was photolithographically patterned on Si arrays, showing high conformity but low ionic conductivity of approximately 2.8 × 10^{-7} S cm^{-1}. The cathode slurry was applied dropwise over the anode array. The microbattery's maximum delivered capacity was found to be 0.55 mA h cm^{-2} at the current density of 0.22 mA cm^{-2}, and after 100 cycles, it was 0.5 mA h cm^{-2} (potential range 2.6–3.7 V). These results were clearly better than for 2D structured microbatteries. However, the silicon pulverization problem, causing non-uniform conductive areas, led to the electrochemical degradation of this structure.[82]

There has been a research of a special stretchable design of micropillar electrodes supported on metallic serpentines. There the polymer electrolyte composed of 0.5 M of LiTFSI in MA-PEG500 was spin-coated onto the innovative structure with LNMO and LTO electrodes, which were deposited by doctor-blade technique and laser ablated to achieve micropatterns (Fig. 4b).[83] Such architecture not only resulted in the increase of capacity by 2.5 times (1 mA h cm^{-2} at C/2) compared to the 2D structure but also showed good performance under the mechanical strain and very small capacity fading over 100 cycles.[83] Thus, this microbattery proved to be a promising approach with a further target to increase the energy density by varying the electrode materials and improving the micropillars' density.

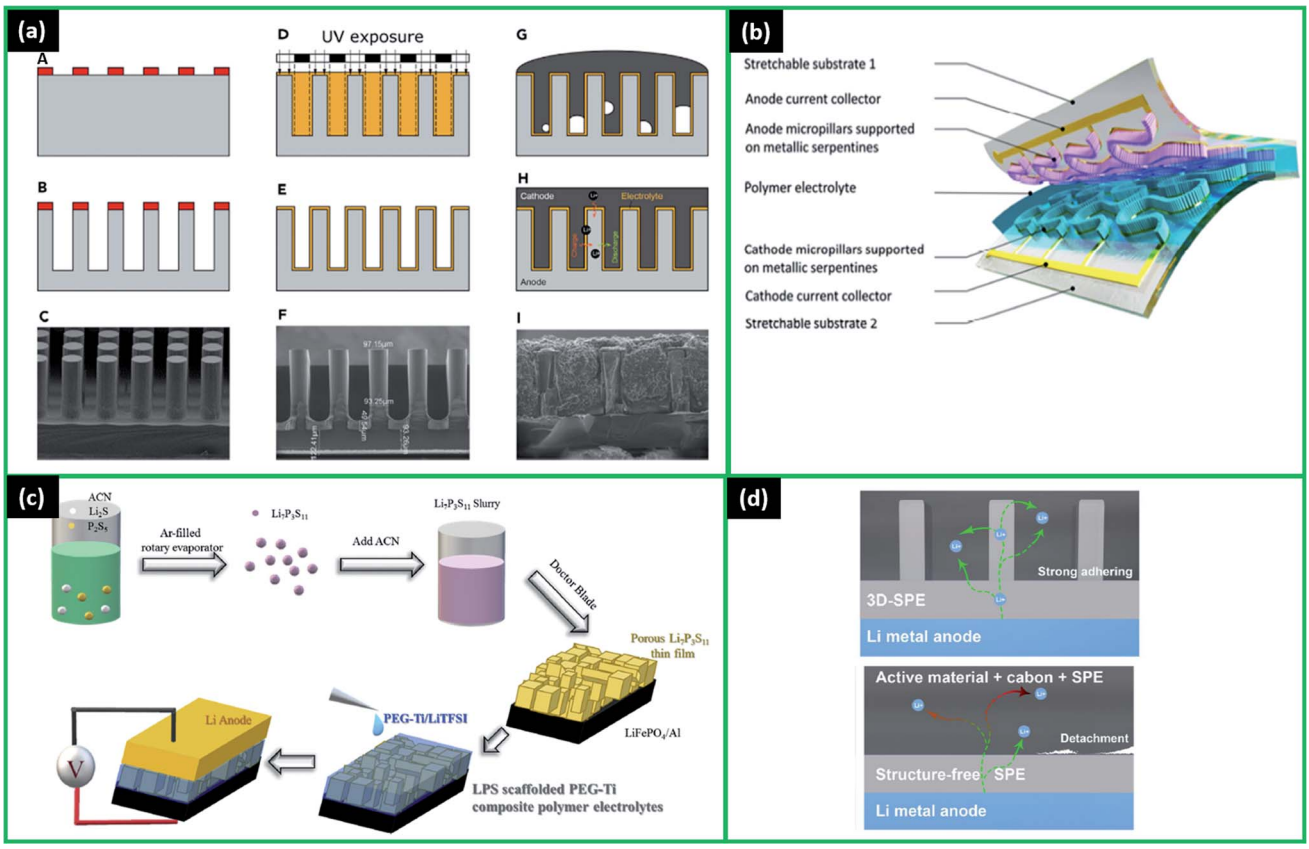

Fig. 4 (a) Fabrication scheme for 3D battery based on SU-8-coated silicon arrays: (A) silicon wafer is coated with oxide and array pattern is etched, (B) 3D post array is etched into silicon, (C) SEM image of silicon array, (D) SU-8 photoresist is selectively cross-linked around the silicon posts by photolithography, (E) uncross-linked SU-8 is removed in a developer bath and base layer is cross-linked, (F) SEM image of SU-8-coated array, (G) vacuum infiltration of cathode slurry, (H) charging schematic of complete 3D battery, (I) SEM image of full 3D battery. Reproduced with permission from ref. 82; (b) schematic view of the stretchable LIMB. Reproduced with permission from ref. 83; (c) schematics of fabrication procedure for Li-ion batteries with LPS-scaffolded solvent-free PEG–Ti composite polymer electrolyte. Reproduced with permission from ref. 62; (d) schematic illustration of all-solid-state Li-metal battery with stereolithography 3D printing SPE and structure-free SPE. Reproduced with permission from ref. 77. Copyright (2020) American Chemical Society.

Other interesting LIBs structures with PEO-based electrolytes have also been tested in coin cells. However, due to promising results, it was concluded that the techniques could potentially be adapted for microbattery technologies. For instance, Cai *et al.* developed a new low-cost processing method of microbatteries, where, firstly, the $Li_7P_3S_{11}$ (LPS) porous scaffold was prepared, and then, PEG–Ti hybrid polymer electrolyte was infiltrated into it (Fig. 4c).[62] The constructed composite electrolyte showed a relatively high ionic conductivity of 1.6×10^{-4} S cm^{-1}. The microbattery with this electrolyte, Li anode and LFP cathode, delivered 103 mA h g^{-1} capacity (2.5–4 V, 0.05C) stable for the first 8 cycles.[62] Therefore, the functionality of this battery manufactured by the innovative method was proved. However, to evaluate the longer cycling performance, more experiments are required. In another study, He *et al.* proposed the adopted method of stereolithography to produce Li/SPE/$LiFePO_4$ 3D microbatteries, where SPE was PEO–succinonitrile (SCN)–LiTFSI (Fig. 4d).[77] The electrolyte had high ionic conductivity (3.7×10^{-4} S cm^{-1}) at room temperature, and cells achieved a higher capacity of 128 mA h g^{-1} after 250 cycles at 0.1C and stable cycling compared to 2D microbattery (32 mA h g^{-1}),[77] hence, proving that this technology is a promising candidate for microbattery fabrication.

3.1.3.2 Non-polyethylene polymers. Several composite polymer electrolytes have also been tested in 2D thin-film batteries with promising results. One of such composite polymer electrolytes included dimethacrylic oligomer bisphenol A ethoxylate dimethacrylate (BEMA), diluent poly(ethyleneglycol) methyl ether methacrylate (PEGMA), ethylene carbonate/diethyl carbonate (EC/DEC), and LiTFSI.[91] It was prepared on the VO electrode using UV-induced photo-polymerization deposition and then assembled with Li anode in a thin-film cell. It delivered a capacity of 130 mA h g^{-1} at the first cycle and 1.5C rate and after 300 cycles at the higher 5C rate, the capacity decreased to 100 mA h g^{-1}.[91] Such good stability was attributed to the electrolyte conformal coating and intimate contact between electrode and electrolyte.[91]

The new method of chemical vapour deposition was applied to deposit a series of copolymer films based on hydroxyethyl methacrylate and ethylene glycol diacrylate on 3D TiO_2nts.[111] The results showed that conformal coating with the electrolyte can be produced, and the tuning of electrolyte properties (ionic, electronic conductivity, mechanical strength) is possible with CVD.[111] However, the full cell testing for these films has not been done yet and needs further investigations.

3.2 Gel polymer electrolytes (GPEs)

GPEs are easily made by heating a mixture containing a polymer matrix, a lithium salt, and a solvent.[92] The mixture is then cast in a hot state and cooled to form a thin film under the pressure of electrodes.[92] GPEs have mainly been investigated for applications in traditional Li-ion batteries. Nevertheless, some studies indicated the fabrication of microbatteries using GPEs due to the possibility of increased ionic conductivity (10^{-3}–10^{-4} S cm^{-1}) compared to common polymer electrolytes as well as shape flexibility.[112–114] In this review, the microbatteries with gel electrolyte having mostly solid phases are considered. Park *et al.* investigated the gel polymer electrolyte poly(vinylidene fluoride-hexafluoro propylene) (PVDF-HFP) fabricated by the solvent casting method and tested in a thin-film battery of Li/PVDF-HFP gel/LCO.[115] The cathode was screen printed onto a platinum current collector/SiO_2/Si wafer using a stainless 400-mesh screen. The cell displayed 164 μA h cm^{-2} capacity at the rate of 20 μA cm^{-2} and in the potential window of 3–4.2 V.[115] This was 23 times higher than that of LiPON as a result of the improved contact area between the cathode and the electrolyte.[115] However, more tests with larger numbers of cycling and stability observations need to be done for further development of this electrolyte.

Similarly, another research group also studied GPE consisting of PVdF-HFP, P13FSI-pyrrolidinium bis(fluorosulfonyl) imide, and LiTFSI.[116] The GPE was coated on Li and macroporous silicon (pSi) to construct the Li/GPE/LCO(sputtered) and pSi/GPE/LCO(sputtered) microbatteries, respectively.[116] The Li/GPE/LCO cell demonstrated good stability in the voltage range of 3–4.2 V and showed 264 μA h cm^{-2} capacity at the high current rate of 333 μA cm^{-2} and 98.9% retention even after 30 cycles.[116] At the same time, pSi/GPE/LCO had the initial capacity of 226 μA h cm^{-2}, which decreased to approximately 180 μA h cm^{-2} after 30 cycles. The high ionic conductivity of the GPE (1.88×10^{-3} S cm^{-1} at 25 °C) and compatibility with electrode materials might have led to the successful functionality of both structures.[116]

Another composite polymer electrolyte (CPE) composed of $LiI_1P(EO)_{20}EC$, 12% (v/v) Al_2O_3 structure was investigated in the thin-film Li/CPE/FeS_{1+x} cell.[117] The cell demonstrated stable behaviour with the initial capacity of around 50 mA h at the current rate of 50 μA cm^{-2} and around 39% capacity loss after 650 cycles, which is considered as significant deterioration.[117] However, a few details are available on the CPE properties and characteristics since a deeper understanding of FeS_{1+x} cathode was targeted for further work.

One of the recent studies tested the new 3D interdigitated structure with VO cathode, Li anode, and GPE composed from PEO, LiTFSI, 1,3-dioxolane (DOL), and 1,2-dimethoxyethane (DME) (Fig. 5a).[78] The innovative microbattery delivered 0.15 mA h cm^{-2} areal capacity, 73% of which was retained after 550 cycles at 1C, proving a good stable behaviour. The peak energy and power densities of 1.2 J cm^{-2} and 75.5 mW cm^{-2}, respectively, were observed at 100C, which is considerably larger than other packaged microbatteries' performance parameters, thus making this 3D microbattery one of the promising candidates for further development and integration in the autonomous devices.[78] Kil *et al.* have done research on 3D pillars structure with UV-curable GPE (ethoxylated trimethylolpropane triacrylate (ETPTA) monomers, liquid electrolytes, and alumina nanoparticles) with ionic conductivity of 1 mS cm^{-1}.[113] The UV curing was used here to promote cross-linking of the polymer matrix for solidification. The structure from micropillar Si anode, micropatterened GPE, and Li as a counter electrode was cycled, and it was found that the initial high-charge capacity 2680 mA h g^{-1} faded to approximately 700 mA h g^{-1} after the 10th cycle.[113] Although the retention is not favorable, it was

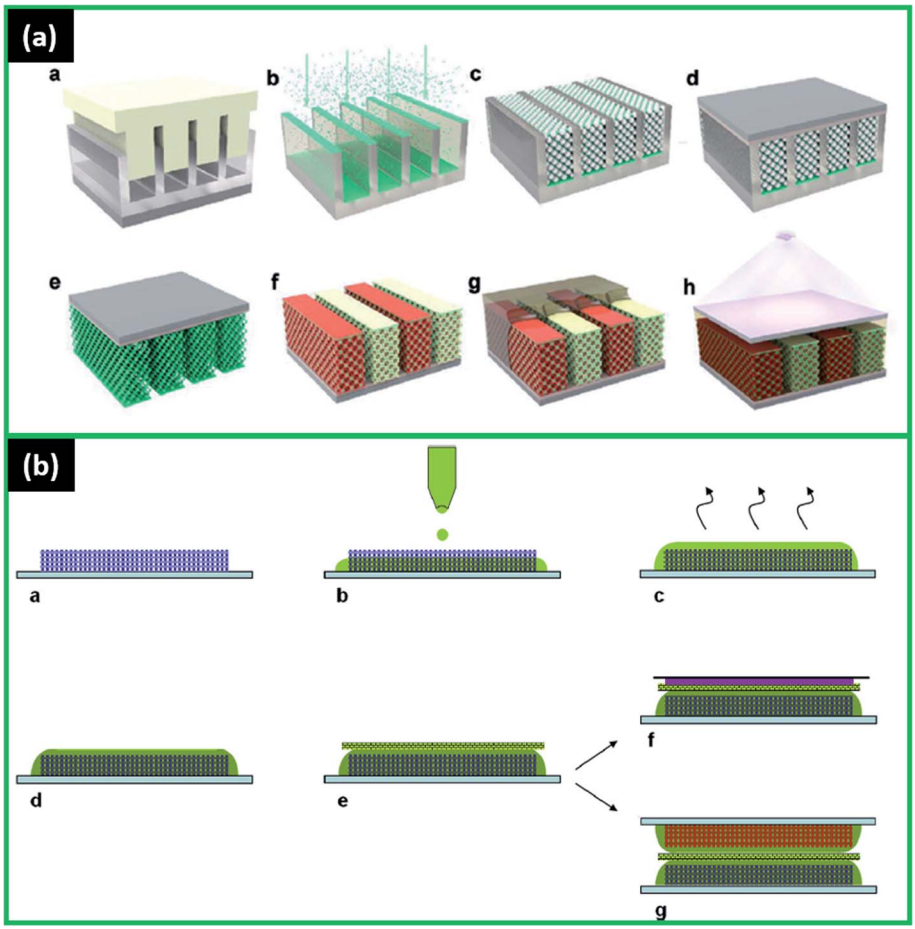

Fig. 5 (a) Schematic of the microbattery fabrication: (a) PMMA template is fabricated by nanoimprinting, (b) vertical e-beam evaporation of Ni on the PMMA template, (c) structure after selective removal of Ni film from the top of the PMMA template, assembly of a PS opal in the PMMA template, and Ni electrodeposition through the PS opal, (d) bonding of (c) to a polyimide film using an epoxy adhesive, (e) etching of the PMMA template and polystyrene opal to expose the interdigitated 3D microelectrodes, (f) VO (cathode) and Li (anode) electrodeposited on the appropriate interdigitated Ni fingers, (g) infiltration of PEO/LiTFSI/DOL/DME gel electrolyte, (h) packaging of the cell with UV-cured NOA. Reproduced with permission from ref. 78; (b) scheme of half cell and Li-ion full cell realization: (a) tape cast porous positive (resp. negative) composite electrode on aluminum current collector, (b) ionogel precursor printing on electrode: filling of the composite electrode porosity and obtaining separator effect, (c) polycondensation of ionogel precursor, (d) all solid positive (resp. negative) electrode and ionogel assembly is obtained, (e) addition of fiberglass separator soaked in ES liquid electrolyte, (f) half-cell with lithium metal counter electrode and copper current foil, (g) Li-ion full-cell formed by face-to-face stacking of negative electrode/ionogel assembly and positive electrode/ionogel assembly separated by fiberglass soaked in ES liquid electrolyte. Reproduced with permission from ref. 14.

shown that optimized alumina content and fabrication technology resulted in the dimensionally stable, conformal, and bendable GPE.

Another type of solid polymer electrolytes – ionogel that consists of molten salt and the inorganic matrix has attracted more attention due to high Li conductivity (up to 10^{-3} S cm^{-1}) and ability to create a conformal layer favourable for 3D structures.[14,118,119] First, testing planar structures, Delannoy *et al.* applied a new method of ink-jetting the silica-based ionogel (PYR13-Li-TFSI: *N*-methyl-*N*-propylpyrrolidinium bis(trifluoromethan) suflonylimide and LiTFSI) on the electrode surfaces (Fig. 5b).[14] The resulting thin-film battery of $Li_4Ti_5O_{12}$/ionogel/LFP appeared to have a steady surface capacity of 300 μA h cm^{-2}, approximately double of liquid electrolyte cell (145 mA h cm^{-2}) after 100 cycles at the C/10 rate and potential window of 1.5–2.5 V.[14] The satisfactory results confirmed that the ink-jet printing, being a fast and cheap technique, could be a good candidate for polymer electrolyte deposition. It might be important to highlight the recent battery is not considered a microbattery, but due to very promising results was proposed for further testing in the microbattery structure. The new 2.5D structure with LFP pillars covered with ionogel and planar Li showed excellent performance with power and energy densities of 2.8 mW cm^{-2} and 3.7 mW h cm^{-2}, respectively, that were attributed to the conformal cover of pillars by the electrolyte.[118] These results are currently best-reported solid-state 3D battery densities. Therefore, more studies on this and other 3D designs and promising ionogel electrolyte applications in microbatteries are required.

In general, there are many SPE preparation methods examined for various polymer materials. The deposition techniques were rather unique in each case as many polymer compositions

have been tested. Among those discussed in this paper, the most common methods include electrodeposition applied for PMMA–PEG,[74,75,108] SPAPE[96,110] and drop-casting used for PMMA–PEG,[73] PEA,[105] PVDF-HFP.[115] Based on the findings, electrodeposition has been proved to be an effective technique, which provided a conformal electrolyte layer and excellent interface with electrodes that directly improved the microbattery performance.[74] The impact of electropolymerization cycles was observed for SPAPE with the optimum cycles determined to be 10.[110] The effect of other electrodeposition conditions needs to be studied more. Parameters of other new methods such as sol–gel,[63] photolithography,[82] stereolithography,[77] ink-jetting,[14] UV-induced photopolymerization,[91] and their influence on SPE characteristics have not been investigated in detail yet and require more attention in the future.

3.3 Transference number

Transference (or transport) number is defined as the proportion of electric current transported by a specific ion.[34,120,121] In LIBs other ions rather than Li^+ do not provide the electrical energy, as their charge cannot be transferred through the external circuit. Thus Li transference number is considered as the main parameter.[120,122] A higher transference number is favourable, as it allows larger power densities by decreasing the electrolytes' concentration polarization.[121] Detailed information on the ion transport mechanisms in solid electrolytes and the ways of measuring the transference number were provided in the review by Quartarone and Mustarelli.[34] Generally, in inorganic ceramic electrolytes, the conduction occurs due to only one mobile ion (Li^+ for LIB electrolytes) with some rare cases of charge transfer through electronic charge carriers, therefore resulting in the transference number close to 1.[120,123] Thus, this parameter is mainly important for polymer electrolytes, where several other species like various anions can be mobile and contribute to the overall conduction.[124] So some earlier studies observed the low cation transference number for polymer electrolytes.[125,126]

For solid PEO-based electrolytes, it was shown that the cationic transference number varied between 0.2 and 0.3 with ionic conductivity in the range of 10^{-8}–10^{-5} S cm^{-1}.[120,122,127,128] One of the best transference numbers of 0.48 with a large ionic conductivity of 10^{-3} S cm^{-1} was obtained for PEG500DME-LiTFSI electrolyte. However, its further testing in LIMB structure is required.[101] To decrease the negative effect of polarization phenomena during cycling for low transport number PEO-based electrolytes, the addition of such fillers as SiO_2 and Al_2O_3 and formation of hybrid polymer electrolytes were attempted and those changes resulted in an improved transference number up to 0.8 due to a larger number of free Li^+ ions.[63,123] Other researchers succeeded in demobilizing anions in PEO structure, leaving only Li ions active, which resulted in the high transport number > 0.85 (with ionic conductivity 1.3 × 10^{-5} S cm^{-1}).[129] Such increased value helped to improve the cell performance even though the ionic conductivity was reduced by one order of magnitude, proving the importance of this parameter.[130]

The relatively low transport number of PEO-based electrolytes led to the investigation of other SPEs. For instance, poly(trimethylene carbonate) (PTMC)-based electrolytes had a transference number higher than 0.6 along with ionic conductivity of 10^{-5} S cm^{-1}, which was attributed to the weaker Li binding in the PTMC structure compared to PEO-based one.[131,132] Another type of SPE – single ion electrolyte having Li source directly on polymer chain rather than from Li salts dissolution-demonstrated an excellent transference number (0.8–1) and high ionic conductivity (10^{-4} S cm^{-1}).[133,134] Such high values were obtained due to this specific attachment of anionic centres to the polymer side chains.[133,134] In addition, the higher Li^+ conductivity (up to 0.6) was achieved for Lewis-acidic polymers like polyboranes as a result of weaker Li^+ and stronger anion coordination.[135] However, more studies are undergoing to investigate other properties and to improve the complex and expensive synthesis of the above-mentioned PEs. The recent review by Zhao *et al.* extensively covered the transference numbers of different types of SPEs together with the various methods to improve these numbers.[122]

Considering the particular case of the discussions of the thin-film or 3D SPEs' transference numbers and their effect on the microbatteries performance, it is noticeable that not all studies investigate the exact values of the applied SPEs. From the available resources, it was reported that LIMBs of PEO with fillers (2D) and polycarbonate-based electrolytes (3D) with transport numbers 0.37 and 0.6, respectively, delivered relatively stable energy with further room for SPEs properties improvement and more experiments to conduct.[63,104]

4. Inorganic crystalline electrolytes

Ceramic materials with a crystal structure that can be designed to have high ionic conductivity and thermal stability are promising candidates for all-solid-state battery electrolytes.[19,136] The bulk properties can be better compared to glass and polymer electrolytes.[136] However, to obtain high total ionic conductivity, it is necessary to increase the grain boundary conductivity since the grain boundaries present a large barrier for ions' migration across the interfaces.[18] As a result, diffusion with a slow ion transfer kinetics in electrolyte becomes the rate-determining step, decreasing the performance of the microbattery. Thus, it is also critical to create a good contact between the electrolyte and electrode. The lack of grain boundaries due to isotopically conductive and intrinsically soft structure in polymer and glass electrolytes helps to build stable mechanical interfaces that significantly diminish the Li-ion diffusion resistance.[136] Considering these properties, it is also easier to fabricate thin films of polymer and glass electrolytes. Moreover, glass electrolytes typically have higher electrochemical decomposition potentials, adding more stability to the material.[19] The above-mentioned difficulties prevented a wide application of ceramic materials with crystal structures in 2D microbatteries so far, while 3D structures presented an even bigger challenge for conformal coating with electrolytes and production of their crystal structure. Nevertheless, high thermal stability of crystalline electrolytes is one of the main advantages of these

materials, which is usually gained through annealing that also helps to improve the electrode–electrolyte interface quality.[19] Several types of crystalline electrolytes can be found and will be discussed below, including the main NASICON, LISICON, perovskite and garnet-type electrolytes. The other crystalline materials, such as argyrodite materials, are promising candidates for microbatteries, but they have not been integrated and studied yet.[137,138]

4.1 Garnet

One of the candidates for SSEs are garnet-type materials with the general formula of $Li_3Ln_3M_2O_{12}$ (M = Te, W; Ln = Er, Tm, Eu, Gd, Tb, Y, Pr, Nd, Sm, Dy, Ho, Yb, Lu).[18] Among them, the outstanding candidate is $Li_7La_3Zr_2O_{12}$ (LLZO)-type electrolyte. It attracted more attention due to its high ionic conductivity found to reach up to 1.02×10^{-3} S cm^{-1} at 30 °C.[139,140] Moreover, LLZO demonstrated good thermal stability and availability of raw materials.[140–143] The typical crystal structure of LLZO consists of dodecahedral LaO_8 and octahedral ZrO_6 (Fig. 6a).[144,145] Many investigations have been done to study LLZO and improve its properties, and they are discussed, for example, in a recent extensive review by Wang *et al.*[140] In it, the effect of phases was discovered, where the higher ionic conductivity was attributed to the prevailing presence of cubic phase over tetragonal.[146] Furthermore, various substitutions and doping were done with cations Al^{3+}, Nb^{5+}, Ta^{5+}, Ga^{3+}, Te^{6+}, Y^{3+}, Ti^{4+}, Ge^{4+}, and Fe^{3+}. In most of the cases, the doping increased the Li-ion conductivity and enhanced the stability against Li.[18,145] LLZO synthesis conditions were also extensively studied, as they directly affect the important structural parameters such as grain boundaries, crystallite size, grain size, and

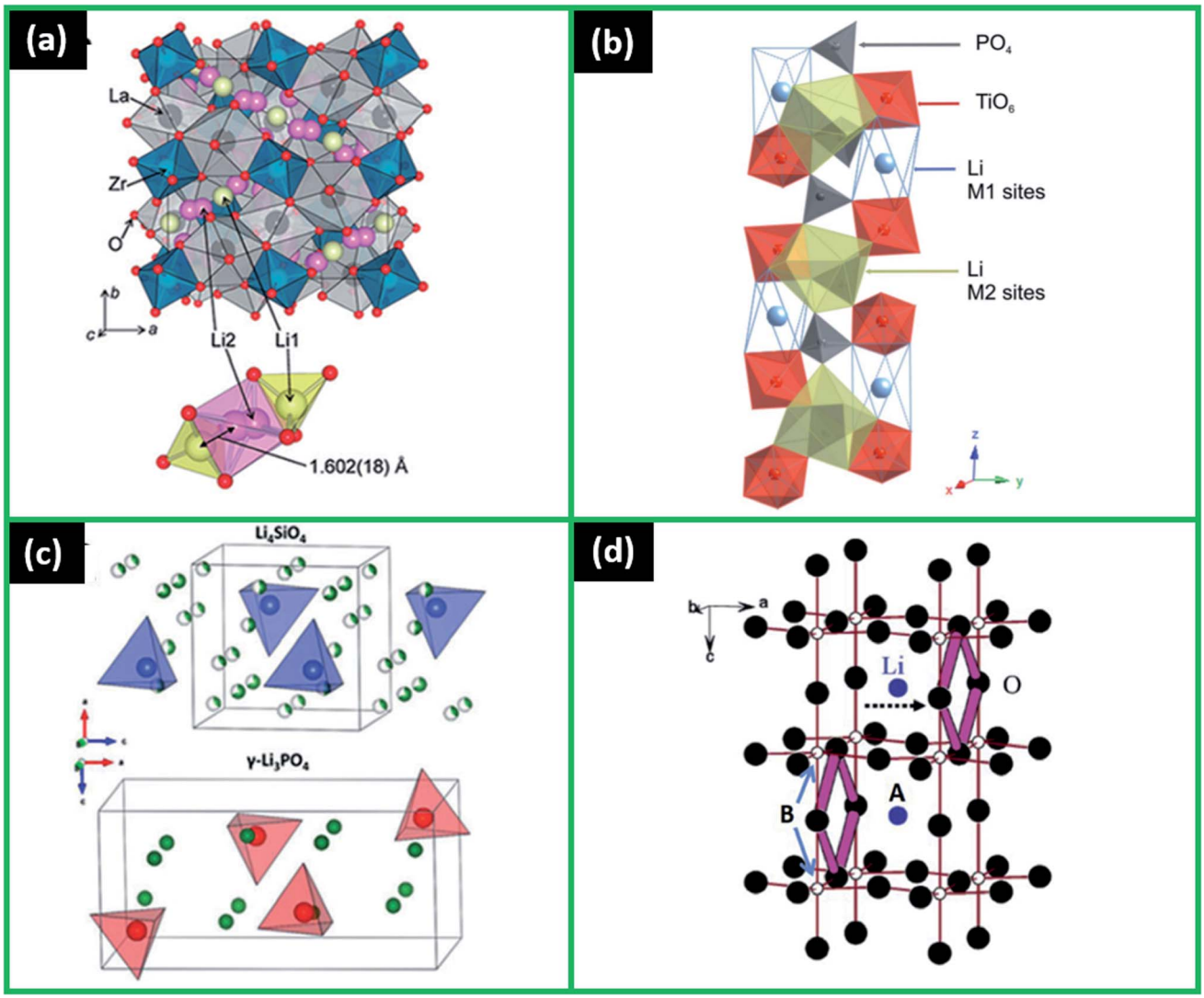

Fig. 6 (a) Crystal structure of cubic $Li_7La_3Zr_2O_{12}$ and coordination polyhedra around the Li_1 and Li_2 sites. Reproduced with permission from ref. 145; (b) part of the NASICON-type crystal structure showing the M1 and M2 crystal sites. Reproduced with permission from ref. 156; (c) schematic representations of the crystal structures of the end-member phases Li_4SiO_4 and g-Li_3PO_4. Reproduced with permission from ref. 145; (d) crystal structure of perovskite-type solid electrolytes $Li_{3x}La_{2/3-x}TiO_3$. Reproduced with permission from ref. 181. Copyright (2003) American Chemical Society.

bulk density. As LLZO is mainly synthesized by the sintering method, the optimal conditions were investigated to decrease the grain boundaries, which, when present in large amounts, significantly reduce the ionic conduction.[145] Moreover, an innovative approach of $Li_{6.25}Al_{0.25}La_3Zr_2O_{12}$ fabrication using a multilayer processing with Li reservoirs (Li_3N) was suggested, which helped to lower the processing temperature by 400 °C while keeping the desired phase of the material and ionic conductivity relatively high (10^{-5} S cm^{-1} order).[147] Similarly, another alternative method to produce $LiCoO_2$–LLZO was proposed, where infiltration is applied to deposit cathode from metal salts directly in a porous LLZO scaffold at a low processing temperature (700 °C), forming a low resistance interface.[148] Further development of these promising processes is required in the future. Another uncommon sol–gel method was applied by Chen *et al.* to successfully deposit thin-film LLZO, also optimizing such parameters as annealing and number of layers to obtain the highest 1.6×10^{-6} S cm^{-1} ionic conductivity.[149]

Although garnet-type materials are promising electrolytes for solid-state batteries challenges like high reactivity with moisture and CO_2 at an ambient atmosphere, crystalline instability at high temperatures, high production cost, and high interfacial resistance with Li need to be addressed.[145,150–152] Particularly for LLZO, it was found that its relatively high electronic conductivity causes the formation of Li dendrites within the electrolyte and results in cell failure.[21] Moreover, the ionic conductivity of thin-film LLZO is 1–3 orders of magnitude lower than of bulk ones due to various microstructural changes.[153] Thus, a few studies are available on microbatteries with LLZO currently, and more studies are ongoing to investigate, for example, amorphous LLZO to tune its Li conductivity and avoid Li dendrites formation.[153]

4.2 NASICON

NASICON, one of the most studied crystal electrolytes, has attracted more attention not only due to high ionic conductivity (reaching up to 10^{-3} S cm^{-1}) but also high oxidation potential, structural and thermal stability.[19,26,154,155] NASICON is typically composed of $LiM_2^{IV}(PO_4)_3$ (M is a tetravalent cation: Ti, Zr, Sn, Ge, Hf).[154] The structure is formed by the PO_4 tetrahedra and MO_6 octahedra, which are forming the 3D tunnels for Li-ions positioned at the interstitial sites (Fig. 6b).[19,156]

The mechanical and electrical properties of NASICON mainly depend on the chemical elements present in the structure. For instance, initially developed $LiTi_2(PO_4)_3$ had ionic conductivity of 10^{-6} S cm^{-1}, which was enhanced to 10^{-3} S cm^{-1} by partial substitution of Ti^{4+} by Al.[157–159] This substitution by the trivalent cations A^{3+} (Al, Ga, In, La, Y, Ti, Sc, Cr, Fe) forming $Li_{1+x}A_xTi_{2-x}(PO_4)_3$ (LATP) with better electric properties happened presumably due to a higher charge carrier number the cations.[157] Although the bulk ionic conductivity was found to be large, thin films were reported to have several orders of magnitude lower conductivities due to hindered glass-ceramic phase control. For example, thin-film LATP fabricated by RF sputtering had the largest Li conductivity of 2.46×10^{-5} S cm^{-1},[160] while prepared by annealing techniques had it in the order of 10^{-6} S cm^{-1}.[161] Similarly, aerosol deposited thin film of $Li_{1.5}Al_{0.5}Ge_{1.5}(PO_4)_3$ (LAGP) demonstrated maximum ionic conductivity of only 5×10^{-6} S cm^{-1}.[162] In addition, Ti^{4+} in LATP structure could be easily reduced by Li,[163,164] making it unstable in batteries with lithium anodes, while structures with Al–Ge and Fe–Hf showed more compatibility with the Li electrode.[18] An attempt to improve the stability of $Li_{1.3}Al_{0.3}Ti_{1.7}(PO_4)_3$ LATP against Li was made recently by Liu *et al.* Al_2O_3 was coated on LATP by ALD and the electrolyte performance was checked in a symmetrical Li/LATP/Li thin-film cell.[165] The results showed that a stable interface was created and the undesired Li penetration and Ti reduction were inhibited.[165] Similarly, a more stable interface was formed between LATP and LCO with the artificial layer of Li_3PO_4 deposited by ALD, where the layer helped to suppress the elemental interdiffusion and the formation of interlayers with low Li conductivity.[166] The properties of NASICON could also be improved by several techniques, such as thermal treatments, sintering process, excessive lithium introduction, and Si doping.[154] For example, $LiZr_2(PO_4)_3$ prepared at 1200 °C underwent the phase transition from monoclinic to rhombohedral when it was heated, resulting in increased ionic conductivity of up to 1.2×10^{-2} S cm^{-1} measured at 300 °C.[18] In general, several reviews considered the recent advances, challenges, and perspectives of NASICON-type electrolytes, and some of their potential in microbattery applications.[16,18,25,38,167,168]

One of a few thin-film batteries with NASICON-type electrolyte was investigated by Hofmann *et al.* $Li_{1.5}Al_{0.5}Ti_{1.5}(PO_4)_3$ electrolyte was deposited by PLD and analysed in the microbattery structure with a Si anode and a $LiCoPO_4$ cathode.[169] The cathode–electrolyte interface was studied particularly and significant inter-diffusion processes that are highly dependent on heat treatment were observed. The results highlighted the difficulty of producing a stable interface, which favours the Li ion diffusion, as it can be done only at low temperatures, while for crystal structures formations much higher temperatures are required.[169] Thus, additional protective layers were suggested for these structures to reduce the inter-diffusion and interface resistance. As the capacity and general performance information of this thin-film battery is absent, more studies are needed in the future.

Although there are numerous NASICON-type electrolytes that have been actively investigated, only a few of them were integrated and evaluated in microbattery systems up to now. Thus, more studies are required on the electrode/electrolyte interface improvement as well as the optimal conditions for deposition and treatment of electrolytes.

4.3 LISICON

Li superionic conductor – LISICON is another good candidate for solid electrolytes due to the obtained high ionic conductivity (up to 10^{-2} S cm^{-1}).[145] LISICON structure is based on the Li_4XO_4 (X = Si, Ge, Ti) and Li_3YO_4 (Y = P, As, V, Cr); Li_2MXO_4 (M = Zn, Mg); Li_2ZO_4 (Z = S, W), which results in g-Li_3PO_4 phases[19,145] (Fig. 6c).

The earliest investigations were done on $Li_{14}Zn(GeO_4)_4$ where the ionic conductivity was found to be 1.3×10^{-6} S cm^{-1} at 33 °C and 2×10^{-6} S cm^{-1} at 50 °C.[170,171] In such structures, the conductivity was enhanced, as Li could diffuse not only through vacancies but also through interstitials.[170,171] Several recent studies revealed other promising structures, which had several orders of magnitude higher conductivities than those of the parent phases. For instance, $_{(1-z)}Li_4SiO_{4-(z)}Li_3PO_4$ ($z = 0.25$, 0.5 and 0.75) families with ionic conductivities of 10^{-3} S cm^{-1} at 300 °C,[172] $Li_{10.42}Si_{1.5}P_{1.5}Cl_{0.08}O_{11.92}$ and $Li_{10.42}Ge_{1.5}P_{1.5}Cl_{0.08}O_{11.92}$ with 1.03×10^{-5} and 3.7×10^{-5} S cm^{-1}, respectively.[173] Various LISICONs were produced with elemental and structural changes. Although most of them had excellent thermal stability, still, the lower ionic conductivity at room temperature compared to other electrolyte candidates prevented the widespread studies of these materials up to now.[145,170,171]

The recent advancement of LISICON-type electrolytes was introduced with the development of thio-LISICON $Li_{4-x}Ge_{1-x}P_xS_4$ ($0 < x < 1$), which had superior properties.[18,174] By replacing the O^{2-} with S^{2-}, the new electrolytes showed higher ionic conductivities due to the weaker interaction between Li^+ and S^{2-} compared to Li^+ and O^{2-}.[18] For instance, $Li_{3.25}Ge_{0.25}P_{0.75}S_4$ had improved ionic conductivity of 2.17×10^{-3} S cm^{-1} at room temperature along with the electrochemical stability of up to 5 V against Li,[175] while $Li_{10}GeP_2S_{12}$ demonstrated even higher ionic conductivity of 1.2×10^{-2} S cm^{-1} at 27 °C.[174] The partial substitution of O^{2-} by S^{2-} for $Li_{10}GeP_2S_{11.7}O_{0.3}$ and $Li_{10}GeP_2S_{11.4}O_{0.6}$ led to ionic conductivities of 1.03×10^{-2} S cm^{-1} and 8.43×10^{-3} S cm^{-1} at 25 °C, respectively, bringing more stability, as sulfide adds more reactivity to the structure.[176] Therefore, another research group also attempted to incorporate Cl and produce the $Li_{9.54}Si_{1.74}P_{1.44}S_{11.7}Cl_{0.3}$ structure, which delivered ionic conductivity comparable to liquid electrolytes of 2.5×10^{-2} S cm^{-1} at 25 °C.[177]

Despite the fact that the recently developed thio-LISICON-based electrolytes have the desired conductivity close to liquid electrolytes, not many were tested in the microbattery structures. It was found that, generally, the sulphide in the structure brings instability at an ambient atmosphere due to its hygroscopic nature, limited operating electrochemical range, generation of H_2S, and high cost of production.[174,178,179]

So far, Gilardi *et al.* deposited a thin-film LISICON-type $Li_{4-x}Ge_{1-x}P_xO_4$ (LGPO) by PLD and characterized it.[180] It was observed that although LGPO fabricated at room temperature had higher porosity, roughness and some contamination on the surface, the ionic conductivity was not much affected by the low-temperature deposition and was in the order of 10^{-6} S cm^{-1}.[180] Therefore, the ease of fabrication, wide electrochemical window, and relatively reasonable conductivity make LGPO a potentially interesting electrolyte for solid-state thin-film batteries, and thus, further testing of this electrolyte in microbattery required. In general, more testing of the microbattery with LISICON-based electrolytes is expected once the appropriate chemical composition of the electrolytes is found that will satisfy the conductivity and stability criteria.

4.4 Perovskite

Lithium lanthanum titanate $Li_{3x}La_{2/3-x}TiO_3$ (LLTO) is one of the perovskite-type electrolytes with a promising ionic conductivity attributed to its crystallographic structure (up to 10^{-3} S cm^{-1}) (Fig. 6d).[18,181] The first developed LLTO, although showing high bulk ionic conductivity of 10^{-3} S cm^{-1}, had lower total ionic conductivity of 2×10^{-5} S cm^{-1} as a result of grain boundary effect.[182] Moreover, the easy reduction of Ti^{4+} in the structure at low voltages (<1.8 V), brought the incompatibility of LLTO with many anodes including Li.[183] Thus, several researchers attempted to substitute Ti with other elements such as Sn^{4+}, Zr^{4+}, Mn^{4+} and Ge^{4+} [184]. It was found that ionic conductivity was increased only slightly with Mn^{4+} and Ge^{4+}.[184] The authors also noticed that only partial Ti^{4+} substitutions should be done in order to avoid the formation of the second phase.[184] Another proposed method to improve LLTO characteristics is to use pulsed laser deposition (PLD) to produce amorphous LLTO films, which not only had the higher ionic conductivity (up to 10^{-3} S cm^{-1}) but also better stability with Li anode.[185,186]

Completely new perovskite structures were also tested, like $Li_{3/8}Sr_{7/16}Ta_{3/4}Zr_{1/4}O_3$ (LSTZ), which had the total ionic conductivity of 10^{-4} S cm^{-1} at 30 °C, with improved grain boundary conductivity and stability at voltages > 1 V *versus* Li.[20] Similarly, $Li_{3/8}Sr_{7/16}Ta_{3/4}Hf_{1/4}O_3$ (LSTH) demonstrated good ionic conductivity (3.8×10^{-4} S cm^{-1} at 25 °C) and electrochemical stability > 1.4 V *versus* Li.[187] Even though these newly developed perovskites had better performance, the problem of high-temperature preparation (>1000 °C) and interfacial issues between electrolyte and electrode require more investigations.[20,187]

Due to the above-mentioned challenges, a few studies are available on microbatteries with perovskite electrolytes up to now. Regardless, Lee *et al.*, investigated amorphous LLTO potential thin film for microbatteries, which was deposited by PLD.[188] By optimizing the PLD parameters, such as temperature and pressure, high Li conductivity was obtained (3×10^{-4} S cm^{-1}).[188] This electrolyte was then tested in a half-cell with LNMO that showed 98% retention of capacity after 50 cycles.[188] More experiments are needed to investigate the interfacial stabilities and to examine the full thin-film cell.

Some investigations were done with the LLTO films coated with other layers, like LiPON, to enhance the stability, prevent the reactions with Li and short-circuits. To illustrate, the LLTO interlayer covered with LiPON from both sides was found to be very stable in the operating voltage window of 0–5.5 V tested by linear sweep voltammetry.[189] Li *et al.* used e-beam evaporation to deposit LLTO thin film on LCO cathode and subsequently sputter a LiPON protection layer followed by thermal evaporation of Li to create a Li/LiPON/LLTO/LCO cell.[190] This cell delivered 50 μA h cm^{-2} μm^{-1} capacity at the first cycle and 24 μA h cm^{-2} μm^{-1} after 100 cycles at electrochemical conditions of 7 μA cm^{-2} current and voltage window of 3–4.4 V. Though the cell provided good cyclability, a large number of grain boundaries yielded low ionic conductivity of 1.8×10^{-7} S cm^{-1}, preventing the microbattery's better performance.[190]

4.5 Synthesis of crystalline SSE thin films

Although many studies have been done on the effect of synthesis and treatment of "bulk" crystalline electrolytes on their intrinsic properties,[18,167,191–193] the influence of deposition methods on these electrolytes and on their microbattery performance has not been reported explicitly. For most of the crystalline materials integrated into microbatteries, the preparation method was limited to the solid-state reaction of mixtures with required composition and then deposition on the electrode. Such methods of deposition as sputtering,[60,194] e-beam evaporation,[190] sol–gel,[149] spin-coating,[195] PLD[186,196] and ALD were applied to produce thin-film crystalline electrolytes, and various preparation conditions were reviewed.[29,44,149,197,198] The other new deposition methods, for instance, for LLZO, are currently under development and optimization as discussed above.[147,148] Up to now, it was observed that the higher e-beam evaporation power (600 W) applied for the LLTO fabrication resulted in a higher ionic conductivity.[190]

The morphology alteration usually accompanies the crystallization process of the electrolyte during sintering at high temperatures, since the amorphous phase of the electrolyte transforms to crystalline with higher density. For the thin films, the shrinkage may also have a critical effect on their properties. For example, PLD-derived LLTO thin films were deposited and then annealed at various temperatures.[196] According to the results of scanning electron microscopy (SEM), the morphology changed, since grains became more expressed in the films at the highest temperatures. However, it did not lead to the short circuit. In another work, PLD allowed deposition of uniform crystalline LLTO on the substrate heated up to 750 to 880 °C and varying gas pressure from 4 to 20 Pa during the fabrication.[186]

Chen *et al.* obtained mostly amorphous LLZO by sol–gel method despite thin film being annealed at temperatures of 600–800 °C. The final film demonstrated defects that particularly could form during the crystallization process.[149] Spin-coated LLTO calcined at 550 °C during 40 hours demonstrated the clear tetragonal phase. Meanwhile, the morphology

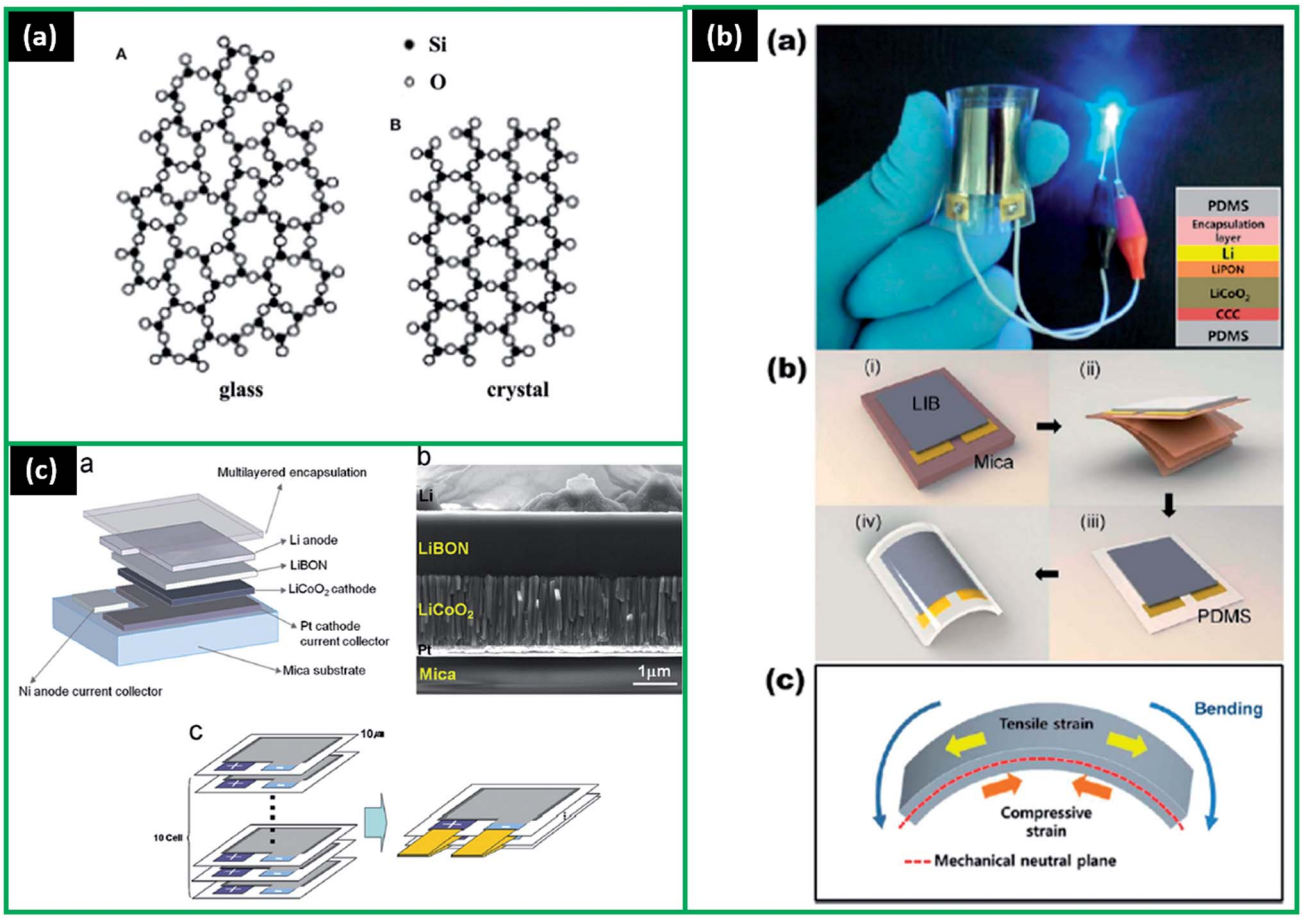

Fig. 7 (a) SiO_2 structure scheme: (A) glass, (B) crystal. Reproduced with permission from ref. 199; (b) (a) photograph of a bendable LIB turning on a blue LED in bent condition, (b) schematic illustration of the process for fabricating flexible LIBs, (c) schematic image of the mechanical neutral plane generated from the counterbalance between tensile and compressive strain. Reproduced with permission from ref. 227. Copyright (2012) American Chemical Society; (c) schematic for (a) the structure and (b) SEM image of cross-section view of the fabricated LiBON-based all-solid state microbattery, Li/LiBON/LCO, and (c) multi-stacks of the microbatteries for the required energy-density. Reproduced with permission from ref. 12.

did not exhibit any cracks, needles or holes in contrast with those that were heated for 5 and 20 hours.[195]

Thus, the SSE thin films can be produced in a crystalline form without the critical impact of post-annealing on film morphology. Besides, the deposition of electrolyte (or its post-annealing) at high temperatures on the electrode should be made carefully, taking into account the electrode material properties, avoiding interfacial problems, and preventing Li loss when the microcell is realized.

5. Inorganic glass electrolytes

Glass electrolytes have been extensively studied as a result of having advantageous parameters, such as isotropic ionic conduction, absence of grain boundary resistance, non-flammability, easy film formation, and a variety of chemical compositions.[199] Most importantly, the amorphous structure leads to higher ionic conductivity compared to the crystal one due to the presence of the so-called "open" structure (Fig. 7a).[199,200] This disordered structure allows easier formation of the diffusion path as the configurational freedom is significantly higher than in the ordered structure.[201] Moreover, the structure with more free space is favourable for compounds where the size of an opening, through which the ions have to diffuse, is the limiting factor, and that is the case for many crystalline materials with a low concentration of the migrating ions.[202]

Glassy electrolytes are typically classified as oxide and sulphide glasses, and among them, lithium phosphate-based electrolytes have attracted much attention due to their stability against lithium and easy processability of thin films.[37] These electrolytes' part will be covered based on the deposition techniques for easier comparison of the electrolytes' and microbatteries' performance parameters.

5.1 Lithium phosphate based electrolytes

5.1.1 Sputtering. LiPON with the composition of $Li_{3.3}PO_{3.9}N_{0.17}$ was first developed at Oak Ridge National Laboratory in 1992 by Radio Frequency (RF) sputtering of Li_3PO_4 in the presence of nitrogen gas. Cross-linking of nitrogen (N) between the phosphate groups resulted in much improved ionic conductivity (3×10^{-6} S cm^{-1}) compared to amorphous Li_3PO_4 without incorporated N.[27,59,65,203] Moreover, LiPON showed desirable low electronic conductivity (10^{-14} S cm^{-1}) and good electrochemical stability in combination with Li metal (0–5.5 V).[27,59,65] Later, more characteristics have been studied, such as decomposition chemistry and electrochemistry of LiPON decomposition, vital for battery safety.[204]

The RF-sputtering method could produce good quality LiPON planar films without cracks. However, it has a low deposition rate (1–10 nm min^{-1}), which was supposed to limit its widespread use and commercialization.[27,205] Recently though, several industrial manufacturers, such as Front Edge Technology, succeeded to improve the deposition rate during the scale-up.[206] Nevertheless, the investigation was continued to find the best parameters for film deposition. It was observed in the study by Choi *et al.* the decrease in power (80 W) led to an increase of N/P ratio in ~2 μm thick LiPON film, and with slower deposition rate, the ionic conductivity could be increased even more significantly.[207] Yet, ambiguous trends of ionic conductivity with N/P ratio were also shown by Hamon *et al.*[208] and Kim *et al.*[209] Another study by Suzuki *et al.* showed that when adding extra Li_2O to Li_3PO_4 target for film sputtering, a higher number of three-coordinated N atoms were detected in the deposited LiPON film. This resulted in enhanced ionic conductivity (3.1×10^{-6} S cm^{-1}) compared to sputtering using conventional target (2.1×10^{-6} S cm^{-1}).[210] Up to now, one of the highest ionic conductivities for LiPON with 4.9×10^{-6} S cm^{-1} at 22 °C was obtained by Su *et al.* using the RF sputtering growth rate of 14 nm min^{-1} (100 W).[211] Generally speaking, reviewing the available works with LiPON film electrolyte showed that the used power was in the wide range of 35–350 W, while thickness was within 0.5–2 μm. The effect of sputtering target temperature was also observed, where the increase of it led to the reduction of LiPON ionic conductivity and worsened performance of the thin-film battery with this electrolyte in general.[212] Such result was attributed to the formation of a closed-packed structure which hindered Li diffusion.[212]

The compatibility of LiPON with common electrode materials, such as Li and LCO, was actively investigated. For instance, using electroanalytical measurements, cryogenic electron microscopy, and *in situ* electron microscopy, it was shown that LiPON forms a stable interface (up to 80 nm) with Li, reducing the Li loss during interface formation and further cycling compared to the liquid electrolytes, therefore providing a stable (de)intercalation of Li.[213–215] The composition of this layer with N and P concentration gradients and their unique spatial distribution acts as an effective passivation layer.[214–216] LiPON/LCO interface, its composition, and electronic structure have been also studied by such techniques as X-ray photoemission spectroscopy, scanning transmission electron microscopy (STEM) coupled with electron energy loss spectroscopy (EELS). It was observed that the interface of a 10 Å layer is usually formed with nitrogen-containing species.[217,218] Excellent cycling stability of thin-film LCO with LiPON was demonstrated, which was explained by the grain size effect with the critical particle size of the cathode being 0.3–1.1 μm.[219] However, another research group found, based on the STEM/EELS analysis, that after extensive cycling Li accumulation at the interface caused an irreversible capacity losses.[220] Moreover, the surface and evolution of the lithium morphologies in thin-film Li/LiPON/LCO (or $LiMN_2O_4$) have been evaluated after extensive cycling, and the cell with LCO showed more uniform Li distribution and stable behaviour while having a hold at the top of charge at 4.2 V.[221] Nevertheless, the observed surface changes attributed to the Li dewetting and residual stress require more investigations on the exact mechanisms in the future to enhance safety.

5.1.1.1 2D structures. In general, the earliest developments of 2D LIMBs with LiPON electrolyte, Li and LCO electrodes had promising results. The first tests of thin-film Li/LiPON/LCO with a 2.5 μm thick LiPON demonstrated approximately 150 μA h capacity with stable cyclability of over 4000 cycles at 0.1

mA.[56] Later, similar microbattery with thinner electrolyte (1 μm) also showed excellent 65 μA h cm^{-2} capacity with a very small 6% loss after 1800 cycles and negligible self-discharge.[28] That made them an attractive candidate for industrial applications. Teledyne Electronic Technologies, for instance, proceeded to manufacture this type of microbattery on a multichip module package.[56] The other commercial Li/LiPON/LCO type LIMBs with different total thicknesses of 170 and 200 μm showed the energy density of 25 and 21 mW h cm^{-3}, respectively, along with good cyclability for at least 500 cycles with approximately 100% capacity retention.[57] Testing of similar microbattery structure Li/LiPON/LCO with cathode thickness of 4.2 μm demonstrated the energy and power density of 1 mW h cm^{-2} and 1 mW cm^{-2}, respectively.[54] Excellent performance for Li/LiPON/LCO microbattery was observed with the capacity remaining stable (approximately 22 μA h cm^{-2}) after 1100 cycles, indicating the importance of cathode properties and its compatibility with electrolyte.[222] Another Li/LiPON/LCO thin-film battery's volumetric capacity was 63.5 μA h cm^{-2} μm^{-1}, corresponding to 92% cathode utilization, which also showed almost no degradation after 500 cycles.[223] Such results were attributed to the formation of crack-free and crystallographically oriented cathode films. The importance of structure–rate relationship in LCO and encapsulation that preserved film morphology was also demonstrated in the study by Song *et al.*, where Li/LiPON/LCO cell delivered a steady volumetric capacity of 35 μA h cm^{-2} μm^{-1} with 85% retention after 800 cycles.[224] Another example of successful Li/LiPON/LCOmicrocell with 45 μA h cm^{-2} μm^{-1} capacity and the retention of 88% over 800 cycles proved good integration of 1.4 μm thick LiPON (350 W) with bias sputtered and heat-treated LCO.[225] Park *et al.* specifically tested LCO cathodes that were bias sputtered at different voltages. It was found that structure of the LCO treated by −50 V bias combined with 1.5 μm LiPON (200 W) and evaporated Li was most suitable to obtain the highest initial capacity battery of around 63 μA h cm^{-2} μm^{-1}.[226] There was a 16% capacity loss after 100 cycles, making it a promising treatment method of electrodes. Due to the good performance of common thin-film microbattery Li/LiPON/LCO, it was attempted to add flexibility to the battery for wearable applications by using sacrificial mica substrates and wrapping by polydimethylsiloxane (PDMS) (Fig. 7b).[227] The new battery demonstrated a relatively high capacity of 106 μA h cm^{-2} that was stable for 100 cycles with 10% loss. Similar behaviour was also obtained for bent samples, indicating the effectiveness of the new approach and a good basis for further energy density improvements of flexible microbatteries.

Several research studies were done to evaluate other cathode materials with LiPON electrolyte. An RF sputtered $LiMn_2O_4$ (LMO) completed by 1 μm LiPON and Li metal demonstrated 48 μA h cm^{-2} μm^{-1} capacity and only 4% loss after 100 cycles in the voltage range of 3.7–4.3 V and current density of 100 μA cm^{-2}, LMO proved to be a promising cathode candidate, though the other properties needed further studies.[228] The same composed thin-film cell Li/LiPON/LMO also showed very stable behaviour with the initial capacity of 110 mA h g^{-1}, which reduced to 105 mA h g^{-1} after 3500 cycles. The increase of the bulk or cathode–electrolyte interface resistances was determined to be the main issue in this battery.[229] Generally, though LMO cathode was reported to have lower performance compared to LCO,[28] Li *et al.* tested another material LNMO, which can operate at higher potential (3.2–5 V) than LMO (up to 4 V) due to partial substitution of Mn.[230] The extensive electrochemical testing (up to 10 000 cycles) of Li/LiPON/LNMO thin-film battery demonstrated excellent results that showed 122 mA h g^{-1} capacity, retention of 90.6% at C/10, and a good rate performance of the solid-state cell due to, as the authors suggested, a reduced thickness of the electrolyte compared to the liquid one, good interfacial compatibility, as well as fast kinetics of the electrodes.[230] Navone *et al.* has attempted to introduce a new safe crystalline cathode V_2O_5 (VO) and compared it with a widely used LCO. However, at the relatively similar theoretical capacity of VO and LCO, the microcell Li/LiPON/LCO delivered a higher capacity of 50 μA h cm^{-2} μm^{-1} after 140 cycles at 10 μA cm^{-2}, while Li/LiPON/VO had 30 μA h cm^{-2} μm^{-1} capacity after 20 cycles at the same current density.[231] Similarly, for another Li/LiPON/VO cell, the low performance and significant reduction of capacity were observed from 8 to 5 μA h after 500 cycles, which was attributed to the high electrode–electrolyte and charge transfer resistances.[232] Better results were observed for the composite $0.5Ag:V_2O_5$ cathode that was tested in Li/LiPON/$0.5Ag:V_2O_5$ thin-film battery with the initial capacity 72 μA h cm^{-2} μm^{-1} faded almost twice after 20 cycles.[233] It was noticed that cyclability was most probably affected by the improved electronic conductivity of $0.5Ag:V_2O_5$ film and electrode–electrolyte interfacial stability. Li *et al.* investigated Li/LiPON/$LiCo_{0.8}Ni_{0.2}O_2$ and Li/LiPON/$LiCo_{0.8}Zr_{0.2}O_2$ thin film batteries with new cathodes attempting to get better electrochemical performance than commercial LCO. The cycling of the batteries showed initial capacities of 62 μA h cm^{-2} μm^{-1} and 50 μA h cm^{-2} μm^{-1} for Ni and Zr-containing cells, respectively, which is quite close to the LCO theoretical capacity (69 μA h cm^{-2} μm^{-1}), therefore these materials were proposed as the new cathode candidates.[234] Zr doped cathode, however, showed better retention than Ni-doped one over 50 cycles.[234] Another cathode material, amorphous $LiFe(WO_4)_2$, was integrated into Li/LiPON/$LiFe(WO_4)_2$ thin-film microbattery that had the initial high capacity of 104 μA h cm^{-2} μm^{-1}, which diminished to 56 μA h cm^{-2} μm^{-1} after 150 cycles.[235] The significant decrease of capacity within the first 15 cycles was a result of the unavoidable crystallization of $LiFe(WO_4)_2$ that led to lower electrochemical activity. The same research group also tested another Li/LiPON/$CuWO_4$ thin-film battery, where the drastic reduction of the capacity from 145 μA h cm^{-2} μm^{-1} to 70 μA h cm^{-2} μm^{-1} happened at the second cycle, and only 43% of that was maintained after 100th cycle.[236] The large initial irreversibility was attributed to the electrochemical reaction occurring at voltages above 2.5 V.

The performance and compatibility of LiPON with materials other than Li were also studied. One of the proposed materials was tin nitride (Sn_xN_y) that was integrated into the thin-film battery Sn_xN_y/LiPON/LCO with 7.6 μm total thickness.[52] The discharge capacity was evaluated at different temperatures and was found to increase from 20 °C to 60 °C and subsequently decrease until 200 °C. Although higher temperatures caused

more active ingredients to function and improve the LiPON conductivity, this also resulted in the enhancement of undesired grain diffusion. The maximum capacity of 200 μA h was observed at 60 °C, while at 100 °C, 193 μA h discharge capacity remained stable only for 15 cycles in the voltage window of 2–4 V.[52]

The structures with both non-commercial cathode and anode and LiPON were investigated as well. The new thin-film structure of Si/LiPON/VO–LiPO showed the capacity fading from the initial 15.7 μA h cm^{-2} to 7.7 μA h cm^{-2} after 30 cycles, which was attributed to the degradation of Si anode due to volume changes.[237] Another thin-film battery ZnO/LiPON/LMO experienced low coulombic efficiency of 55% in the first cycle as a result of the reaction between ZnO and Li-ions.[238] Thus, it further delivered the capacity of only 22 μA h cm^{-2} at the current density of 5 μA cm^{-2} and in the potential window 0.5–5 V. Approximately 10% of this capacity was also lost after 50 cycles. As no heat treatments were done to this battery, it was proposed to be a candidate for low-power and low-temperature substrate applications.[238] Very unusual behaviour was observed for VO/LiPON/LMO thin-film battery, where the capacity significantly increased from 0.1 μA h cm^{-2} to 10 μA h cm^{-2} after 20 cycles and then remained steady.[239] It was attributed to the so-called "forming process", where the possible gradual decrease of interface resistances led to such performance. However, further studies on this phenomenon have not been done yet. Nevertheless, later, the research group Nakazawa *et al.* tested a similar thin-film structure battery and observed stable performance with around 80% retention of the initial capacity of 1.1 mA h after 100 cycles.[240] The cell was even tested in a real digital watch, which was working for 1 month without additional charging.[240] Nevertheless, as VO has some safety limitations of toxic nature, the same group also investigated Nb_2O_5/LiPON/$Li_2Mn_2O_4$ thin-film battery with an alternative anode, which had a very thin LiPON layer (100 nm) and demonstrated stable behaviour for 500 cycles and optimal anode thickness of 100 nm.[241] Nb_2O_5 was not actively implemented in microbatteries though due to its relatively lower capacity compared to Li. The innovative structure of a "Li-free" battery, where Li is electrochemically plated between the substrate and LiPON to form anode, was also studied in the thin-film battery of overlayer (LiPON or parylene C)/Cu/LiPON/LCO/Au.[242] The cell delivered 85 μA h cm^{-2} of initial capacity with a 38% loss after 500 cycles. The considerable capacity fading was explained by the further development of unfavourable morphology of the plated Li and its irreversible consumption. Moreover, the importance of the overlayer, which covered the anode current collector and formed the tight gas seal, therefore reducing the formation of electrochemically inactive Li_2O and LiOH, was highlighted.[242] A similar "Li-free" inverted stack battery of stainless substrate (SUS)/PtLiPON/LCO/Au was also tested.[243] It was observed that the cell with 7.5 μm-thick LiPON had the stable capacity of approximately 100 mA h g^{-1} at 5 μA cm^{-2} for 100 cycles due to good protection from the short circuit and the undesired reactions of plated Li. At the same time, the cell with 1.5 μm-thick LiPON was short-circuited due to insufficient mechanical strength of thin LiPON layer.[243] Further investigations on the improvement of energy density in "Li-free" microbatteries are in progress nowadays.

Several ideas were proposed to improve the properties of LiPON. Xiao *et al.*, for example, focused on the effect of fabrication conditions on LiPON properties and compared the LiPON produced by sputtering a sintered standard Li_3PO_4 and Li-rich $Li_{3.3}PO_4$ in a widely used Li/LiPON/LCO microbattery.[58] It was observed that Li-rich LiPON thin-film battery, besides providing a slightly higher capacity of 64.5 μA h cm^{-2} μm^{-1} also had larger capacity retention of 98% after 26 cycles at 0.1C. In addition, at the discharge rate of 4C, Li-rich LiPON thin-film battery showed 89.5% capacity retention ratio, while standard LiPON battery had 83.1%. Such improvements were reported to be the result of the weakened space-charge layer effect induced by Li-ion defects in the Li-rich target.[58] Generally, however, Lacivita *et al.* systematically studied the dependence of ionic conductivities on LiPON composition and actually found the optimal Li : P ratio to be 2.9 : 1, which provided the maximum ionic conductivity.[244] Moreover, it was found that the small integration of boron into LiPON (LiPONB) introduced enhanced chemical and thermal stability while the electrical properties remained unchanged.[245] This electrolyte was used in Li/LiPONB/TiOS thin-film battery, which had a large capacity (90 μA h cm^{-2} μm^{-1}) in the voltage range of 1–3 V (*versus* Li) and current density of 100 μA cm^{-2} along with a long cycle life (>1000 cycles) and low self-discharge (<5%/year).[245] Similarly, LiPONB was used in the microbattery Li/LiPONB/LCO, which had the initial capacity of 34.5 μA h cm^{-2} that was retained to 95.3% after 15 cycles at the current rate 10 μA cm^{-2} and voltage window 3.4–4.2 V.[246] In another study, LiPONB with Si anode and Li cathode demonstrated excellent electrochemical performance with 571 μA h cm^{-2} μm^{-1} capacity and almost no fading for over 1500 cycles.[247] Good mechanical properties and strong adhesion of LiPONB to Si prevented the initiation of cracks in the anode. Furthermore, solid electrolyte helped to avoid the formation of undesirable products at the electrode–electrolyte interface, unlike liquid electrolyte, indicating the promising use of silicon and LiPONB in solid-state microbatteries.[247] Later, Song *et al.* have attempted to fully replace phosphorus (P) with boron and test the resulted electrolyte $Li_{3.09}BO_{2.53}N_{0.52}$ (LiBON) in a thin-film battery Li/LiBON/LCO on a flexible substrate (Fig. 7c).[12] As finding the exact electrolyte composition is very challenging with just one technique, this research team used several methods, such as inductively coupled plasma atomic emission spectroscopy (ICP-AES), elastic recoil detection-time of flight (ERD-TOF), as well as XPS to check the N-doping. The outstanding performance with the initial capacity of 55 μA h cm^{-2} μm^{-1} and 90% retention after 1000 cycles was observed for the cell. Therefore, LIBON was again noted to be a good candidate for flexible devices.[12] It was also attempted to integrate Si in LiPON to improve the ionic conductivity of the electrolyte. One of the recent research papers demonstrated a higher ionic conductivity (up to 2.06×10^{-5} S cm^{-1}) for LiSiPON compared to LiPON.[248] LiSiPON produced by single-target sputtering has a potential for further development with processing optimization. However, instability of LiSiPON with Li anode remains an obstacle for a wide application.[248]

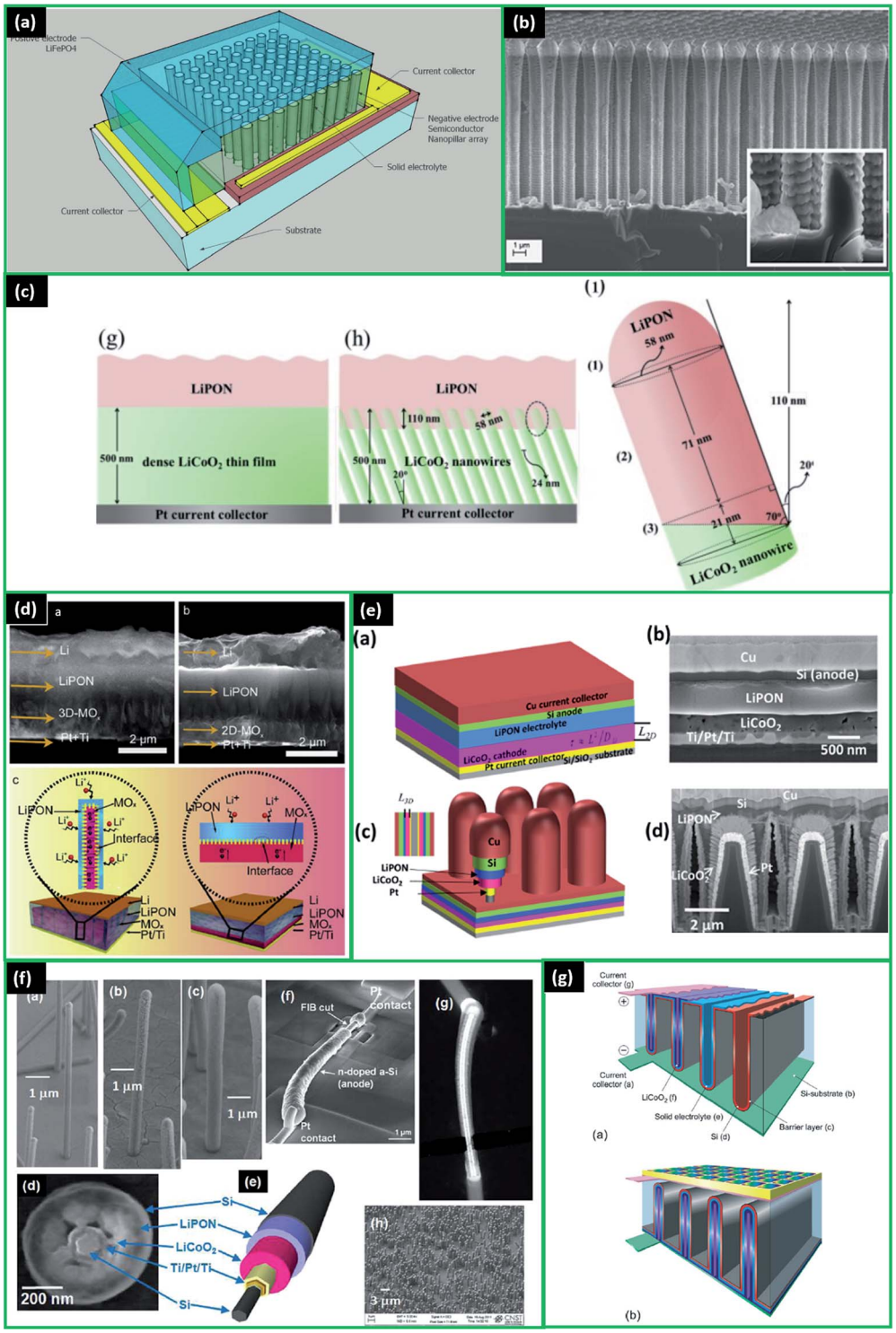

Fig. 8 (a) Overview of the lithium ion solid state micro-battery. Reproduced with permission from ref. 76; (b) overview of the SiNPL array covered by the LiPON/LFP sputtered thin films. Reproduced with permission from ref. 76; (c) (a) dense thin film cathode, (b) slanted nanowires cathode, (i) enlarged the LiPON-deposited slanted nanowire cathode. Reproduced with permission from ref. 70; (d) cross-section field emission scanning electron microscope (FESEM) images of (a) the 3D and (b) the 2D thin film battery, (c) schematic illustration of the structural comparison between 3D and 2D thin film battery. Reproduced with permission from ref. 79; (e) (a) schematic of a planar thin film battery, (b) focused ion beam (FIB) cross section of a thin film battery, (c) schematic of a 3D battery, (d) focused ion beam cross sections of 3D battery with nominally 500 nm thick LiPON. Reproduced with permission from ref. 71. Copyright (2016) American Chemical Society; (f) FESEM images of nanowire LIBs following deposition of (a) Ti/Pt/Ti, (b) $LiCoO_2$, and (c) LiPON/Si; (d) a FIB cut cross section FESEM image and (e) a nanowire LIB schematic; (f) a nanowire LIB contacted with Pt electrodes on a Si/SiO_2 substrate, (g) HAADF STEM of a Nanowire LIB on SiN_x membrane with Pt contacts showing its internal structural arrangement, and (h) a panoramic FESEM of the Nanowire LIBs on the wafer. Reproduced with permission from ref. 72. Copyright (2012) American Chemical Society; (g) (a) 3-D integrated all-solid-state Li-ion battery for which surface enlargement has been accomplished by electrochemical or reactive ion etching (RIE) of a silicon substrate, (b) autonomous energy-generating and storage device, combining a Si-solar cell with an integrated all-solid-state battery. Reproduced with permission from ref. 263.

It is also known that LiPON interfaces mainly contributed to the internal cell resistance.[54] The effect of interfacial resistance was previously described by Wang *et al.* for LiPON with 2×10^{-6} S cm^{-1} ionic conductivity.[249] It was speculated that the performance of the battery was negatively affected due to increased cathode–electrolyte resistance resulting from significant strain-induced degradation of the LCO cathode at the interface region.[249] Nevertheless, several researchers found that the interface resistance might not be the main limitation for some cases. For example, for the thin-film microbattery of Li/LiPON/$Li_4Ti_5O_{12}$(LTO) cycled 5 times at 3.5 mA cm^{-2}, the ionic charge transfer resistance between cathode and electrolyte was not a rate-limiting factor, rather the phase changes of LTO had mainly contributed to the cell impedance.[250] Similarly, the study of Li/LiPON/LCO showed the stability of LiPON during ageing at 60 °C, where LCO caused a significant increase in cell resistance due to phase conversions.[251] In addition, Wang *et al.* observed that at the highly delithiated state, the cathode tended to form a layer of rocksalt CoO and Li_2O/Li_2O_2 structure, which accumulated Li and led to the larger amount of inactive cathode material.[252]

In general, the interface still plays a crucial role in battery performance and is one of the causes of the limited practical development of all-solid-state batteries. The quality of the interface and the interfacial resistance magnitude vary depending on many factors, including the deposition conditions, surface roughness, used electrode materials. Thus, the electrode–electrolyte interfaces, their behaviour, and strategies to overcome the issues have been extensively studied for various electrolytes and discussed in numerous review articles in detail.[24,26,145,253–258] One proposed way to reduce the resistance was to do thermal treatment that could not only improve the ionic conductivity of LiPON but also enhance the number of electrochemically active sites at the interface of electrode and electrolyte.[52,242,259] So, thermal treatment of LCO/LiPON interface at the temperature of 200 °C significantly reduced the resistance.[260] In another study by Jeong *et al.*, thermally treated Al_2O_3 film (400 °C) at the interface of LiPON and LCO also diminished the resistance while enlarging the capacity and stability during cycling.[261]

5.1.1.2 3D structures. Although 2D microbatteries are able to provide good electrochemical performance, increasing the surface area by moving to 3D architecture is the obvious way to decrease the interfacial resistance that, in a balance with a properly constructed cathode, can enhance both the power and the energy densities of microbatteries. Several 3D architectures with LiPON have been designed and studied. One of the earliest investigations was done by Xu *et al.*, where the ionic conductivities of the planar LiPON film were found to be in the range of $1–2 \times 10^{-6}$ S cm^{-1}, whereas when trying to RF-sputter LiPON on the 3D structures (porous membranes, column arrays), inhomogeneous and rough deposition of LiPON was observed.[11]

Later, various micro- and nano-rod designs were tested by several research groups. For instance, successful 3D microrod patterning was done by Lethien *et al.*, where LiPON was sputtered on the silicon nanopillars (SiNPL) negative electrodes to form SiNPL/LiPON/LFP microbattery with a conformal coverage of SiNPL (Fig. 8a and b).[76] Although no electrochemical performance of the battery was discussed, LiPON ionic conductivity was measured to be 1.5×10^{-6} S cm^{-1}.[76] The functioning 3D microbatteries (Li/LiPON/LCO) with well-aligned slanted LCO nanowire structure were investigated recently (Fig. 8c).[70] This 3D structure had a higher normalized discharge capacity than a 2D thin-film battery at 0.1C most probably due to the larger contact area of electrode–electrolyte. Furthermore, nanowires maintained a high specific capacity (73%, ~70 mA h g^{-1}) even after 400 cycles in the voltage range of 3–4.2 V due to the ability to accommodate the stress of the volume changes during cycling.[70] Sun *et al.* have recently investigated another successful 3D structure, where vertically aligned oxygen-deficient α-MoO_{3-x} nanoflake arrays were sputtered along with LiPON electrolyte and Li anode (Fig. 8d).[79] The microbattery demonstrated good capacity (266 mA h g^{-1} at 500 mA g^{-1} and 1.5–3.5 V) and stable cycle performance (92.7% capacity retention after 1000 cycles) higher than of a 2D battery made out of the same materials.[79] The following structure allowed not only a greater cathode–electrolyte interface with a short Li diffusion path but also accommodation for the volume change, which enhanced the mechanical integrity of the microbattery. Moreover, the microcolumnar 3D structures of Si/LiPON/LCO constructed with the sputtering technique were electrochemically tested (Fig. 8e).[71] The results indicated that although the capacity of the 3D sample was higher (25 μA h cm^{-2}) than that of 2D's (20 μA h cm^{-2}), at the higher rates, the 3D sample had a significantly lower capacity (80% or less).[71] It was speculated that the structural inhomogeneity with low ionic conductivity of the LiPON (2.5×10^{-7} S cm^{-1}) led to the poor performance of this microbattery. The sputtering method was also used to deposit Ti/Pt/Ti current collector, LCO, LiPON, and Si anode on the Si nanowires (Fig. 8f) creating a microbattery with 0.5–1 μm diameter.[72] This microbattery with only 110 nm LiPON film showed increased electric field in the electrolyte that resulted in the pinhole formation at the LCO/LiPON interface, rapid self-discharge, and short-circuiting. However, for the samples with larger LiPON thickness (>180 nm), the self-discharge diminished significantly, therefore confirming that the optimal thickness for electrolyte should be not smaller than 110 nm in order to avoid compromising the space-charge limited electronic conduction.[72] In terms of LiPON thickness discussion, another research group Put *et al.* obtained the thinnest RF-sputtered plane LiPON, which was electronically insulating, retaining good ionic conductivity. Such behaviour deviating from other studies was explained by the possible difference in LiPON stoichiometry and the substrate effect, whereas in a real microbattery, LCO with sharp crystallite edges could reinforce local electric fields.[262]

A new concept to create the 3D structure was proposed in the form of trenches using Si-substrate, TiN or TaN film to protect the Si-substrate from Li penetration and Si/LiPON/LCO components (Fig. 8g).[263] It was predicted that for a surface enhancement factor of 25, the energy density can achieve 5 mW h cm^{-2} μm^{-1} for 1 μm thick LCO cathode. Moreover, LiPON film on the Si electrode had steadier cyclability due to the

stable solid-electrolyte interface (SEI) compared to the liquid electrolyte, which had a significant decrease in capacity after 30 cycles.[263]

Baggetto *et al.* focused on analyzing the Ta, TiN, TaN barrier layers for that 3D structure.[264] Among them, TiN has demonstrated the most promising results with Li-ions migration prevention due to the lowest reactivity with Li. In general, in the 3D Si/LiPON/LCO microbattery with TiN barrier layer, the capacity is expected to deliver energy and power density of approximately 1.5 mA h cm^{-2} μm^{-1} and 5 mW h cm^{-2} μm^{-1}, respectively, at the voltage of 3.5 V.[264] However, the exact electrochemical testing of this battery has not been conducted.

LiPON was also tested as a barrier layer for both sides of the lithium phosphorus tungsten oxynitride (LiPWON) a potential electrolyte. Although the protected electrolyte structure LiPON/LiPWON/LiPON was less vulnerable for short circuits, the ionic conductivity (1.2–1.5 $\times$ 10^{-7} S cm^{-1}) was relatively low compared to conventional LiPON.[265] Similarly, LiPON/LLTO/LiPON structure was studied, and it showed stable operation in the voltage window of 0–5.5 V. However, the same issue of low conductivity, which was in the range of 10^{-7} S cm^{-1}, remained for that electrolyte.[189]

5.1.2 Pulsed laser deposition (PLD). Although the sputter deposition method produced several successful electrolyte layers for microbatteries, it still suffers from the low deposition rate (1–10 nm min^{-1}).[19] Thus, other methods have also been investigated, such as Pulsed Laser Deposition (PLD). Previously, LiPON deposited by PLD had a relatively high deposition rate (40 nm min^{-1}).[266] However, the film was initially having an unsatisfying quality, which restricted its wide application in microbatteries.[266] Another research group managed to use PLD to deposit cathode $Ag_{0.3}V_2O_5$ and electrolyte LiPON thin films with a uniform interface.[29] The Li/LiPON/$Ag_{0.3}V_2O_5$ had demonstrated the stable specific capacity of 40 μA h cm^{-2} μm^{-1} after 100 cycles at a current density of 7 μA cm^{-2} and voltage range 1–3.5 V.[29] An interesting result was obtained by West *et al.*, where the amorphous LiPON film was deposited by PLD (LiPON-PLD) between the cathode $LiMn_{1.485}Ni_{0.45}Cr_{0.05}O_4$ (LNM) and RF-sputtered LiPON electrolyte.[267] That helped to reduce the charge-transfer resistance by at least 5 times compared to the samples without LiPON-PLD film.[267] This result was attributed to the produced higher N/P ratio and the larger amount of triply coordinated Nitrogen content in LiPON by PLD technique.[267] Matsuda *et al.* has also succeeded to fabricate Li/Li_3PO_4/LCO thin-film battery using PLD to deposit amorphous electrolyte a-Li_3PO_4 and LCO.[268] Besides achieving the high rate deposition of 5–7.2 μm h^{-1} (83–120 nm min^{-1}), the functional cell with 60 μA h cm^{-2} capacity stable for 10 cycles was also obtained.[268] Nevertheless, further capacity improvement was limited due to the crack formation in cathode film as a result of volume changes during cycling.[268]

5.1.3 Atomic layer deposition (ALD). The emerging ALD technique was also used to successfully deposit LiPON with ionic conductivity of 10^{-7} S cm^{-1}. Several processes were attempted, such as ALD with two precursors, lithium bis(-trimethylsilyl)amide (LiHMDS), and diethyl phosphoramidate (DEPA),[269] or utilizing (trisdimethylaminophosphorus $-$ O_2) + (LiO*t*Bu $-$ NH_3)[270] and [lithium *tert*-butoxide (LiO*t*Bu) $-$ H_2O] + (trimethyl phosphate $-$ plasma N_2).[271,272] So, Put *et al.* successfully deposited a very thin layer of LiPON (70 nm) with ionic conductivity of 5 $\times$ 10^{-7} S cm^{-1} on top of 200 nm LTO using ALD and tested the thin-film battery with Li anode at 5C and voltage window of 0–2.5 V.[271] This cell was demonstrated to be functional with the capacity of 0.3 A h cm^{-3} after 1 cycle.[271] Later, Pearse *et al.* deposited uniform, conformal, and ultrathin (<100 nm) LiPON film with 6.51 $\times$ 10^{-7} S cm^{-1} ionic conductivity using DEPA and LiO*t*Bu precursors and then investigated Si/LiPON(Li_2PO_2N)/LCO thin-film battery.[273] The battery showed stable behaviour and delivered 20 μA h cm^{-2} capacity, 80% of which was retained after 150 cycles at 300 μA cm^{-2}.[273] The same research group investigated the 3D structure where LiPON was deposited on the cylindrical pore arrays, forming SnN_x/LiPON(Li_2PO_2N)/LiV_2O_5 battery (Fig. 9a).[31] Testing of this structure demonstrated good electrochemical stability with the capacity of approximately 30 μA h cm^{-2} (area enhancement factor = 10) in the voltage range of 0.5–3.5 V *vs.* Li^+/Li for 100 cycles.[31] This was 9.3 times larger capacity than that of the planar cell made from the same materials. In addition, Létiche *et al.* research group has studied pure ALD deposited-Li_3PO_4 electrolyte onto the 3D pillar novel structure of Li/Li_3PO_4/TiO_2 (Fig. 9b).[274] It was found that single microtubes (SMT) and double microtubes (DMT) had significantly higher capacities compared to planar thin films. Hence, for SMT the initial capacity was approximately 100 μA h cm^{-2}, while for DMT, it was 300 μA h cm^{-2} (at C/16), which corresponded to 33-fold and 100-fold increase compared to thin-film counterparts.[274] Both structures had stable behaviour for at least 10 cycles. Thus, such configuration and materials were proved to be good candidates for 3D microbatteries.

In general, ALD proved to be a promising technique to develop 3D solid-state batteries due to the ability to produce the ultrathin, uniform, and conformal films for high aspect ratio structures.

5.1.4 Other techniques. One of the other LiPON deposition methods was the Ion Beam Assisted Deposition (IBAD), which had a high deposition rate (60 nm min^{-1}).[19] It was found that although the LiPON's ionic conductivity was high (1.6 $\times$ 10^{-6} S cm^{-1}), the film was easily cracked under large tensile stresses.[19] Another approach of E-beam (EB) evaporation was applied to Li_3PO_4 target in the presence of reactive nitrogen plasma with a relatively low rate of 8 nm min^{-1}.[275] The resulting LiPON film had the ionic conductivity of 10^{-7}–10^{-8} S cm^{-1}.[275] However, it was noticed that the increased nitrogen concentration and the kinetic energy of N in plasma had caused the crystalline formations in LiPON, which diminished its ionic conductivity.[275] To improve the deposition rate even more plasma-assisted directed vapour deposition method based on EB evaporation was also tried. Besides the relatively similar ionic conductivity (10^{-7}–10^{-9} S m^{-1}) to that of RF sputtered one, the rate was significantly higher compared to RF-sputtering (up to 45 times).[276] Moreover, the advantage of this method was that the direct change of the plasma current allowed controlling the nitrogen incorporation and the ionic conductivity of LiPON. Furthermore, it was attempted to deposit

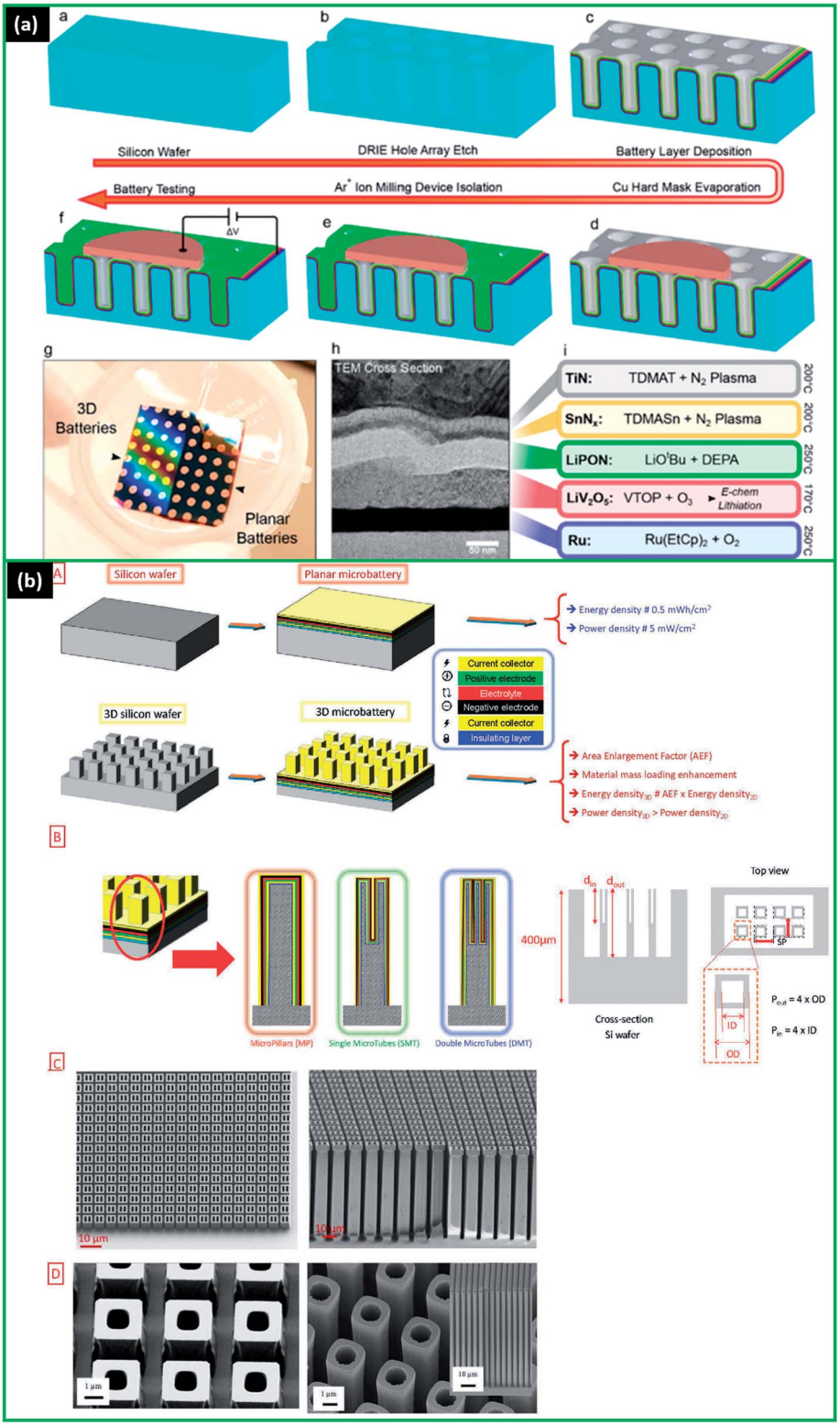

Fig. 9 (a) Fabrication and characterization of 3D solid-state thin-film batteries. (a–d) Schematic of fabrication of devices, (e) isolation of individual batteries *via* Ar^+ ion milling through anode current collector and anode films, (f) battery testing through contact with top electrode and cathode current collector layers, (g) optical photograph of finished battery "chip". Each chip is dual sided, with 3D batteries on the left and planar batteries on the right. Optical iridescence from the 3D array causes the visible coloration, (h) cross-sectional TEM image of an all-ALD solid-state battery with 40 nm Ru/70 nm LiV_2O_5/50 nm Li_2PO_2N/10 nm SnN_x/25 nm TiN, (i) overview of ALD chemistry and process temperature for each layer visible in (h). Reproduced with permission from ref. 31. Copyright (2018) American Chemical Society; (b) (A) schematic of 2D and 3D microbatteries fabricated on silicon wafer, (B) description of the proposed 3D scaffold: micropillars, simple microtubes and double microtubes (MP, SMT and DMT) are successfully fabricated on 3 in. silicon wafer, (C and D) SEM images of the fabricated DMT (SMT, respectively): photoresist mask (left) and 3D silicon scaffold (right) after the deep reactive ion etching of the wafer selectively to the mask. Reproduced with permission from ref. 274.

the LiPON on Si 3D substrate with the line/space = 2 μm/2 μm and the aspect ratio of 1 using metalorganic-chemical vapour deposition (MOCVD).[32] The resulting film was uniform, having a relatively large ionic conductivity of $\sim 10^{-6}$ S cm^{-1}.[32] The functionality of the MOCVD-produced LiPON was tested and confirmed in the thin-film battery a-Si:H/LiPON/LCO.[32] All in all, the new methods that showed satisfactory results of LiIPON deposition are currently under development, and a few studies are available yet.

As the deposition technique's parameters play a crucial role in the material properties, a lot of attention was brought to improve the methods and develop the electrolyte with the most favourable characteristics. Major techniques of solid electrolyte fabrication and their specifications are generally covered in several review reports.[36–38] The RF sputtering being a dominating LiPON preparation method was discussed in numerous articles, where the effect of sputtering power, pressure, target–substrate distance, target density, N_2 deposition pressure, deposition rate, and other conditions on the electrochemical properties of LiPON were investigated.[58,207,208,277–280] Considering the examples of LiPON integrated into the thin-film or 3D microbattery performance, firstly, it was found that by changing the RF power, the boron content was varied in LiPONB and at the optimum 50 W : 20 W (Li_3PO_4 : Li_3BO_4) power, the highest ionic conductivity was observed.[246] The importance of the composition of the sputtering target was also shown, where usage of Li-rich $Li_{3.3}PO_4$ target compared to normal Li_3PO_4 target led to superior LiPON conductivity and higher microbattery initial capacity.[58] It was suggested that Li-rich LiPON helped to diminish the space-charge layer effect.[58] Moreover, *in situ* (without breaking vacuum after VO electrode growth) and *ex situ* (with breaking vacuum) LiPON depositions demonstrated that the *in situ* process resulted in lower interfacial and charge transfer resistances and thus better microbattery performance.[232] The full review article on the RF sputtering conditions and their impact on LiPON used in solid-state batteries has been provided recently by Ko and Yoon.[281] Other techniques, like PLD and ALD, are gaining more attention in LiPON studies due to the promising results, and these techniques' features are discussed in the recent reviews by Julien *et al.*,[29] and Liu *et al.*,[43] Meng *et al.*,[44] Fenech and Sharma.[198] In short, for PLD, the importance of N_2 gas pressure and laser fluence was highlighted so far,[266] while for ALD, the precursors and the temperature window were mentioned to be important parameters.[43,44] Thorough studies on PLD/ALD conditions and their impact on LiPON's direct performance in the microbatteries are still limited. Similarly, other techniques, like IBAD and CVD, also lack extensive investigations and need research on the methods' limitations in more detail.

5.2 Other glass electrolytes

Other glass electrolytes generally classified as oxide- and sulphide-based were attempted to be developed by various research groups using mainly RF sputtering and vacuum evaporation techniques.[19] However, these materials have gained less attention compared to LiPON due to several reasons. Most of the oxide-based electrolytes produced by the conventional physical vapour deposition method showed smaller or comparable ionic conductivity and poor electrochemical stability relative to LiPON.[19,65,282–284] At the same time, sulphide-based electrolytes, having a promising ionic conductivity that is much closer to liquid electrolytes, are less favourable due to hygroscopic nature and chemical instability in the air.[19,285] Therefore, the number of reported studies on these materials is limited up to now.

One of the glass electrolyte examples is Li_2O–V_2O_5–SiO_2 (LVSO). It showed the ionic conductivity of 10^{-5}–10^{-7} S cm^{-1} and low electronic conductivity (10^{-10} S cm^{-1}).[19,286] Using this electrolyte, the microbattery Li/LVSO/MoO_3 delivered 290 μA h cm^{-2} μm^{-1} capacity with 4.66 μm thickness of cathode in the voltage window of 1.5–3.5 V and at the current density of 10 μA cm^{-2}.[287] This performance was successfully maintained for 40 cycles.[287] Another LVSO based microbatteries (SnO/LVSO/LCO and SnO/LVSO/LMO), where electrolyte was deposited by PLD, could deliver 9 μA h cm^{-2} (2–3 V) and 1.5 μA h cm^{-2} (1–3 V) capacities, respectively.[288] In this case, the annealing of the cathodes helped to increase the roughness and thus the active interface area between the electrolyte and cathode leading to the larger capacities.[288] Later, the same research group also tested SnO/LVSO/$LiNi_{0.8}Co_{0.2}O_2$ microbattery with the annealed cathode and observed stable operation for 20 cycles with a small loss of the capacity from 19 to 16.1 μA h cm^{-2} μm^{-1}.[289] Brazier *et al.* studied similar PLD-fabricated-SnO/LVSO/LCO microbattery and observed that at the 4.4 μA cm^{-2} current, the capacity had a large irreversible loss and quickly faded due to the chemical elements' migration between LVSO and both the cathode and the anode. In addition, the delamination of SnO was detected.[290] An attempt to improve LVSO's ionic conductivity was done by adding the $LiBO_2$ in LVSO, which resulted in the maximum conductivity of 6.4×10^{-4} S cm^{-1} that was attributed to the porosity decrease.[291] Although there were several successful tests of LVSO-based electrolytes, it still had lower or similar ionic conductivities compared to commercial LiPON in most of the cases.[19,286,292] It was speculated that the possible amorphous Li_2O reaction with air and the formation of LiOH or Li_2CO_3 decreased LVSO's conductivity.[19,293] Most importantly, LVSO lacked electrochemical stability, therefore, it has not been widely utilized for microbatteries yet.

Another interesting electrolyte, Li_2O–SiO_2–P_2O_5 (LiSiPON) with the ionic conductivity of 1.24×10^{-5} S cm^{-1}, was used in a thin-film battery of $Si_{0.7}V_{0.3}$/$Li_{1.9}Si_{0.28}P_{1.0}O_{1.1}N_{1.0}$/LCO.[294] The microbattery showed excellent cycling stability with the capacity of 50 μA h cm^{-2} μm^{-1} (2–3.9 V) lasting for 1500 cycles.[294] However, at higher voltages (>3.9 V) the degradation of the battery happened, which was speculated to be due to the over-extraction of Li from the cathode.[294,295]

It was found that sulphide matrix-based oxysulfide glass electrolytes could greatly enhance Li^+ conductivity (10^{-4}–10^{-3} S cm^{-1}) compared to oxide-matrix ones (10^{-8}–10^{-5} S cm^{-1}).[285] This was attributed to the weaker bonding of Li with the non-bridging S anion, which resulted in easier diffusion. Nevertheless, the sulphide-based electrolytes have not been widely commercialized because of the complicated

synthesis process and difficult handling of the corrosive component.[285] Therefore, among the available glass electrolytes, LiPON is currently the most prominent candidate so far, since it has relatively high ionic conductivity, low electronic conductivity, and excellent electrochemical stability.

6. 2D *vs.* 3D LIMB

Obviously, the main difference between 2D and 3D is the geometry of the cell. However, even small shape distinctions may result in significant changes of intrinsic kinetics and thermodynamics. The main advantages of 3D architecture are an increased amount of active sites and greater surface area, free infusion and electrolyte ion access, and room for volume variations. 3D shape provides minimized ionic transport length between battery components, which simplifies the low diffusivity in solids; increased electrolyte-accessible surface, which decreases current density per unit area during cycling and lowers the overpotential required for charge transfer; mitigated mechanical degradation of the electrode. Besides, energy and areal capacity can be controlled easily by electrode height.[49,296] Below are several examples where the 2D and 3D micro cells were studied and compared.

For example, the larger contact area between LCO nanowire electrode and LiPON electrolyte allowed an increase of discharge capacity when compared to the corresponding planar cell.[70] 2D battery built with α-MoO_{3-x} cathode, LiPON electrolyte, and Li anode was not able to deliver the performance that was achieved by its 3D counterpart.[79] Along with improved electrode–electrolyte interface, accommodation for the volume change played an important role in the better mechanical properties of the cell. The microcolumnar Si/LiPON/LCO microbattery showed that the poor structural inhomogeneity and low ionic conductivity of the LiPON can bring a negative effect on cycling of 3D sample at higher rates compared to the 2D one.[71]

He *et al.* reported the cells with 3D spiral solid polymer electrolyte, the superior performance of which was caused not only by shortened Li-ion pathways between electrode and electrolyte but also due to reinforced interfacial adhesion and ability of 3D structures to maintain more mass loading of active materials.[77]

Edström *et al.* stated that the large surface area of the anode and cathode provides improved capacity per footprint area and high power capabilities if the 3D cell offers a short transport distance between the electrodes and thin layers of the electrode materials on the current collectors. Thus, the capacity can be increased by a factor of 10–30 per footprint area by using the appropriate 3D design.[297] Werner *et al.* reported that the capacity of the gyroidal 3D nanoscaled cells was three orders of magnitude higher than a theoretical capacity of flat architecture with the same nanoscale dimensions and footprint area.[81] Similarly, the 3D MoO_yS_z/hybrid polymer electrolyte/lithiated graphite cell exhibited a capacity of about 30 times higher than that of a 2D battery keeping the same footprint and same electrode thickness. It was explained by the high surface area of the nanosize molybdenum oxysulfide. The additional reason was suggested to be the material's heightened sensitivity to the environment, since the surface of the electrodeposited cathode is usually highly oxidized.[3] In another study of 3D thin film LIB with electrodes' pillars, the areal energy density was increased due to prolonged height of the pillars resulting in an increase of the loading of the active material per areal footprint.[298] The simulation of three types of 3D-shaped LCO/polymer + LiTFSI/graphite cells with interdigitated, concentric, and trench electrode arrangements revealed that the former two own low polarization to higher positive electrode–electrolyte surface area with enhanced contact area in contrast with the third one. Besides, the concentric architecture provided the lowest average cell temperatures for all investigated charge rates and the highest capacity.[299] The design advantage of interdigitated 3D architectures over simple thick films is that a short and uniform diffusion path maintained between the anode and cathode enables thick electrodes with high power.[82]

However, 3D-shaped battery structures have more challenges than 2D one for all types of electrolyte, such as manufacturing difficulties, high risks of a short circuit, compatibility of current collector–electrolyte–electrodes materials to provide a good contact between components, and an uneven current distribution that may cause nonuniform heat generation.[300]

7. Outlook on the 3D structures fabrication processes

It is known that for complex 3D architectures, conformal and thin uniform coating is crucial for the effective functionality of the microbatteries. Thus, the deposition techniques play an important role and can be compared based on their possibility to deposit pinhole-free, step-conformal films and applicability for battery materials. In this section, the general outlook on to the common and developing fabrication processes of 3D microbatteries' solid electrolytes is provided.

For organic electrolytes, the widely applied for 2D structures drop casting and dip coating methods were attempted on 3D structures, such as nanotubes. It was observed that, for example, the deposition of SPE on TiO_2nts was not conformal and the surface area of nanotubes was only partially covered by the electrolyte.[73,104] Later, the electrodeposition was found to be able to deposit more homogeneous, stepwise conformal layers of electrolyte on nanotubes, which significantly improved the microbatteries' performance.[74,75,96,108,110] This method also introduced easier control of film's thickness by potential and time variation and lower electrolyte–electrode interface resistances.[109,301] However, this method is cumbersome and requires relatively complex material preparations. Thus, other techniques are also under development.

For instance, organic electrolyte deposition methods, such as spin coating and photolithography, also underwent testing and showed some promising results with functional microbatteries.[82,83] Spin coating on micropillars, being a relatively simple process, was determined to have more adaptability for various polymer electrolytes,[83] while photolithography of SU-8

photoresist electrolyte provided conformal coating of 3D arrays, allowing the use of Si as both the scaffold and anode.[82]

Another innovative approach is 3D printing, which is a common tool to build 3D architectures due to low-cost and various designs' flexibility.[1,7] Therefore, the development of its application for electrolyte printing is expected to be a very important step for all-solid-state microbatteries. 3D printing includes such methods as stereolithography, direct ink-writing, ink-jetting, selective laser melting, and others.[77,302–306] One successful investigation was done on 3D spiral SPE deposited by stereolithography, where the 3D structure tested in the coin cell had stable and better cycle performance compared to the 2D structure, proving that this technology is a promising candidate for SPE fabrication.[77] This relatively simple printing method, where complex inks preparation and postprocessing of printed parts are not needed, has great potential and requires further adoption for the microbattery.[77] Most probably, as a result of low viscosity requirements for the materials printing process, only a few articles are available on SPE 3D printing up to now.[1] Currently, this field is in its formative stage.

Another research group demonstrated deposition of conformal SPEs on nanopillars, nanopores, and arrays by CVD.[111] The main advantage of this method is the ability to tune polymer properties, like ionic conductivity, by varying the compositions and copolymer network polarity.[111] Similarly, further testing of this technique is needed in a real microbatteries' environment.

UV-polymerization has also been applied to fabricate solid GPE on the Si pillars' structure. The films were proved to be not only conformable to 3D micropatterned architectures but also highly ion-conductive and bendable, thus opening more opportunities for the development of flexible devices.[113] Currently, further studies on fabrication process optimization are required.

For inorganic solid electrolytes, like LiPON, the most common method applied for 3D structures' coating was RF-sputtering. Several successful structures, such as nanopillars, slanted nanowires, nanoflake arrays and microcolumns, were conformally sputtered with LiPON, and most of them have been cycled and demonstrated generally stable performance.[70,71,76,79] However, in some cases, the poor performance of

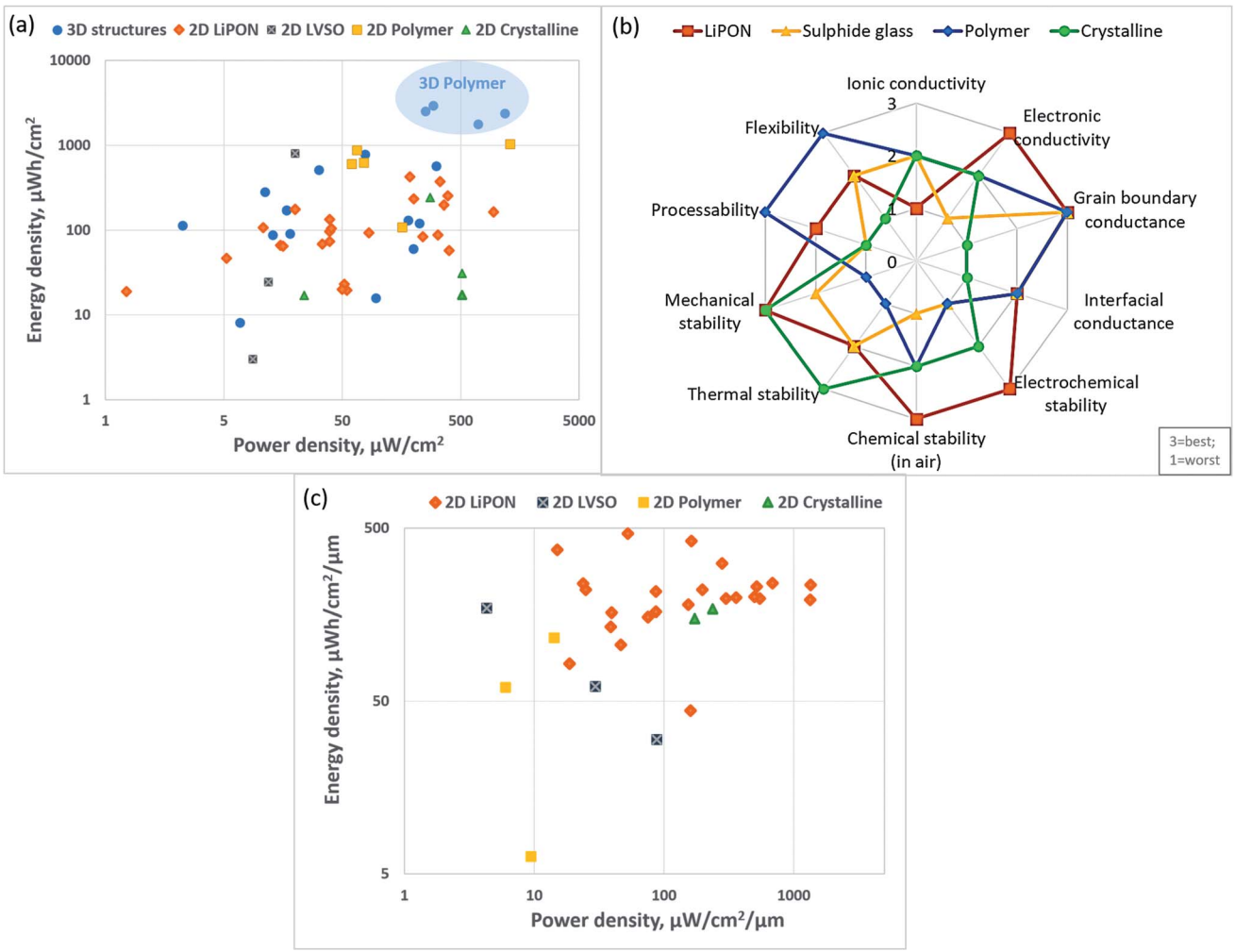

Fig. 10 (a) Ragone plot of 2D and 3D LIMBs; (b) spider chart comparing parameters of solid electrolytes integrated into microbatteries; (c) Ragone plot of only 2D lithium microbatteries with consideration of cathode thickness.

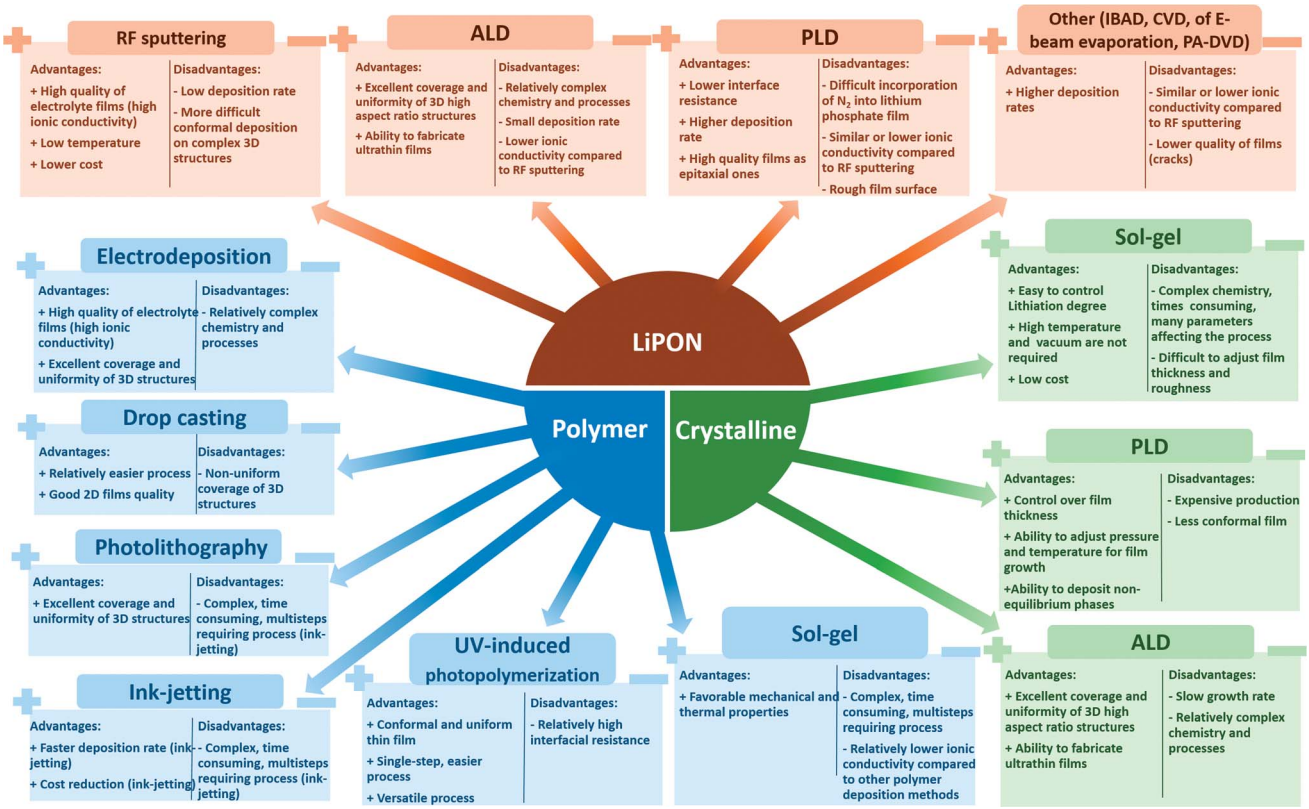

Fig. 11 Solid electrolytes' deposition techniques advantages and disadvantages.

microbatteries was attributed to the structural inhomogeneity in deposited LiPON.[71]

In addition, ALD is proved to be one of the emerging and promising techniques for 3D microbatteries' and solid electrolytes' deposition. As with ALD, it is possible to tune films composition at the precision level of atoms, control the growth and thickness of the films at the atomic scale, as well as fabricate the high-quality conformal thin films on various complicated architectures.[43,44] Moreover, ALD is more compatible with microbatteries' technologies and materials due to a relatively low deposition temperature.[43,44] The research done using ALD to deposit LiPON on nanopore arrays and Li_3PO_4 on microtubes to form microbatteries showed that besides the enhanced capacity as a result of 3D structuring, the cells were electrochemically stable.[31,274] Nevertheless, the relative complexity of the used chemistry and ALD process itself as well as smaller deposition rates than sputtering range prevented the wide commercialization of this technique as of today.[43,44]

8. Summary

Solid-state microbattery gained a lot of attention due to rapidly developing microelectronics used in various applications, such as smart cards, memory chips, biomedical devices, and others. Along with the thin-film structures, 3D structures with different materials have been developed recently to improve both the energy and power densities. One of the major components of a battery – electrolyte – plays an important role by transporting the ions between electrodes and enables the battery to function. The solid electrolyte, which is of great interest for the microbattery technology, provides additional safety by introducing a leakage-free feature and acts as a separator to prevent short circuits. Thus, in this review, the focus was on solid electrolytes of different types, including polymer, crystalline, and glass, which were successfully introduced in the 2D or 3D microbattery and electrochemically tested.

The promising candidate for solid electrolytes – polymer-based one mainly demonstrated high ionic conductivity (up to 10^{-4} S cm^{-1}), easy processability as well as flexibility. So, several successful 3D structures with innovative architectures and/or application of electrodeposition that helped to create a good electrode–electrolyte interface showed appealing results with both high power and energy density (Fig. 10a). Other innovative deposition techniques for SPE, such as photolithography and others, have been also tested providing some appealing results, so they are under further active investigation as well (Fig. 11). Nevertheless, cells with solid polymer electrolytes still suffer from mechanical integrity problems and thermal and electrochemical instabilities compared to LiPON, requiring further studies and development.

Similarly, most of the crystalline electrolytes, including NASICON, LISICON, garnet-based and perovskites, despite attracting high bulk ionic conductivities, still have low grain boundary conductivities and difficult processability as major issues in addition to some of the electrochemical and phase

Table 2 Electrochemical properties of all-solid-state 2D thin film and 3D microbatteries with glass, solid polymer and crystalline electrolytes

#	Electrolyte	Preparation method	Preparation conditions notes	Ionic conductivity	Microbattery	Structure (thin film, 2D/3D)	Initial discharge capacity	Voltage range	Current rate	Number of cycles	Retention	Ref.
1	LiPON	RF magnetron sputtering (MS)	2.5 μm (cathode)	NA	Li/LiPON/$LiCoO_2$	2D	150 μA h	3–4.2 V	0.1 mA	4000	99%	56
2	LiPON	RF MS	170 μm 200 μm (total thickness)	NA	Li/LiPON/$LiCoO_2$	2D	25 21 mW h cm^{-3}	3.6–4.1 V	1C	500	∼100%	57
3	N–LiPON (normal) Li–LiPON (Li-rich)	RF MS	Li_3PO_4 $Li_{3.3}PO_4$ (targets); 2.7 W cm^{-2}	2.4 μS cm^{-1} 3.2 μS cm^{-1}	Li/LiPON/$LiCoO_2$	2D	62.1 64.5 μA h cm^{-2} μm^{-1}	3.2–4.2 V	0.1C	26	98% 90%	58
4	LiPON	RF MS	1 μm (LiPON)	2 μS cm^{-1}	Li/LiPON/$LiMn_2O_4$	2D	48 μA h cm^{-2} μm^{-1}	3.7–4.3 V	100 μA cm^{-2}	100	96%	228
5	LiPON	RF MS	1–1.5 μm (LiPON)	NA	Li/LiPON/$LiMn_2O_4$	2D	110 mA h g^{-1}	2.5–4.2 V	20 μA cm^{-2}	3500	95%	229
6	LiPON	RF MS	1 μm (LiPON); 350 W	NA	Li/LiPON/$LiCoO_2$ Li/LiPON/V_2O_5	2D	55 45 μA h cm^{-2} μm^{-1}	2.15–3.8 V	10 μA cm^{-2}	140 20	90% 67%	231
7	LiPON	RF MS	2.4 μm (LiPON); 35 W	NA	Li/LiPON/$LiFe(WO_4)_2$	2D	104 μA h cm^{-2} μm^{-1}	1–4 V	28 μA cm^{-2}	150	54%	235
8	LiPON	RF MS	2.4 μm (LiPON)	NA	Li/LiPON/$CuWO_4$	2D	145 μA h cm^{-2} μm^{-1}	1–4 V	14 μA cm^{-2}	100	21%	236
9	LiPON	RF MS	5.5 W cm^2; heat treatment 1 h at 200 °C	3.2 μS cm^{-1}	Sn_xN_y/LiPON/$LiCoO_2$	2D	193 μA h (cycling at 100 °C) 200 μA h (cycling at 60 °C)	2–4.2 V	15 μA	15	∼100%	52
10	LiPON	RF MS	1.5 μm (LiPON)	NA	Si/LiPON/VO–LiPO	2D	15.7 μA h cm^{-2}	0.5–3 V	0.3 μA	30	49%	237
11	LiPON	RF MS	100 W	NA	ZnO/LiPON/$LiMn_2O_4$	2D	22 μA h cm^{-2}	0.5–5 V	5 μA cm^{-2}	50	95%	238
12	LiPON	RF MS	1 μm	NA	V_2O_5/LiPON/$LiMn_2O_4$	2D	0.1 μA h cm^{-2} (1^{st} cycle) 10 μA h cm^{-2} (20^{th} cycle)	0.5–3.5 V	2 μA cm^{-2}	35	98% (of 20^{th} cycle)	239
13	LiPON	RF MS	2 μm	NA	Overlayer (LiPON or parylene C)/Cu/LiPON/$LiCoO_2$/Au	2D	85 μA h cm^{-2}	3–4.2 V	5 mA cm^{-2}	500	60%	242
14	LiPON	RF MS	7.5 μm; 40 W; Ar;	NA	SUS/Pt/LiPON/$LiCoO_2$/Au	2D	110 mA h g^{-1} 55 μA h cm^{-2} μm^{-1}	2–4.2 V	5 μA cm^{-2}	100	∼81%	243
15	LiPON	RF MS	100 W	0.7–1 μS cm^{-1}	Li/LiPON/$Li_4Ti_5O_{12}$(LTO)	2D	31 μA h cm^{-2}	1–2 V	3.5 μA cm^{-2}	5	∼95%	250
16	LiPON	RF MS	1.5 μm 100 W	NA	Li/LiPON/$LiCoO_2$	2D	22 μA h cm^{-2}	3–4.3 V	80 μA cm^{-2}	1100	100%	222
17	LiPON	RF MS	1.5 μm	NA	Li/LiPON/$LiCoO_2$	2D	60 μA h cm^{-2} μm^{-1}	3–4.2 V	5C	500	100%	223
18	LiPON ($Li_{2.64}P_{1.0}O_{2.81}N_{0.33}$)	RF MS	1.45–1.5 μm 3.53 W cm^{-2}	1.5 μS cm^{-1}	Li/LiPON/$LiCoO_2$	2D	35 μA h cm^{-2} μm^{-1}	3–4.2 V	0.73C	800	85%	224
19	LiPON	RF MS	1.4 μm	NA	Li/LiPON/$LiCoO_2$	2D		3–4.2 V	10 μA cm^{-2}	900	88%	225

Table 2 (*Contd.*)

#	Electrolyte	Preparation method	Preparation conditions notes	Ionic conductivity	Microbattery	Structure (thin film, 2D/3D)	Initial discharge capacity	Voltage range	Current rate	Number of cycles	Retention	Ref.
			350 W				42 μA h cm^{-2} μm^{-1}					
20	LiPON	RF MS	1.5 μm 200 W	NA	Li/LiPON/$LiCoO_2$	2D	63 μA h cm^{-2} μm^{-1} ($V = -50$ V)	3–4.2 V	1C	100	90%	226
21	LiPON	RF MS	1.5 μm	NA	Li/LiPON/$LiCoO_2$	2D	16 μA h	3–5 V	10 μA cm^{-2}	100	50%	308
22	LiPON	NA	NA	NA	Li/LiPON/$LiCoO_2$	2D	106 μA h cm^{-2}	3–4.2 V	46.5 μA cm^{-2}	100	90%	227
23	LiPON	RF MS	*In situ* (no vacuum break); *ex situ*	0.943 μS cm^{-1}	Li/LIPON/V_2O_5	2D	8 μA h 6 μA h	2.7–3.6 V	20 μA cm^{-2}	500	62.5% 58%	232
24	LiPON	RF MS	2.4 μm	NA	Li/LiPON/$LiCo_{0.8}Ni_{0.2}O_2$	2D	62 μA h cm^{-2} μm^{-1}	3–4.2 V	14 μA cm^{-2}	50	86%	234
			35 W		Li/LiPON/$LiCo_{0.8}Zr_{0.2}O_2$		50 μA h cm^{-2} μm^{-1}				98%	
25	LiPON	RF MS	1 μm	2 μS cm^{-1}	Li/LiPON/$LiNi_{0.5}Mn_{1.5}O_4$	2D	122 mA h g^{-1}	3.2–5 V	C/10	10 000	90.6%	230
26	LiPON	RF MS	1 μm 100 mm × 100 mm (cell size) 200 mm × 20 0 mm	NA	V_2O_5/LiPON/$Li_{2-x}Mn_2O_4$	2D	1.1 mA h 8 mA h	0.3–3.5 V	0.4 mA 1 mA	98	81% 69%	240
27	LiPON	RF MS	100 nm	NA	Nb_2O_5/LiPON/$Li_2Mn_2O_4$	2D	500 mA h cm^{-3}	0.3–3.5 V	0.1 mA	500	76%	241
28	LiPON	RF MS	1 μm	NA	Li/LiPON/$LiCoO_2$	2D	65 μA h cm^{-2}	3.3–4.5 V	100 μA cm^{-2}	1800	94%	28
					Li/LiPON/$LiMn_2O_4$		55 μA h cm^{-2}	3–4.2 V		500	77%	
29	LiPON	RF MS	150 W; post anneal. At 550 °C	1.5 μS cm^{-1}	SiNPL/LiPON/$LiFePO_4$	3D; nanopillars	NA	NA	NA	NA	NA	76
30	LiPON	RF MS	5 mTorr	NA	Li/LiPON/$LiCoO_2$	3D, slanted nanowires	96 mA h g^{-1}	3–4.2 V	1C	400	73%	70
31	LiPON	RF MS	2 μm (LiPON)	NA	Li/LiPON/α-MoO_{3-x}	3D, nanoflake arrays	266 mA h g^{-1}	1.5–3.5 V	500 mA g^{-1}	1000	92.7%	79
32	LiPON	RF MS	500 nm (LiPON)	0.25 μS cm^{-1}	Si/LiPON/$LiCoO_2$	3D, microcolumns	25 μA h cm^{-2} 4.5 μA h cm^{-2}	3–4 V	0.16C 1.2C	20	~87.5%	71
33	LiPON	Physical vapor deposition	Nanowires: 2 μm length; 0.5–1 μm diameter	NA	Si/LiPON/$LiCoO_2$	3D, nanowires	NA	NA	NA	NA	NA	72
34	LiPON (Li_2PO_2N)	Atomic layer deposition (ALD)	0.6 Å per cycle; 250 °C	NA	SnN_x/LiPON/LiV_2O_5	3D, pore arrays	30 μA h cm^{-2} (area enhancement factor = 10)	0.5–3.5 V	100 μA cm^{-2}	100	56%	31
35	LiPON	ALD	70 nm (LiPON)	0.5 μS cm^{-1}	Li/LiPON/$Li_4Ti_5O_{12}$	2D	0.3 A h cm^{-3}	0.8–2.6 V	5C	1	NA	271
36	LiPON	ALD	90 nm (LiPON)	0.651 μS cm^{-1}	Si/LiPON/$LiCoO_2$	2D	20 μA h cm^{-3}	2.5–4.2 V	300 μA cm^{-2}	150	80%	273
37	LiPON		N_2, O_2 atm	1.6 μS cm^{-1}	Li/LiPON/$Ag_{0.3}V_2O_5$	2D	40 μA h cm^{-2}	1–3.5 V	7 μA cm^{-2}	100	NA	29

Table 2 (*Contd.*)

#	Electrolyte	Preparation method	Preparation conditions notes	Ionic conductivity	Microbattery	Structure (thin film, 2D/3D)	Initial discharge capacity	Voltage range	Current rate	Number of cycles	Retention	Ref.
		Pulsed laser deposition (PLD)										
38	LiPON	E-beam reaction evaporation	2 μm, nitrogen-plasma assisted deposition	NA	Li/LiPON/0.5Ag:V_2O_5	2D	72 μA h cm^{-2} μm^{-1}	1–3.5 V	7 μA cm^{-2}	20	58%	233
39	LiPON	Metalorganic-chemical vapor deposition (MOCVD)	190 nm	5.3 μS cm^{-1}	Si/LiPON/$LiCoO_2$	2D	5.2 μA h cm^{-2}	2.8–3.8 V	12.7 μA cm^{-2}	1	NA	32
40	LiPONB	RF MS	2.0 W cm^2; Li_3PO_4–$LiBO_2$ 95/5	2.6 μS cm^{-1}	Li/LiPONB/TiO_yS_z	2D	90 μA h cm^{-2} μm^{-1}	1–3 V	100 μA cm^{-2}	500	89%	245
41	LiPONB	RF MS	50 W (Li_3PO_4)	1.628 μS cm^{-1}	Li/LiPONB/$LiCoO_2$	2D	34.5 μA h cm^{-2}	3.4–4.2 V	10 μA cm^{-2}	15	95.3%	246
42	LiPONB	RF MS	1.4 μm; 2 W cm^{-2}	NA	Si/LIPONB/Li	2D	40 μA h cm^{-2} 571 μA h cm^{-2} μm^{-1}	0.05–1 V	100 μA cm^{-2} (2C)	1500	~100%	247
43	$Li_{3.09}BO_{2.53}N_{0.52}$ (LiBON)	RF MS	3.53 W cm^{-2}	NA	Li/LiBON/$LiCoO_2$	2D	55 μA h cm^{-2} μm^{-1}	2.8–4.2 V	1C	1000	90%	12
44	Li_2O–V_2O_5–SiO_2 (LVSO)	RF MS	1 : 1 Ar/O_2 atm; 100 W; 50 °C	1 μS cm^{-1}	Li/LVSO/MoO_3	2D	400 μA h cm^{-2}	1.5–3.5 V	10 μA cm^{-2}	40	72.5%	287
45	LVSO	PLD	1 : 1 Ar/O_2 atm; 100 W; 50 °C	NA	SnO/LVSO/$LiCoO_2$ SnO/LVSO/$LiMn_2O_4$	2D	9 μA h cm^{-2} 1.5 μA h cm^{-2}	2–3 V 1–3 V	4.4 μA cm^{-2}	3	85% 93%	288
46	LVSO	PLD	1 : 1 Ar/O_2 atm; 100 W; c	0.3 μS cm^{-1}	SnO/LVSO/$LiCoO_2$	2D	NA	1.4–3.5 V	4.4 μA cm^{-2}	10	NA	290
47	$Li_{3.4}V_{0.6}Si_{0.4}O_4$ (LVSO)	Solid state reaction	NA	NA	SnO/LVSO/ $LiNi_{0.8}Co_{0.2}O_2$	2D	20 μA h cm^{-2} μm^{-1}	0–3 V	NA	20	84%	289
48	Polymethyl methacrylate–polyethylene glycol (PMMA–PEG)	Drop casting	19 μm (PMMA–PEG)	NA	TiO_2nts/PMMA–PEG/ $LiNi_{0.5}Mn_{1.5}O_4$ (LNMO)	3D, nanotubes (nts)	30 μA h cm^{-2} μm^{-1} (=80 mA h g^{-1})	1–3.3 V	C/10	35	91.5%	73
49	PMMA–PEG	Electrodeposition of nts + drop casting	Cyclic voltammetry	NA	TiO_2nts/PMMA–PEG/ $LiNi_{0.5}Mn_{1.5}O_4$ (LNMO)	3D, nanotubes (nts)	175 mA h g^{-1}	1–3.3 V	C/10	10	88%	74
50	PMMA–PEG	Electrodeposition	1 μm	NA	Li/PEO–PMMA(LiTFSI)/ TiO_2nts	3D, nanotubes (nts)	190 μA h cm^{-2} μm^{-1} (1^{st} cycle) 83 μA h cm^{-2} μm^{-1} (2^{nd} cycle)	0.5–2.6 V	C/5	50	78%	301
51	PMMA–PEG	Electrodeposition	100 electropolymerization cycles	NA	TiO_2nts/PMMA–PEG/ LNMO	3D, nanotubes (nts)	125 mA h g^{-1}	1–3.3 V	C/10	10	72%	75
52	SiO_2–PEG	Sol–gel; organic polymerization	0.8–1 μm	26 μS cm^{-1}	Li/SiO_2–PEG/ $Li_4Ti_5O_{12}$	2D	2.7 mA h g^{-1}	1–2 V	1 mA cm^{-2}	500	30%	63
53	PEG based BAB block	Prepared by Nippon Soda Company Limited	NA	0.2 mS cm^{-1}	$Li_{4/3}Ti_{5/3}O_4$/PEG-BAB/$LiMn_2O_4$	2D	8.48 μW h cm^{-2}	1.6–2.7 V	NA	1	NA	64
54	LiTFSI in MA-PEG500	Spin-coating	NA	0.4 mS cm^{-1}			1 mA h cm^{-2}	1–3.5 V	C/2	100	80%	83

Table 2 (*Contd.*)

#	Electrolyte	Preparation method	Preparation conditions notes	Ionic conductivity	Microbattery	Structure (thin film, 2D/3D)	Initial discharge capacity	Voltage range	Current rate	Number of cycles	Retention	Ref.
					$Li_4Ti_5O_{12}$/LiTFSI-MA-PEG500/$LiNi_{0.5}Mn_{1.5}O_4$	3D, micropillars						
55	SU-8	Photolithography	Structure similar to PEG	0.1–0.3 μS cm^{-1}	Si/SU-8/$LiNi_{0.8}Co_{0.15}Al_{0.05}O_2$ (NCA)	3D, arrays	0.55 mA h cm^{-2}	2.6–3.7 V	0.22 mA cm^{-2}	100	93%	82
56	Poly(ether amine) (PEA)-based monomer	Chemical reaction, solution casting on electrode	1 μm	8 μS cm^{-1}	Li/SPE/$LiFePO_4$	2D	140 mA h g^{-1}	2.2–4.2 V	C/50; cycled at 60 °C	12	21%	103
57	Poly(trimethylene carbonate) (PTMC)	Chemical reaction, dip coating	Functionalized by caprolactone (CL); <5 μm	NA	Li/P(TMC-CL)–LiTFSI/Cu_2O (nanopillar)	3D, nanopillars	0.2 mA h cm^{-2}	0.2–3.2 V	0.008 mA cm^2	10	95%	104
58	*P*-Sulfonated poly(allyl phenyl ether) (SPAPE)	Electrodeposition	300 nm	NA	Li/SPAPE/TiO_2nts	3D, nanotubes	88 μA h cm^{-2}	1–3 V	C/8	4	60%	96
59	SPAPE	Electrodeposition	NA	NA	Li/SPAPE/CNT	3D, nanotubes	11 000 mA h g^{-1} (1^{st} cycle) 1600 mA h g^{-1} (2^{nd} cycle)	0.01–2 V	1C	50	50% (of 2^{nd} cycle)	110
60	Poly(propylene glycol) diacrylate (PPDGA) and polyetheramine (glyceryl poly(oxypropylene)) (PEA) blend with LiTFSI	Drop casting	NA	NA	Li/PPDGA–PEA–LiTFSI/Cu_2Sb	3D, nanopillar	0.3 mA h cm^{-2} (1^{st} cycle) 0.15 mA h cm^{-2} (2^{nd} cycle)	0.01–1.5 V	C/50; cycled at 60 °C	50	50%	105
61	Poly(vinylidene fluoride-hexafluoro propylene) (PVDF-HFP)	Solvent casting	Addition of $LiPF_6$	NA	Li/PVDF-HFP(gel)/$LiCoO_2$	2D	164 μA h cm^{-2}	3–4.2 V	20 μA cm^{-2}	1	NA	115
62	Gel polymer electrolyte (GPE): (PVdF-HFP, P13FSI-pyrrolidinium bis(fluorosulfonyl)imide, LiTFSI)	Hand casting	Electrolyte prepared by chemical reaction	1.88 mS cm^{-1}	Li/GPE/$LiCoO_2$	2D	264 μA h cm^{-2}	3–4.2 V	333 μA cm^{-2}	30	98.9%	116
					pSi/GPE/$LiCoO_2$		226 μA h cm^{-2}	0–1.2 V	17 μA cm^{-2}	32	80%	
					Li/GPE/pSi-Cu		270 μA h cm^{-2}		400 μA cm^{-2}	30	93%	
63	GPE: PEO, LiTFSI, 1,3-dioxolane (DOL), and 1,2-dimethoxyethane (DME)	Drop casting	Stepwise infiltration of GPE components	4 mS cm^{-1}	Li/GPE/V_2O_5	3D, interdigitated	0.15 mA h cm^{-2}	1.5–3.7 V	1C	550	73%	78
64	GPE: ethoxylated trimethylolpropane triacrylate (ETPTA) polymer matrix, liquid electrolyte (1 M $LiPF_6$ in ethylene carbonate (EC)/propylene carbonate (PC) = 1/1 (v/v)), and Al_2O_3 nanoparticles	UV-curing	18 μm	1 mS cm^{-1}	Si pillars/GPE/Li	3D, micropillars	2680 mA h g^{-1}	0.01–1.5 V	0.5C	10	26%	113

Table 2 (*Contd.*)

#	Electrolyte	Preparation method	Preparation conditions notes	Ionic conductivity	Microbattery	Structure (thin film, 2D/3D)	Initial discharge capacity	Voltage range	Current rate	Number of cycles	Retention	Ref.
65	Ionogel (PYR13-Li-TFSI: *N*-methyl-*N*-propylpyrrolidinium bis(trifluoromethan) suflonylimide and LiTFSI)	Ink-jetting	NA	~0.05 S cm^{-1}	$LiFePO_4$/ionogel/ $Li_4Ti_5O_{12}$	2D	300 μA h cm^{-2}	1.5–2.5 V	C/10	100	85%	14
66	Solid polymer electrolyte (SPE): dimethacrylic oligomer bisphenol A ethoxylate dimethacrylate (BEMA), diluent poly(ethyleneglycol) methyl ether methacrylate (PEGMA), ethylene carbonate/ diethyl carbonate (EC/DEC) and LiTFSI	UV-induced photo-polymerization deposition	25 ± 5 μm	NA	Li/SPE/V_2O_5	2D	130 mA h g^{-1}	2.5–3.8 V	1.5C	300	96%	91
67	Composite polymer electrolyte (CPE): $LiI_1P(EO)_{20}EC$, 12% (v/v) Al_2O_3	NA	NA	NA	Li/CPE/FeS_{1+x}	2D	50 mA h	1–2.3 V	50 μA cm^{-2}	650	61%	117
68	Poly(phenylene oxide) (PPO)	Electrodeposition	10–15 nm	NA	3D carbon/PPO/V_2O_5 gel	3D, microporous anode	9 mA h g^{-1}	1.6–3.3 V	10–20 μA	10	11%	80
69	Poly(phenylene oxide) (PPO)	Electrodeposition	10 nm	NA	Mesoporous carbon/ PPO/lithium sulfide	3D, gyroid	0.225 mA h cm^{-2}	1.5–3 V	0.125 mA cm^{-2}	10	~100%	81
70	Li_3PO_4	PLD	4 J cm^{-2}	0.33 μS cm^{-1}	Li/Li_3PO_4/$LiCoO_2$ SnO/LVSO/$LiCoO_2$	2D	10 μA h cm^{-2} 5.5 μA h cm^{-2}	2–4.2 V	166 μA cm^{-2}	20	100% 33%	309
71	Li_3PO_4	PLD	300 mJ	0.8 μS cm^{-1}	Li/Li_3PO_4/$LiCoO_2$	2D	60 μA h cm^{-2}	3–4.4 V	69 μA cm^{-2}	10	98%	268
72	Li_3PO_4	ALD	2 mbar	0.62 μS cm^{-1}	Li/Li_3PO_4/TiO_2	3D, microtubes (MT)	100 μA h cm^{-2} (double DMT) 300 μA h cm^{-2} (single SMT)	1.1–2.3 V	C/10 C/16	20	~100%	274
73	Li_4SiO_4	Prepared by Wako Pure Chemical Industries, Ltd	NA	0.4 μS cm^{-1}	Li/Li_4SiO_4/$LiCoO_2$	2D	10 μA h cm^{-2}	3–4.2 V	NA	77	96.6%	310
74	Li_2O–SiO_2–P_2O_5 (LiSiPON)	RF MS	N_2; 75 W	8.8 μS cm^{-1}	$Si_{0.7}V_{0.3}$/ $Li_{1.9}Si_{0.28}P_{1.0}O_{1.1}N_{1.0}$/ $LiCoO_2$	2D	60 μA h cm^{-2} μm^{-1}	2–3.9 V	10 μA	1500	83%	295
75	$Li_{3x}La_{2/3-x}TiO_3$ (LLTO)	Solid-state reaction, e-beam evaporation on electrode	1500 nm (LLTO)	0.18 μS cm^{-1}	Li/LiPON/LLTO/ $LiCoO_2$	2D	50 μA h cm^{-2} μm^{-1}	3–4 V	7 μA cm^{-2}	100	50%	190

instabilities, preventing their wide usage in commercial microbatteries.

Thus, many investigations have been done on glass-based electrolytes, especially LiPON, which, among the various candidates, satisfies most of the criteria for the appropriate electrolyte, such as low electronic conductivity, good chemical, electrochemical, thermal and mechanical stabilities, relatively low interfacial resistances, and good processability (Fig. 10b). However, the critical parameter of LiPON's ionic conductivity is still significantly lower (10^{-7} S cm^{-1}) than standard liquid electrolytes' (10^{-2} S cm^{-1}). Although it is less critical for microbatteries with a very thin layer of electrolyte and short Li ion diffusion path length, several studies have been focusing on the improvement of this and other stability parameters by varying deposition conditions, integrating boron in the LiPON structure, and others, which were discussed in this review. Moreover, analysing the various deposition techniques of LiPON and the performance of these films in microbatteries, it was found that up until now, RF sputtering remains the prevailing method due to a higher quality of films and a less complex and energy-demanding process. However, the emerging techniques like ALD show promising results especially for 3D high-aspect-ratio structures (Fig. 11). The other glass electrolytes, such as sulphide-based, although having higher ionic conductivity (up to 10^{-3} S cm^{-1}), showed unfavourable electrochemical instabilities. Generally, up until now, LiPON remained as one of the most examined and the most successful candidates for solid-state microbatteries, showing good performance in several innovative 3D structures and especially in thin-film 2D designs (Fig. 10c). However, the other electrolytes with higher ionic conductivities are under the investigation of various research groups all over the world, which put a lot of effort to tackle the existing challenges. Table 2 summarizes all critical information on Li solid electrolytes and their integration in microbatteries including the electrolyte composition, ionic conductivity, preparation methods and conditions, microbattery electrodes, structure, electrochemical test conditions, and performance in order to find favourable electrolyte candidates and their microbattery structures with high capacity and long cycle life.

To sum up, this review has provided information on many aspects of solid electrolytes used in various microbatteries, covering the recent advancements, performance, and current issues of such structures. To significantly improve solid-state microbatteries, it is vital to face the ongoing situation with solid electrolytes and resolve their problems. Therefore, this review objectively summarizes the information on existing studies that will help researchers to understand the actual status of solid electrolytes and find new solutions to their further development and integration in high-performance solid microbatteries.

Author contributions

A. J., A. M., B. U. conceived the idea, gathered data, analysed, processed it, and wrote the manuscript; S.-T. M. and Z. B. supervised and organized the work, revised the manuscript and assisted in the data processing and analysis. A. M. and Z. B. secured funding for this work.

Conflicts of interest

There are no conflicts to declare.

Acknowledgements

This work was supported by a research grant AP08052231 "Development of solid-state electrolytes with high ionic conductivity for the next generation of lithium-ion batteries" from the Ministry of Education and Science of the Republic of Kazakhstan and a research project No. SOE2019001 "Development of 3D solid state thin film materials for durable and safe Li-ion microbatteries" from Nazarbayev University.

References

1 S. Ferrari, M. Loveridge, S. D. Beattie, M. Jahn, R. J. Dashwood and R. Bhagat, *J. Power Sources*, 2015, **286**, 25–46.
2 W. Li, T. L. Christiansen, C. Li, Y. Zhou, H. Fei, A. Mamakhel, B. B. Iversen and J. J. Watkins, *Nano Energy*, 2018, **52**, 431–440.
3 M. Nathan, D. Golodnitsky, V. Yufit, E. Strauss, T. Ripenbein, I. Shechtman, S. Menkin and E. Peled, *J. Microelectromech. Syst.*, 2005, **14**, 879–885.
4 D. Golodnitsky, M. Nathan, V. Yufit, E. Strauss, K. Freedman, L. Burstein, A. Gladkich and E. Peled, *Solid State Ionics*, 2006, **177**, 2811–2819.
5 N. Nitta, F. Wu, J. T. Lee and G. Yushin, *Mater. Today*, 2015, **18**, 252–264.
6 M. Li, J. Lu, Z. Chen and K. Amine, *Adv. Mater.*, 2018, **30**, 1–24.
7 Y. Wang, B. Liu, Q. Li, S. Cartmell, S. Ferrara, Z. D. Deng and J. Xiao, *J. Power Sources*, 2015, **286**, 330–345.
8 N. J. Dudney, *Electrochem. Soc. Interface*, 2008, **17**, 44–48.
9 J. W. Long, B. Dunn, D. R. Rolison and H. S. White, *Chem. Rev.*, 2004, **104**, 4463–4492.
10 J. W. Long, B. Dunn, D. R. Rolison and H. S. White, *Adv. Energy Mater.*, 2020, **10**, 1–6.
11 F. Xu, N. J. Dudney, G. M. Veith, Y. Kim, C. Erdonmez, W. Lai and Y. M. Chiang, *J. Mater. Res.*, 2010, **25**, 1507–1515.
12 S. W. Song, K. C. Lee and H. Y. Park, *J. Power Sources*, 2016, **328**, 311–317.
13 J. H. Pikul, H. Gang Zhang, J. Cho, P. V. Braun and W. P. King, *Nat. Commun.*, 2013, **4**, 1732–1735.
14 P. E. Delannoy, B. Riou, B. Lestriez, D. Guyomard, T. Brousse and J. Le Bideau, *J. Power Sources*, 2015, **274**, 1085–1090.
15 T. Zhang, W. He, W. Zhang, T. Wang, P. Li, Z. M. Sun and X. Yu, *Chem. Sci.*, 2020, **11**, 8686–8707.
16 Y. Zhu, J. C. Gonzalez-Rosillo, M. Balaish, Z. D. Hood, K. J. Kim and J. L. M. Rupp, *Nat. Rev. Mater.*, 2020, 1–19.

17 Y. Zheng, Y. Yao, J. Ou, M. Li, D. Luo, H. Dou, Z. Li, K. Amine, A. Yu and Z. Chen, *Chem. Soc. Rev.*, 2020, **49**, 8790–8839.
18 F. Zheng, M. Kotobuki, S. Song, M. O. Lai and L. Lu, *J. Power Sources*, 2018, **389**, 198–213.
19 H. Xia, H. L. Wang, W. Xiao, M. O. Lai and L. Lu, *Int. J. Surf. Sci. Eng.*, 2009, **3**, 23–43.
20 C. H. Chen, S. Xie, E. Sperling, A. S. Yang, G. Henriksen and K. Amine, *Solid State Ionics*, 2004, **167**, 263–272.
21 F. Han, A. S. Westover, J. Yue, X. Fan, F. Wang, M. Chi, D. N. Leonard, N. J. Dudney, H. Wang and C. Wang, *Nat. Energy*, 2019, **4**, 187–196.
22 V. Thangadurai and W. Weppner, *Ionics*, 2006, **12**, 81–92.
23 D. Grazioli, V. Zadin, D. Brandell and A. Simone, *Electrochim. Acta*, 2019, **296**, 1142–1162.
24 Y. Chen, K. Wen, T. Chen, X. Zhang, M. Armand and S. Chen, *Energy Storage Mater.*, 2020, **31**, 401–433.
25 K. J. Kim, M. Balaish, M. Wadaguchi, L. Kong and J. L. M. Rupp, *Adv. Energy Mater.*, 2021, **11**, 1–63.
26 R. C. Xu, X. H. Xia, S. Z. Zhang, D. Xie, X. L. Wang and J. P. Tu, *Electrochim. Acta*, 2018, **284**, 177–187.
27 X. Yu, J. B. Bates, G. E. Jellison and F. X. Hart, *J. Electrochem. Soc.*, 1997, **144**, 524–532.
28 N. J. Dudney, *Mater. Sci. Eng., B*, 2005, **116**, 245–249.
29 C. M. Julien and A. Mauger, *Coatings*, 2019, **9**, 386.
30 F. Vereda, R. B. Goldner, T. E. Haas and P. Zerigian, *Electrochem. Solid-State Lett.*, 2002, **5**, 239–241.
31 A. Pearse, T. Schmitt, E. Sahadeo, D. M. Stewart, A. Kozen, K. Gerasopoulos, A. A. Talin, S. B. Lee, G. W. Rubloff and K. E. Gregorczyk, *ACS Nano*, 2018, **12**, 4286–4294.
32 T. Fujibayashi, Y. Kubota, K. Iwabuchi and N. Yoshii, *AIP Adv.*, 2017, **7**, 085110.
33 C. Chen, R. A. Eichel and P. H. L. Notten, *J. Electroceram.*, 2017, **38**, 230–247.
34 E. Quartarone and P. Mustarelli, *Chem. Soc. Rev.*, 2011, **40**, 2525–2540.
35 A. Levasseur, M. Menetrier, R. Dormoy and G. Meunier, *Mater. Sci. Eng., B*, 1989, **3**, 5–12.
36 X. Liang, F. Tan, F. Wei and J. Du, *IOP Conf. Ser.: Earth Environ. Sci.*, 2019, **218**, 012138.
37 J. F. M. Oudenhoven, L. Baggetto and P. H. L. Notten, *Adv. Energy Mater.*, 2011, **1**, 10–33.
38 M. Balaish, J. C. Gonzalez-Rosillo, K. J. Kim, Y. Zhu, Z. D. Hood and J. L. M. Rupp, *Nat. Energy*, 2021, **6**, 227–239.
39 L. Liu, Q. Weng, X. Lu, X. Sun, L. Zhang and O. G. Schmidt, *Small*, 2017, **13**, 1–12.
40 T. M. Clancy and J. F. Rohan, *J. Energy Storage*, 2019, **23**, 1–8.
41 C. Yue, J. Li and L. Lin, *Front. Mech. Eng.*, 2017, **12**, 459–476.
42 C. M. Julien, A. Mauger and O. M. Hussain, *Materials*, 2019, **12**, 1–26.
43 J. Liu, H. Zhu and M. H. A. Shiraz, *Front. Energy Res.*, 2018, **6**, 1–5.
44 X. Meng, *Energy Storage Mater.*, 2020, **30**, 296–328.
45 B. O'Regan and M. Grätzel, *Nature*, 1991, **353**, 737–740.
46 I. B. Sprague and P. Dutta, *Appl. Phys. Lett.*, 2012, **101**, 113903.
47 Y. Yang, K. C. Pradel, Q. Jing, J. M. Wu, F. Zhang, Y. Zhou, Y. Zhang and Z. L. Wang, *ACS Nano*, 2012, **6**, 6984–6989.
48 W. C. West, J. F. Whitacre, V. White and B. V. Ratnakumar, *J. Micromech. Microeng.*, 2002, **12**, 58–62.
49 J. Ni, A. Dai, Y. Yuan, L. Li and J. Lu, *Matter*, 2020, **2**, 1366–1376.
50 R. Salot, S. Martin, S. Oukassi, M. Bedjaoui and J. Ubrig, *Appl. Surf. Sci.*, 2009, **256**, 54–57.
51 J. P. Carmo, R. P. Rocha, A. F. Silva, L. M. Goncalves and J. H. Correia, *Procedia Chem.*, 2009, **1**, 453–456.
52 D. Li, Z. Ma, J. Xu, Y. Li and K. Xie, *Mater. Lett.*, 2014, **134**, 237–239.
53 S. Shiraki, H. Oki, Y. Takagi, T. Suzuki, A. Kumatani, R. Shimizu, M. Haruta, T. Ohsawa, Y. Sato, Y. Ikuhara and T. Hitosugi, *J. Power Sources*, 2014, **267**, 881–887.
54 N. J. Dudney and Y. Il Jang, *J. Power Sources*, 2003, **119–121**, 300–304.
55 Y. N. Zhou, M. Z. Xue and Z. W. Fu, *J. Power Sources*, 2013, **234**, 310–332.
56 J. B. Bates, N. J. Dudney, B. Neudecker, A. Ueda and C. D. Evans, *Solid State Ionics*, 2000, **135**, 33–45.
57 B. Laïk, I. Ressejac, C. Venet and J. P. Pereira-Ramos, *Thin Solid Films*, 2018, **649**, 69–74.
58 D. L. Xiao, J. Tong, Y. Feng, G. H. Zhong, W. J. Li and C. L. Yang, *Solid State Ionics*, 2018, **324**, 202–206.
59 J. B. Bates, N. J. Dudney, G. R. Gruzalski, R. A. Zuhr, A. Choudhury, C. F. Luck and J. D. Robertson, *J. Power Sources*, 1993, **43**, 103–110.
60 J. F. Whitacre and W. C. West, *Solid State Ionics*, 2004, **175**, 251–255.
61 H. S. Kim, Y. Oh, K. H. Kang, J. H. Kim, J. Kim and C. S. Yoon, *ACS Appl. Mater. Interfaces*, 2017, **9**, 16063–16070.
62 T. J. Cai, Y. H. Lo and J. J. Wu, *Mater. Today Energy*, 2019, **13**, 119–124.
63 J. F. Vélez, M. Aparicio and J. Mosa, *Electrochim. Acta*, 2016, **213**, 831–841.
64 H. Nakano, K. Dokko, J. ichi Sugaya, T. Yasukawa, T. Matsue and K. Kanamura, *Electrochem. Commun.*, 2007, **9**, 2013–2017.
65 J. B. Bates, N. J. Dudney, G. R. Gruzalski, R. A. Zuhr, A. Choudhury, C. F. Luck and J. D. Robertson, *Solid State Ionics*, 1992, **53–56**, 647–654.
66 V. Zadin, H. Kasemägi, A. Aabloo and D. Brandell, *J. Power Sources*, 2010, **195**, 6218–6224.
67 S. Moitzheim, B. Put and P. M. Vereecken, *Adv. Mater. Interfaces*, 2019, **6**, 1–17.
68 B. L. Ellis, P. Knauth and T. Djenizian, *Adv. Mater.*, 2014, **26**, 3368–3397.
69 R. W. Hart, H. S. White, B. Dunn and D. R. Rolison, *Electrochem. Commun.*, 2003, **5**, 120–123.
70 M. Yoon, S. Lee, D. Lee, J. Kim and J. Moon, *Appl. Surf. Sci.*, 2017, **412**, 537–544.
71 A. A. Talin, D. Ruzmetov, A. Kolmakov, K. McKelvey, N. Ware, F. El Gabaly, B. Dunn and H. S. White, *ACS Appl. Mater. Interfaces*, 2016, **8**, 32385–32391.

72 D. Ruzmetov, V. P. Oleshko, P. M. Haney, H. J. Lezec, K. Karki, K. H. Baloch, A. K. Agrawal, A. V. Davydov, S. Krylyuk, Y. Liu, J. Huang, M. Tanase, J. Cumings and A. A. Talin, *Nano Lett.*, 2012, **12**, 505–511.
73 N. Plylahan, M. Letiche, M. K. S. Barr and T. Djenizian, *Electrochem. Commun.*, 2014, **43**, 121–124.
74 G. D. Salian, C. Lebouin, A. Demoulin, M. S. Lepihin, S. Maria, A. K. Galeyeva, A. P. Kurbatov and T. Djenizian, *J. Power Sources*, 2017, **340**, 242–246.
75 G. D. Salian, C. Lebouin, A. Galeyeva, A. P. Kurbatov and T. Djenizian, *Front. Chem.*, 2019, **7**, 1–8.
76 C. Lethien, M. Zegaoui, P. Roussel, P. Tilmant, N. Rolland and P. A. Rolland, *Microelectron. Eng.*, 2011, **88**, 3172–3177.
77 Y. He, S. Chen, L. Nie, Z. Sun, X. Wu and W. Liu, *Nano Lett.*, 2020, **20**, 7136–7143.
78 P. Sun, X. Li, J. Shao and P. V. Braun, *Adv. Mater.*, 2020, **2006229**, 1–7.
79 S. Sun, Q. Xia, J. Liu, J. Xu, F. Zan, J. Yue, S. V. Savilov, V. V. Lunin and H. Xia, *J. Materiomics*, 2019, **5**, 229–236.
80 N. S. Ergang, M. A. Fierke, Z. Wang, W. H. Smyrl and A. Stein, 2007, 1135–1139.
81 J. G. Werner, G. G. Rodríguez-Calero, H. D. Abruña and U. Wiesner, *Energy Environ. Sci.*, 2018, **11**, 1261–1270.
82 J. I. Hur, L. C. Smith and B. Dunn, *Joule*, 2018, **2**, 1187–1201.
83 M. Nasreldin, R. Delattre, C. Calmes, M. Ramuz, V. A. Sugiawati, S. Maria, J. L. de B. de la Tocnaye and T. Djenizian, *Energy Storage Mater.*, 2020, **33**, 108–115.
84 D. Fang, K. Huang, S. Liu and Z. Li, *J. Alloys Compd.*, 2008, **464**, L5.
85 W. Wei, G. Oltean, C. W. Tai, K. Edström, F. Björefors and L. Nyholm, *J. Mater. Chem. A*, 2013, **1**, 8160–8169.
86 T. Djenizian, I. Hanzu and P. Knauth, *J. Mater. Chem.*, 2011, **21**, 9925–9937.
87 J. Xie, J. F. M. Oudenhoven, D. Li, C. Chen, R.-A. Eichel and P. H. L. Notten, *J. Electrochem. Soc.*, 2016, **163**, A2385–A2389.
88 S. Moitzheim, J. E. Balder, R. Ritasalo, S. Ek, P. Poodt, S. Unnikrishnan, S. De Gendt and P. M. Vereecken, *ACS Appl. Energy Mater.*, 2019, **2**, 1774–1783.
89 Q. Zhang, K. Liu, F. Ding and X. Liu, *Nano Res.*, 2017, **10**, 4139–4174.
90 Q. Zhou, J. Zhang and G. Cui, *Macromol. Mater. Eng.*, 2018, **303**, 1–14.
91 C. Gerbaldi, M. Destro, J. R. Nair, S. Ferrari, I. Quinzeni and E. Quartarone, *Nano Energy*, 2013, **2**, 1279–1286.
92 K. S. Ngai, S. Ramesh, K. Ramesh and J. C. Juan, *Ionics*, 2016, **22**, 1259–1279.
93 K. Murata, S. Izuchi and Y. Yoshihisa, *Electrochim. Acta*, 2000, **45**, 1501–1508.
94 R. C. Agrawal and G. P. Pandey, *J. Phys. D: Appl. Phys.*, 2008, **41**, 223001.
95 Z. Ogumi, *J. Electrochem. Soc.*, 1989, **136**, 625.
96 I. V. Ferrari, M. Braglia, T. Djenizian, P. Knauth and M. L. Di Vona, *J. Power Sources*, 2017, **353**, 95–103.
97 Y. Ito, K. Syakushiro, M. Hiratani, K. Miyauchi and T. Kudo, *Solid State Ionics*, 1986, **18–19**, 277–281.
98 N. Boaretto, L. Meabe, M. Martinez-Ibañez, M. Armand and H. Zhang, *J. Electrochem. Soc.*, 2020, **167**, 070524.
99 P. Yao, H. Yu, Z. Ding, Y. Liu, J. Lu, M. Lavorgna, J. Wu and X. Liu, *Front. Chem.*, 2019, **7**, 1–17.
100 S. B. Aziz, T. J. Woo, M. F. Z. Kadir and H. M. Ahmed, *J. Sci.: Adv. Mater. Devices*, 2018, **3**, 1–17.
101 R. Bernhard, A. Latini, S. Panero, B. Scrosati and J. Hassoun, *J. Power Sources*, 2013, **226**, 329–333.
102 L. Han, M. L. Lehmann, J. Zhu, T. Liu, Z. Zhou, X. Tang, C. Te Heish, A. P. Sokolov, P. Cao, X. C. Chen and T. Saito, *Front. Energy Res.*, 2020, **8**, 1–19.
103 B. Sun, I. Y. Liao, S. Tan, T. Bowden and D. Brandell, *J. Power Sources*, 2013, **238**, 435–441.
104 B. Sun, H. D. Asfaw, D. Rehnlund, J. Mindemark, L. Nyholm, K. Edström and D. Brandell, *ACS Appl. Mater. Interfaces*, 2018, **10**, 2407–2413.
105 S. Tan, E. Perre, T. Gustafsson and D. Brandell, *Solid State Ionics*, 2012, **225**, 510–512.
106 S. Tan, S. Walus, J. Hilborn, T. Gustafsson and D. Brandell, *Electrochem. Commun.*, 2010, **12**, 1498–1500.
107 N. Plylahan, S. Maria, T. N. T. Phan, M. Letiche, H. Martinez, C. Courrèges, P. Knauth and T. Djenizian, *Nanoscale Res. Lett.*, 2014, **9**, 1–8.
108 N. A. Kyerematen, F. Dumur, P. Knauth, B. Pecquenard and T. Djenizian, *C. R. Chim.*, 2013, **16**, 80–88.
109 M. E. Abdelhamid, T. Rüther, J.-P. Veder, T. Rodopoulos, A. I. Bhatt, J. Lee, A. F. Hollenkamp, M. D. Horne, T. Huynh, A. Ong, K. J. Putman, G. Rowe and P. de Souza, *J. Electrochem. Soc.*, 2019, **166**, A5462–A5469.
110 V. A. Sugiawati, F. Vacandio, Y. Ein-Eli and T. Djenizian, *APL Mater.*, 2019, **7**, 031506.
111 W. Li, L. C. Bradley and J. J. Watkins, *ACS Appl. Mater. Interfaces*, 2019, **11**, 5668–5674.
112 R. He, M. Echeverri, D. Ward, Y. Zhu and T. Kyu, *J. Membr. Sci.*, 2016, **498**, 208–217.
113 E. H. Kil, K. H. Choi, H. J. Ha, S. Xu, J. A. Rogers, M. R. Kim, Y. G. Lee, K. M. Kim, K. Y. Cho and S. Y. Lee, *Adv. Mater.*, 2013, **25**, 1395–1400.
114 Y. Kang, H. J. Kim, E. Kim, B. Oh and J. H. Cho, *J. Power Sources*, 2001, **92**, 255–259.
115 M. S. Park, S. H. Hyun, S. C. Nam and S. B. Cho, *Electrochim. Acta*, 2008, **53**, 5523–5527.
116 V. Chaudoy, E. Luais, F. Ghamouss, T. Defforge, S. Desplobain, G. Gautier, J. Wolfman, J.-C. Houdbert, F. Tran-Van and J. Sakai, *ECS Trans.*, 2015, **66**, 31–39.
117 V. Yufit, K. Freedman, M. Nathan, L. Burstein, D. Golodnitsky and E. Peled, *Electrochim. Acta*, 2004, **50**, 417–420.
118 D. S. Ashby, C. S. Choi, M. A. Edwards, A. A. Talin, H. S. White and B. S. Dunn, *ACS Appl. Energy Mater.*, 2020, **3**, 8402–8409.
119 D. S. Ashby, R. H. DeBlock, C. H. Lai, C. S. Choi and B. S. Dunn, *Joule*, 2017, **1**, 344–358.
120 J. W. Fergus, *J. Power Sources*, 2010, **195**, 4554–4569.
121 L. Ye and Z. Feng, *Polym. Electrolytes*, 2010, 550–582.
122 Y. Zhao, L. Wang, Y. Zhou, Z. Liang, N. Tavajohi, B. Li and T. Li, *Adv. Sci.*, 2021, **2003675**, 2003675.

123 P. Kurzweil and J. Garche, *Overview of batteries for future automobiles*, Elsevier B.V., 2017.
124 M. J. C. Plancha, *Polym. Electrolytes*, 2010, 340–377.
125 K. Hayamizu, A. Yuichi, W. S. Price, N. Hiroe and N. Toshiyuki, *J. Phys. Chem. B*, 2004, **108**, 19527–19532.
126 K. E. Thomas, S. E. Sloop, J. B. Kerr and J. Newman, *J. Power Sources*, 2000, **89**, 132–138.
127 W. Gorecki, M. Jeannin, E. Belorizky, C. Roux and M. Armand, *J. Phys.: Condens. Matter*, 1995, **7**, 6823–6832.
128 O. Borodin and G. D. Smith, *Macromolecules*, 2006, **39**, 1620–1629.
129 R. Bouchet, S. Maria, R. Meziane, A. Aboulaich, L. Lienafa, J. P. Bonnet, T. N. T. Phan, D. Bertin, D. Gigmes, D. Devaux, R. Denoyel and M. Armand, *Nat. Mater.*, 2013, **12**, 452–457.
130 M. Doyle, T. F. Fuller and J. Newman, *Electrochim. Acta*, 1994, **39**, 2073–2081.
131 J. Mindemark, B. Sun, E. Törmä and D. Brandell, *J. Power Sources*, 2015, **298**, 166–170.
132 B. Sun, J. Mindemark, E. V. Morozov, L. T. Costa, M. Bergman, P. Johansson, Y. Fang, I. Furó and D. Brandell, *Phys. Chem. Chem. Phys.*, 2016, **18**, 9504–9513.
133 M. Zhang, S. Yu, Y. Mai, S. Zhang and Y. Zhou, *Chem. Commun.*, 2019, **55**, 6715–6718.
134 Q. Ma, H. Zhang, C. Zhou, L. Zheng, P. Cheng, J. Nie, W. Feng, Y. S. Hu, H. Li, X. Huang, L. Chen, M. Armand and Z. Zhou, *Angew. Chem., Int. Ed.*, 2016, **55**, 2521–2525.
135 B. M. Savoie, M. A. Webb and T. F. Miller, *J. Phys. Chem. Lett.*, 2017, **8**, 641–646.
136 L. Wang, J. Li, G. Lu, W. Li, Q. Tao, C. Shi, H. Jin, G. Chen and S. Wang, *Front. Mater.*, 2020, **7**, 1–5.
137 K. J. Kim, J. J. Hinricher and J. L. M. Rupp, *Nat. Energy*, 2020, **5**, 278–279.
138 M. V. Reddy, C. M. Julien, A. Mauger and K. Zaghib, *Nanomaterials*, 2020, **10**, 1–80.
139 C. Deviannapoorani, L. Dhivya, S. Ramakumar and R. Murugan, *J. Power Sources*, 2013, **240**, 18–25.
140 C. Wang, K. Fu, S. P. Kammampata, D. W. McOwen, A. J. Samson, L. Zhang, G. T. Hitz, A. M. Nolan, E. D. Wachsman, Y. Mo, V. Thangadurai and L. Hu, *Chem. Rev.*, 2020, **120**, 4257–4300.
141 R. Murugan, V. Thangadurai and W. Weppner, *Angew. Chem., Int. Ed.*, 2007, **46**, 7778–7781.
142 J. van den Broek, S. Afyon and J. L. M. Rupp, *Adv. Energy Mater.*, 2016, **6**, 1600736.
143 C. Hänsel, S. Afyon and J. L. M. Rupp, *Nanoscale*, 2016, **8**, 18412–18420.
144 J. Awaka, A. Takashima, K. Kataoka, N. Kijima, Y. Idemoto and J. Akimoto, *Chem. Lett.*, 2011, **40**, 60–62.
145 L. Liang, X. Sun, J. Zhang, J. Sun, L. Hou, Y. Liu and C. Yuan, *Mater. Horiz.*, 2019, **6**, 871–910.
146 C. A. Geiger, E. Alekseev, B. Lazic, M. Fisch, T. Armbruster, R. Langner, M. Fechtelkord, N. Kim, T. Pettke and W. Weppner, *Inorg. Chem.*, 2011, **50**, 1089–1097.
147 R. Pfenninger, M. Struzik, I. Garbayo, E. Stilp and J. L. M. Rupp, *Nat. Energy*, 2019, **4**, 475–483.
148 K. J. Kim and J. L. M. Rupp, *Energy Environ. Sci.*, 2020, **13**, 4930–4945.
149 R. J. Chen, M. Huang, W. Z. Huang, Y. Shen, Y. H. Lin and C. W. Nan, *J. Mater. Chem. A*, 2014, **2**, 13277–13282.
150 G. Larraz, A. Orera and M. L. Sanjuán, *J. Mater. Chem. A*, 2013, **1**, 11419–11428.
151 W. Xia, B. Xu, H. Duan, X. Tang, Y. Guo, H. Kang, H. Li and H. Liu, *J. Am. Ceram. Soc.*, 2017, **100**, 2832–2839.
152 H. Peng, Q. Wu and L. Xiao, *J. Sol-Gel Sci. Technol.*, 2013, **66**, 175–179.
153 I. Garbayo, M. Struzik, W. J. Bowman, R. Pfenninger, E. Stilp and J. L. M. Rupp, *Adv. Energy Mater.*, 2018, **8**, 1–14.
154 H. Rusdi, N. S. Mohamed, R. H. Y. Subban and R. Rusdi, *J. Sci.: Adv. Mater. Devices*, 2020, **5**, 368–377.
155 Y. Zhu, X. He and Y. Mo, *J. Mater. Chem. A*, 2016, **4**, 3253–3266.
156 H. El-Shinawi and J. Janek, *RSC Adv.*, 2015, **5**, 14887–14891.
157 P. Maldonado-Manso, E. R. Losilla, M. Martínez-Lara, M. a. G. Aranda, S. Bruque, F. E. Mouahid and M. Zahir, *Chem. Mater.*, 2003, **15**, 1879–1885.
158 J. Fu, *Solid State Ionics*, 1997, **96**, 195–200.
159 E. C. Bucharsky, K. G. Schell, A. Hintennach and M. J. Hoffmann, *Solid State Ionics*, 2015, **274**, 77–82.
160 H. Chen, H. Tao, X. Zhao and Q. Wu, *J. Non-Cryst. Solids*, 2011, **357**, 3267–3271.
161 X. M. Wu, S. Chen, F. R. Mai, J. H. Zhao and Z. Q. He, *Ionics*, 2013, **19**, 589–593.
162 R. Inada, K. Ichi Ishida, M. Tojo, T. Okada, T. Tojo and Y. Sakurai, *Ceram. Int.*, 2015, **41**, 11136–11142.
163 P. Knauth, *Solid State Ionics*, 2009, **180**, 911–916.
164 K. Arbi, J. M. Rojo and J. Sanz, *J. Eur. Ceram. Soc.*, 2007, **27**, 4215–4218.
165 Y. Liu, Q. Sun, Y. Zhao, B. Wang, P. Kaghazchi, K. R. Adair, R. Li, C. Zhang, J. Liu, L. Y. Kuo, Y. Hu, T. K. Sham, L. Zhang, R. Yang, S. Lu, X. Song and X. Sun, *ACS Appl. Mater. Interfaces*, 2018, **10**, 31240–31248.
166 Y. Liu, Q. Sun, J. Liu, M. Norouzi Banis, Y. Zhao, B. Wang, K. Adair, Y. Hu, Q. Xiao, C. Zhang, L. Zhang, S. Lu, H. Huang, X. Song and X. Sun, *ACS Appl. Mater. Interfaces*, 2020, **12**, 2293–2298.
167 W. Xiao, J. Wang, L. Fan, J. Zhang and X. Li, *Energy Storage Mater.*, 2019, **19**, 379–400.
168 M. Hou, F. Liang, K. Chen, Y. Dai and D. Xue, *Nanotechnology*, 2020, **31**, 132003.
169 P. Hofmann, F. Walther, M. Rohnke, J. Sann, W. G. Zeier and J. Janek, *Solid State Ionics*, 2019, **342**, 115054.
170 D. Mazumdar, D. N. Bose and M. L. Mukherjee, *Solid State Ionics*, 1984, **14**, 143–147.
171 U. v. Alpen, M. F. Bell, W. Wichelhaus, K. Y. Cheung and G. J. Dudley, *Electrochim. Acta*, 1978, **23**, 1395–1397.
172 Y. Deng, C. Eames, J. N. Chotard, F. Laleìre, V. Seznec, S. Emge, O. Pecher, C. P. Grey, C. Masquelier and M. S. Islam, *J. Am. Chem. Soc.*, 2015, **137**, 9136–9145.
173 S. Song, J. Lu, F. Zheng, H. M. Duong and L. Lu, *RSC Adv.*, 2015, **5**, 6588–6594.
174 N. Kamaya, K. Homma, Y. Yamakawa, M. Hirayama, R. Kanno, M. Yonemura, T. Kamiyama, Y. Kato, S. Hama, K. Kawamoto and A. Mitsui, *Nat. Mater.*, 2011, **10**, 682–686.

175 R. Kanno and M. Murayama, *J. Electrochem. Soc.*, 2001, **148**, A742.
176 Y. Sun, K. Suzuki, K. Hara, S. Hori, T. A. Yano, M. Hara, M. Hirayama and R. Kanno, *J. Power Sources*, 2016, **324**, 798–803.
177 Y. Kato, S. Hori, T. Saito, K. Suzuki, M. Hirayama, A. Mitsui, M. Yonemura, H. Iba and R. Kanno, *Nat. Energy*, 2016, **1**, 1–7.
178 H. Muramatsu, A. Hayashi, T. Ohtomo, S. Hama and M. Tatsumisago, *Solid State Ionics*, 2011, **182**, 116–119.
179 Y. Wang, Z. Liu, X. Zhu, Y. Tang and F. Huang, *J. Power Sources*, 2013, **224**, 225–229.
180 E. Gilardi, G. Materzanini, L. Kahle, M. Döbeli, S. Lacey, X. Cheng, N. Marzari, D. Pergolesi, A. Hintennach and T. Lippert, *ACS Appl. Energy Mater.*, 2020, **3**, 9910–9917.
181 S. Stramare, V. Thangadurai and W. Weppner, *ChemInform*, 2003, **34**, 3974–3990.
182 M. Itoh, Y. Inaguma, W.-H. Jung, L. Chen and T. Nakamura, *Solid State Ionics*, 1994, **70–71**, 196–202.
183 C. H. Chen and K. Amine, *Solid State Ionics*, 2001, **144**, 51–57.
184 H. T. Chung, J. G. Kim and H. G. Kim, *Solid State Ionics*, 1998, **107**, 153–160.
185 S. I. Furusawa, H. Tabuchi, T. Sugiyama, S. Tao and J. T. S. Irvine, *Solid State Ionics*, 2005, **176**, 553–558.
186 O. Maqueda, F. Sauvage, L. Laffont, M. L. Martínez-Sarrión, L. Mestres and E. Baudrin, *Thin Solid Films*, 2008, **516**, 1651–1655.
187 B. Huang, B. Xu, Y. Li, W. Zhou, Y. You, S. Zhong, C. A. Wang and J. B. Goodenough, *ACS Appl. Mater. Interfaces*, 2016, **8**, 14552–14557.
188 J. Z. Lee, Z. Wang, H. L. Xin, T. A. Wynn and Y. S. Meng, *J. Electrochem. Soc.*, 2017, **164**, A6268–A6273.
189 J. m. Lee, S. h. Kim, Y. Tak and Y. S. Yoon, *J. Power Sources*, 2006, **163**, 173–179.
190 C. L. Li, B. Zhang and Z. W. Fu, *Thin Solid Films*, 2006, **515**, 1886–1892.
191 R. Rajagopalan, Z. Zhang, Y. Tang, C. Jia, X. Ji and H. Wang, *Energy Storage Mater.*, 2021, **34**, 171–193.
192 J. Huang, F. Liang, M. Hou, Y. Zhang, K. Chen and D. Xue, *Appl. Mater. Today*, 2020, **20**, 100750.
193 R. DeWees and H. Wang, *ChemSusChem*, 2019, **12**, 3713–3725.
194 P. Birke, F. Salam, S. Döring and W. Weppner, *Solid State Ionics*, 1999, **118**, 149–157.
195 K. P. Abhilash, P. Sivaraj, P. C. Selvin, B. Nalini and K. Somasundaram, *Ceram. Int.*, 2015, **41**, 13823–13829.
196 J. K. Ahn and S. G. Yoon, *Electrochim. Acta*, 2004, **50**, 371–374.
197 S. A. Yoon, N. R. Oh, A. R. Yoo, H. G. Lee and H. C. Lee, *J. Korean Ceram. Soc.*, 2017, **54**, 278–284.
198 M. Fenech and N. Sharma, *Chem.–Asian J.*, 2020, **15**, 1829–1847.
199 C. Cao, Z. Bin Li, X. L. Wang, X. B. Zhao and W. Q. Han, *Front. Energy Res.*, 2014, **2**, 1–10.
200 M. Tatsumisago, *Solid State Ionics*, 2004, **175**, 13–18.
201 T. Minami, *J. Non-Cryst. Solids*, 1985, **73**, 273–284.
202 V. Lacivita, N. Artrith and G. Ceder, *Chem. Mater.*, 2018, **30**, 7077–7090.
203 N. J. Dudney, J. B. Bates, R. A. Zuhr, C. F. Luck and J. D. Robertson, *Solid State Ionics*, 1992, **53–56**, 655–661.
204 B. Put, P. M. Vereecken and A. Stesmans, *J. Mater. Chem. A*, 2018, **6**, 4848–4859.
205 J. B. Bates and X. Yu, *J. Vac. Sci. Technol., A*, 1996, **14**, 34–37.
206 V. Krasnov, K.-W. Nieh, S.-J. Ting, P. Tang, F.-H. Chang and C.-T. Lin, *U.S. Pat.*, No. US6863699B1, 2000.
207 C. H. Choi, W. I. Cho, B. W. Cho, H. S. Kim, Y. S. Yoon and Y. S. Tak, *Electrochem. Solid-State Lett.*, 2002, **5**, 14–17.
208 Y. Hamon, A. Douard, F. Sabary, C. Marcel, P. Vinatier, B. Pecquenard and A. Levasseur, *Solid State Ionics*, 2006, **177**, 257–261.
209 B. Kim, Y. S. Cho, J. G. Lee, K. H. Joo, K. O. Jung, J. Oh, B. Park, H. J. Sohn, T. Kang, J. Cho, Y. S. Park and J. Y. Oh, *J. Power Sources*, 2002, **109**, 214–219.
210 N. Suzuki, S. Shirai, N. Takahashi, T. Inaba and T. Shiga, *Solid State Ionics*, 2011, **191**, 49–54.
211 Y. Su, J. Falgenhauer, A. Polity, T. Leichtweiß, A. Kronenberger, J. Obel, S. Zhou, D. Schlettwein, J. Janek and B. K. Meyer, *Solid State Ionics*, 2015, **282**, 63–69.
212 A. Sepúlveda, F. Criscuolo, B. Put and P. M. Vereecken, *Solid State Ionics*, 2019, **337**, 24–32.
213 A. S. Westover, R. L. Sacci and N. Dudney, *ACS Energy Lett.*, 2020, **5**, 3860–3867.
214 D. Cheng, T. A. Wynn, X. Wang, S. Wang, M. Zhang, R. Shimizu, S. Bai, H. Nguyen, C. Fang, M. c. Kim, W. Li, B. Lu, S. J. Kim and Y. S. Meng, *Joule*, 2020, **4**, 2484–2500.
215 Z. D. Hood, X. Chen, R. L. Sacci, X. Liu, G. M. Veith, Y. Mo, J. Niu, N. J. Dudney and M. Chi, *Nano Lett.*, 2021, **21**, 151–157.
216 Z. D. Hood and M. Chi, *J. Mater. Sci.*, 2019, **54**, 10571–10594.
217 S. Jacke, J. Song, G. Cherkashinin, L. Dimesso and W. Jaegermann, *Ionics*, 2010, **16**, 769–775.
218 R. Hausbrand, A. Schwöbel, W. Jaegermann, M. Motzko and D. Ensling, *Z. Phys. Chem.*, 2015, **229**, 1387–1414.
219 Y.-I. Jang, N. J. Dudney, D. A. Blom and L. F. Allard, *J. Electrochem. Soc.*, 2002, **149**, A1442.
220 D. Santhanagopalan, D. Qian, T. McGilvray, Z. Wang, F. Wang, F. Camino, J. Graetz, N. Dudney and Y. S. Meng, *J. Phys. Chem. Lett.*, 2014, **5**, 298–303.
221 N. J. Dudney, *J. Electroceram.*, 2017, **38**, 222–229.
222 M. Takahashi, M. Hayashi and T. Shodai, *J. Power Sources*, 2009, **189**, 191–196.
223 Y. S. Yoon, S. H. Lee, S. B. Cho and S. C. Nam, *J. Electrochem. Soc.*, 2011, **158**, A1313.
224 S. W. Song, H. Choi, H. Y. Park, G. B. Park, K. C. Lee and H. J. Lee, *J. Power Sources*, 2010, **195**, 8275–8279.
225 S. Tintignac, R. Baddour-Hadjean, J. P. Pereira-Ramos and R. Salot, *Electrochim. Acta*, 2014, **146**, 472–476.
226 H. Y. Park, S. R. Lee, Y. J. Lee, B. W. Cho and W. I. Cho, *Mater. Chem. Phys.*, 2005, **93**, 70–78.
227 M. Koo, K. Il Park, S. H. Lee, M. Suh, D. Y. Jeon, J. W. Choi, K. Kang and K. J. Lee, *Nano Lett.*, 2012, **12**, 4810–4816.

228 Y. S. Park, S. H. Lee, B. Il Lee and S. K. Joo, *Electrochem. Solid-State Lett.*, 1999, **2**, 58–59.
229 N. J. Dudney, J. B. Bates, R. A. Zuhr, S. Young, J. D. Robertson, H. P. Jun and S. A. Hackney, *J. Electrochem. Soc.*, 1999, **146**, 2455–2464.
230 J. Li, C. Ma, M. Chi, C. Liang and N. J. Dudney, *Adv. Energy Mater.*, 2015, **5**, 1401408.
231 C. Navone, S. Tintignac, J. P. Pereira-Ramos, R. Baddour-Hadjean and R. Salot, *Solid State Ionics*, 2011, **192**, 343–346.
232 E. J. Jeon, Y. W. Shin, S. C. Nam, W. Il Cho and Y. S. Yoon, *J. Electrochem. Soc.*, 2001, **148**, A318.
233 F. Huang, Z. W. Fu, Y. Q. Chu, W. Y. Liu and Q. Z. Qin, *Electrochem. Solid-State Lett.*, 2004, **7**, 180–184.
234 C. Li, W. Liu and Z. Fu, *Chin. J. Chem. Phys.*, 2006, **19**, 493–498.
235 C. L. Li and Z. W. Fu, *Electrochim. Acta*, 2008, **53**, 6434–6443.
236 C. L. Li and Z. W. Fu, *Electrochim. Acta*, 2008, **53**, 4293–4301.
237 S. Kanazawa, T. Baba, K. Yoneda, M. Mizuhata and I. Kanno, *Thin Solid Films*, 2020, **697**, 137840.
238 L. Li, S. Liu, H. Zhou, Q. Lei and K. Qian, *Mater. Lett.*, 2018, **216**, 135–138.
239 M. Baba, N. Kumagai, N. Fujita, K. Ohta, K. Nishidate, S. Komaba, H. Groult, D. Devilliers and B. Kaplan, *J. Power Sources*, 2001, **97–98**, 798–800.
240 H. Nakazawa, K. Sano and M. Baba, *J. Power Sources*, 2005, **146**, 758–761.
241 H. Nakazawa, K. Sano, T. Abe, M. Baba and N. Kumagai, *J. Power Sources*, 2007, **174**, 838–842.
242 B. J. Neudecker, N. J. Dudney and J. B. Bates, *J. Electrochem. Soc.*, 2000, **147**, 517.
243 T. Yamamoto, H. Iwasaki, Y. Suzuki, M. Sakakura, Y. Fujii, M. Motoyama and Y. Iriyama, *Electrochem. Commun.*, 2019, **105**, 106494.
244 V. Lacivita, A. S. Westover, A. Kercher, N. D. Phillip, G. Yang, G. Veith, G. Ceder and N. J. Dudney, *J. Am. Chem. Soc.*, 2018, **140**, 11029–11038.
245 B. Fleutot, B. Pecquenard, F. Le Cras, B. Delis, H. Martinez, L. Dupont and D. Guy-Bouyssou, *J. Power Sources*, 2011, **196**, 10289–10296.
246 Y. Yoon, C. Park, J. Kim and D. Shin, *Electrochim. Acta*, 2013, **111**, 144–151.
247 V. P. Phan, B. Pecquenard and F. Le Cras, *Adv. Funct. Mater.*, 2012, **22**, 2580–2584.
248 T. Famprikis, J. Galipaud, O. Clemens, B. Pecquenard and F. Le Cras, *ACS Appl. Energy Mater.*, 2019, **2**, 4782–4791.
249 B. Wang, J. B. Bates, F. X. Hart, B. C. Sales, R. A. Zuhr and J. D. Robertson, *J. Electrochem. Soc.*, 1996, **143**, 3203–3213.
250 P. Schichtel, M. Geiß, T. Leichtweiß, J. Sann, D. A. Weber and J. Janek, *J. Power Sources*, 2017, **360**, 593–604.
251 S. Larfaillou, D. Guy-Bouyssou, F. Le Cras and S. Franger, *J. Power Sources*, 2016, **319**, 139–146.
252 Z. Wang, D. Santhanagopalan, W. Zhang, F. Wang, H. L. Xin, K. He, J. Li, N. Dudney and Y. S. Meng, *Nano Lett.*, 2016, **16**, 3760–3767.
253 K. Nie, Y. Hong, J. Qiu, Q. Li, X. Yu and H. Li, *Front. Chem.*, 2018, **6**, 616.
254 S. Xia, X. Wu, Z. Zhang, Y. Cui and W. Liu, *Chem*, 2019, **5**, 753–785.
255 C. Sångeland, J. Mindemark, R. Younesi and D. Brandell, *Solid State Ionics*, 2019, **343**, 115068.
256 Z. Ding, J. Li, J. Li and C. An, *J. Electrochem. Soc.*, 2020, **167**, 070541.
257 H. Lim, J. Park, H. Shin, J. Jeong, J. T. Kim, K. Nam, H. Jung and K. Y. Chung, *Energy Storage Mater.*, 2020, **25**, 224–250.
258 A. Gurung, J. Pokharel, A. Baniya, R. Pathak, K. Chen, B. S. Lamsal, N. Ghimire, W. H. Zhang, Y. Zhou and Q. Qiao, *Sustainable Energy Fuels*, 2019, **3**, 3279–3309.
259 J. B. Bates, N. J. Dudney, B. J. Neudecker, F. X. Hart, H. P. Jun and S. A. Hackney, *J. Electrochem. Soc.*, 2000, **147**, 59.
260 Y. Iriyama, T. Kako, C. Yada, T. Abe and Z. Ogumi, *Solid State Ionics*, 2005, **176**, 2371–2376.
261 E. Jeong, C. Hong, Y. Tak, S. C. Nam and S. Cho, *J. Power Sources*, 2006, **159**, 223–226.
262 B. Put, P. M. Vereecken, J. Meersschaut, A. Sepúlveda and A. Stesmans, *ACS Appl. Mater. Interfaces*, 2016, **8**, 7060–7069.
263 P. H. L. Notten, F. Roozeboom, R. A. H. Niessen and L. Baggetto, *Adv. Mater.*, 2007, **19**, 4564–4567.
264 L. Baggetto, R. A. H. Niessen, F. Roozehoom and P. H. L. Notten, *Adv. Funct. Mater.*, 2008, **18**, 1057–1066.
265 S. H. Jee, M. J. Lee, H. S. Ahn, D. J. Kim, J. W. Choi, S. J. Yoon, S. C. Nam, S. H. Kim and Y. S. Yoon, *Solid State Ionics*, 2010, **181**, 902–906.
266 S. Zhao, Z. Fu and Q. Qin, *Thin Solid Films*, 2002, **415**, 108–113.
267 W. C. West, Z. D. Hood, S. P. Adhikari, C. Liang, A. Lachgar, M. Motoyama and Y. Iriyama, *J. Power Sources*, 2016, **312**, 116–122.
268 Y. Matsuda, N. Kuwata and J. Kawamura, *Solid State Ionics*, 2018, **320**, 38–44.
269 M. Nisula, Y. Shindo, H. Koga and M. Karppinen, *Chem. Mater.*, 2015, **27**, 6987–6993.
270 A. C. Kozen, A. J. Pearse, C. F. Lin, M. Noked and G. W. Rubloff, *Chem. Mater.*, 2015, **27**, 5324–5331.
271 B. Put, M. J. Mees, N. Hornsveld, S. Hollevoet, A. Sepúlveda, P. M. Vereecken, W. M. M. Kessels and M. Creatore, *J. Electrochem. Soc.*, 2019, **166**, A1239–A1242.
272 S. Shibata, *J. Electrochem. Soc.*, 2016, **163**, A2555–A2562.
273 A. J. Pearse, T. E. Schmitt, E. J. Fuller, F. El-Gabaly, C. F. Lin, K. Gerasopoulos, A. C. Kozen, A. A. Talin, G. Rubloff and K. E. Gregorczyk, *Chem. Mater.*, 2017, **29**, 3740–3753.
274 M. Létiche, E. Eustache, J. Freixas, A. Demortière, V. De Andrade, L. Morgenroth, P. Tilmant, F. Vaurette, D. Troadec, P. Roussel, T. Brousse and C. Lethien, *Adv. Energy Mater.*, 2017, **7**, 1–12.
275 W. Y. Liu, Z. W. Fu, C. L. Li and Q. Z. Qin, *Electrochem. Solid-State Lett.*, 2004, **7**, 36–40.
276 Y. G. Kim and H. N. G. Wadley, *J. Vac. Sci. Technol., A*, 2008, **26**, 174–183.
277 C. S. Nimisha, K. Y. Rao, G. Venkatesh, G. M. Rao and N. Munichandraiah, *Thin Solid Films*, 2011, **519**, 3401–3406.

278 S. Nowak, F. Berkemeier and G. Schmitz, *J. Power Sources*, 2015, **275**, 144–150.
279 M. Haruta, S. Shiraki, T. Suzuki, A. Kumatani, T. Ohsawa, Y. Takagi, R. Shimizu and T. Hitosugi, *Nano Lett.*, 2015, **15**, 1498–1502.
280 B. Uzakbaiuly, A. Mukanova, I. Kurmanbayeva and Z. B. Bakenov, *Eurasian J. Phys. Funct. Mater.*, 2019, **3**, 174–182.
281 J. Ko and Y. S. Yoon, *Ceram. Int.*, 2020, **46**, 20623–20632.
282 K. H. Joo, P. Vinatier, B. Pecquenard, A. Levasseur and H. J. Sohn, *Solid State Ionics*, 2003, **160**, 51–59.
283 L. Q. Nguyen, L. Chen and V. Van Truong, *Thin Solid Films*, 1997, **293**, 175–178.
284 B. V. R. Chowdari and K. Radhakrishnan, *Solid State Ionics*, 1991, **44**, 325–329.
285 T. Minami, A. Hayashi and M. Tatsumisago, *Solid State Ionics*, 2006, **177**, 2715–2720.
286 J. Kawamura, N. Kuwata, K. Toribami, N. Sata, O. Kamishima and T. Hattori, *Solid State Ionics*, 2004, **175**, 273–276.
287 H. Ohtsuka and Y. Sakurai, *Solid State Ionics*, 2001, **144**, 59–64.
288 N. Kuwata, R. Kumar, K. Toribami, T. Suzuki, T. Hattori and J. Kawamura, *Solid State Ionics*, 2006, **177**, 2827–2832.
289 R. Baskaran, N. Kuwata, O. Kamishima, J. Kawamura and S. Selvasekarapandian, *Solid State Ionics*, 2009, **180**, 636–643.
290 A. Brazier, L. Dupont, L. Dantras-Laffont, N. Kuwata, J. Kawamura and J. M. Tarascon, *Chem. Mater.*, 2008, **20**, 2352–2359.
291 S. S. Gundale and A. V. Deshpande, *Electrochim. Acta*, 2018, **265**, 65–70.
292 S. Zhao and Q. Qin, *J. Power Sources*, 2003, **122**, 174–180.
293 H. Ohtsuka and J. i. Yamaki, *Solid State Ionics*, 1989, **35**, 201–206.
294 S. J. Lee, J. H. Bae, H. W. Lee, H. K. Baik and S. M. Lee, *J. Power Sources*, 2003, **123**, 61–64.
295 S. J. Lee, H. K. Baik and S. M. Lee, *Electrochem. Commun.*, 2003, **5**, 32–35.
296 Q. Chen, R. Xu, Z. He, K. Zhao and L. Pan, *J. Electrochem. Soc.*, 2017, **164**, A1852–A1857.
297 K. Edström, D. Brandell, T. Gustafsson and L. Nyholm, *Electrochem. Soc. Interface*, 2011, **20**, 41–46.
298 R. Sheil and J. P. Chang, *J. Vac. Sci. Technol., A*, 2020, **38**, 032411.
299 P. Priimägi, H. Kasemägi, A. Aabloo, D. Brandell and V. Zadin, *Electrochim. Acta*, 2017, **244**, 129–138.
300 B. Sun, D. Rehnlund, M. J. Lacey and D. Brandell, *Electrochim. Acta*, 2014, **137**, 320–327.
301 N. A. Kyerematen, F. Dumur, P. Knauth, B. Pecquenard and T. Djenizian, *Electrochem. Commun.*, 2011, **13**, 894–897.
302 K. Sun, T. S. Wei, B. Y. Ahn, J. Y. Seo, S. J. Dillon and J. A. Lewis, *Adv. Mater.*, 2013, **25**, 4539–4543.
303 D. W. McOwen, S. Xu, Y. Gong, Y. Wen, G. L. Godbey, J. E. Gritton, T. R. Hamann, J. Dai, G. T. Hitz, L. Hu and E. D. Wachsman, *Adv. Mater.*, 2018, **30**, 1–7.
304 C. Y. Yap, C. K. Chua, Z. L. Dong, Z. H. Liu, D. Q. Zhang, L. E. Loh and S. L. Sing, *Appl. Phys. Rev.*, 2015, **2**(4), 041101.
305 A. Ambrosi and M. Pumera, *Chem. Soc. Rev.*, 2016, **45**, 2740–2755.
306 C. Zhu, T. Liu, F. Qian, W. Chen, S. Chandrasekaran, B. Yao, Y. Song, E. B. Duoss, J. D. Kuntz, C. M. Spadaccini, M. A. Worsley and Y. Li, *Nano Today*, 2017, **15**, 107–120.
307 N. A. Kyerematen and R. Hahn, *ACS Energy Lett.*, 2018, **3**, 1172–1175.
308 Y. Il Jang, N. J. Dudney, D. A. Blom and L. F. Allard, *J. Power Sources*, 2003, **119–121**, 295–299.
309 N. Kuwata, N. Iwagami, Y. Matsuda, Y. Tanji and J. Kawamura, *ECS Trans.*, 2009, **16**, 53–60.
310 A. Nakagawa, N. Kuwata, Y. Matsuda and J. Kawamura, *ECS Trans.*, 2010, **25**, 155–161.

